Giant magnetoresistance in spin-valves with thin Ru layers and NiO exchange-biased structures

Strijkers, G.J.

Award date:
1995

Eindhoven University of Technology
Department of Physics
Group Cooperative Phenomena

Giant magnetoresistance in spin-valves with thin Ru layers and NiO exchange-biased structures

Gustav J. Strijkers

June 1995

Report of a graduation research project carried out in the group *Cooperative Phenomena* at the Eindhoven University of Technology. This project is part of a collaboration with Philips Research Laboratories Eindhoven.

Supervisors	:	dr. ir. H.J.M. Swagten ir. M.M.H. Willekens
Professor	:	prof. dr. ir. W.J.M. de Jonge

Abstract

We have investigated the magnetoresistance of uncoupled Co/Cu/Co spin-valves. In these Co/Cu/Co spin-valves thin Ru layers were introduced at the interface of Co and Cu or in the middle of the Cu layer. From analyzing the magnetoresistance results and comparison with the Camley-Barnas model, we came to the conclusion that a Co/Ru interface has a smaller spin-dependent scattering asymmetry for electrons, compared to a Co/Cu interface. This can explain the low magnetoresistance ratios observed in Co/Ru/Co spin-valves and multilayers as compared to Co/Cu/Co.

The longest of the mean free paths in Co was determined by analyzing the magnetoresistance ratios as a function of a shifting Ru barrier layer through **Co** in Co/Cu/**Co** spin-valves. Mean free paths were found ranging from about 100 Å at 300K to approximate 200 Å at 10K, in agreement with literature. We tried to determine the mean free path of Cu by analyzing the magnetoresistance ratios of Co/Cu/Co/**Cu** with a shifting Ru layer through the **Cu** back layer. Although it turned out from analysis with the Camley-Barnas model, that this structure is not the most suitable tool to determine the mean free path of Cu, we estimated the mean free path for Cu at 300K and 250K to be about 360 Å and 440 Å respectively. From comparison of the longest of the mean free paths ($\lambda^{long} = \lambda^{\uparrow}$) with the conductivity ($\sigma \propto \lambda^{\uparrow} + \lambda^{\downarrow}$) we found no evidence for the existance of considerable bulk spin-dependent scattering in Co.

We have measured the magnetoresistance of exchange biased spin-valves of Co/Cu/Co and $Ni_{80}Fe_{20}$/Cu/$Ni_{80}Fe_{20}$ sandwiched between insulating NiO. One of the magnetic layers was exchange biased to NiO. For Co/Cu/Co spin-valves magnetoresistance ratios up to 24% have been measured at 10K, which is about a factor 2 higher than the highest magnetoresistance ratios reported in literature. These high magnetoresistance ratios can be explained with the Camley-Barnas model if one takes into account reflections of electrons at the impenetrable NiO layers. Experiments, however, have yielded no proof for reflections at the NiO layers.

For the $Ni_{80}Fe_{20}$/Cu/$Ni_{80}Fe_{20}$ spin-valves sandwiched between NiO magnetoresistance ratios up to 15% at 10K have been found, which also is higher as compared to magnetoresistance results in literature for these spin-valves (maximum 9%). These NiO exchange biased $Ni_{80}Fe_{20}$/Cu/$Ni_{80}Fe_{20}$ spin-valves may be promising for magnetic sensing devices in future.

Contents

Chapter 1

Introduction

Since it is possible to grow alternating thin layers of magnetic and non-magnetic materials on top of each other in what we call magnetic multilayers, this field of research has developed enormously. For about ten years sputtering and evaporation techniques make it possible to grow these multilayers with such high quality that layer thicknesses down to the atomic scale have become possible. These structures have no counterparts in nature and therefore it is not surprising that several new phenomena were discovered. The magnetic moments of two magnetic layers separated by a non-magnetic layer tend to align parallel or anti-parallel. This alignment oscillates between parallel and anti-parallel as a function of the non-magnetic layer thickness. This was called magnetic interlayer coupling. It was also discovered that a change of alignment of these two magnetic moments from parallel to anti-parallel was accompanied by a large change in resistance of the structure. This was called the Giant MagnetoResistance effect (GMR). The research was and is still stimulated by technological applications in for example discs and heads for magnetic recording.

In recent years much research has been done to understand the giant magnetoresistance effect from a fundamental point of view. One of the problems is that, although the origin of the giant magnetoresistance effect is generally accepted to be spin-dependent scattering, the relative role of bulk and interface spin-dependent scattering is not clear. Also the role of reflections of electrons at interfaces between the layers has not been clarified experimentally.

In this respect we have studied the Giant MagnetoResistance effect in Co/Cu/Co and $Ni_{80}Fe_{20}$/Cu/$Ni_{80}Fe_{20}$. In chapter 2 we will introduce the magnetoresistance effect and we will give a simplified physical picture to understand the GMR effect. A brief literature overview is given of the main studies on the origin of the magnetoresistance effect. Chapter 3 is about the Camley-Barnas model for the magnetoresistance. In the last section of this chapter a brief description of the Falicov and Hood model is given, which is an extension of the Camley-Barnas model. The experimental equipment for measuring magnetoresistance and magnetization is briefly outlined in chapter 4. We use X-ray diffraction to determine the crystalline orientation of our layers. Therefore, a short description of this technique is given. In chapter 5 the sample preparation technique sputtering is explained, which we have used to grow our samples. Three possible spin-valve designs are shown. In chapter 6 measurements are presented on Co/Cu-based spin-valves. We have changed the interfaces by adding thin Ru layers at the interfaces of Co and Cu in the spin-valve. This is done to investigate the role of the Co/Cu and Co/Ru interfaces in the magnetoresistance. In chapter 7 calculations and measurements are presented on Co/Cu/**Co** and Co/Cu/Co/**Cu** spin-valves with a Ru barrier layer shifted through **Co** and **Cu** respectivily. We have calculated under what condition these experiments can be used to extract the longest of the mean free paths in **Co** and **Cu**. The longest of the mean free paths λ^{long} is compared with the conductivity to see if decisive evidence about the role of bulk spin-dependent scattering can be found. Finally we present in chapter 8 measurements on Co/Cu/Co and $Ni_{80}Fe_{20}$/Cu/$Ni_{80}Fe_{20}$ spin-valves sandwiched between NiO. One of the magnetic layers of the spin-valves is exchange biased to NiO. Effects on the magnetoresistance of the insulating NiO layers are investigated.

Chapter 2

Giant Magnetoresistance

In this chapter the magnetoresistance effect is introduced. After this introduction we will concentrate on the origin of the magnetoresistance effect, which is known to be spin-dependent scattering. A brief survey is given of the main studies on interfacial spin-dependent scattering.

2.1 Magnetoresistance

Magnetoresistance is the effect that a material changes its resistance if it is exposed to a magnetic field. Magnetoresistance in ferromagnetic materials has long been known. A ferromagnet changes its resistivity if its internal magnetization direction is changed (by applying a field) with respect to the current. This is called the anisotropic magnetoresistance effect (AMR).

In 1986, however, it was discovered that two ferromagnetic layers separated by a non-magnetic layer can show antiferromagnetic coupling [Grün86]. This antiferromagnetic alignment of the magnetic moments of two magnetic layers can be overcome by applying a magnetic field. In 1988 it was observed that this change in alignment of the ferromagnetic layers was accompanied by a change in resistivity [Bai88]. This effect was called the *Giant Magnetoresistance Effect* (GMR, but in this study mostly simply called magnetoresistance or MR). The change in resistivity was larger than the anisotropic magnetoresistance effect and therefore called giant. The *GMR*-ratio is defined as the relative resistance change between the two states with magnetic moments parallel (*Rp*) and anti-parallel (*Rap*):

$$GMR = 100 \cdot \frac{Rap - Rp}{Rp} \%. \tag{2.1}$$

The origin of this magnetoresistance effect was related to spin-dependent scattering of spin-polarized electrons at the interface and in the bulk of the magnetic layers. In the so-called two current model the electrons are considered to be divided into two channels, one channel with spin-up electrons and one channel with spin-down electrons. Electrons with a spin-polarization direction opposite to the magnetization direction in a magnetic layer experience more resistance than electrons with equal spin-polarization direction as the magnetization direction. Figure 2.1 is a schematic drawing of two magnetic layers (*M1* and *M2*) separated by a non-magnetic layer *NM*. The magnetization directions of *M1* and *M2* are considered either anti-parallel (figure 2.1.a) or parallel (figure 2.1.b) with respect to each other. In the case of anti-parallel alignment of the two magnetic layers, both spin-up and spin-down electrons experience large resistance in one of the magnetic layers and at the interface between magnetic and non-magnetic materials. The resistance of such a structure can be seen as two equal resistors, each representing the resistance of one spin-channel, connected parallel. In the case of parallel alignment, however, one spin channel acts as a shunt with a low resistance (spin-up

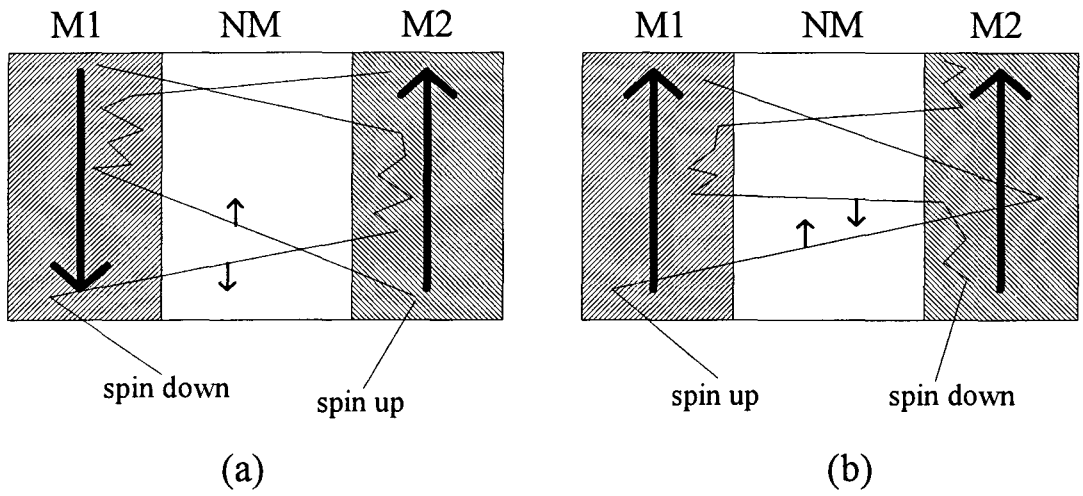

Figure 2.1: *Two magnetic layers (M1 and M2) separated by a non-magnetic layer NM in the case of (a) anti-parallel alignment of the magnetic moments and (b) parallel alignment of the magnetic moments. Also drawn are fictive paths of polarized electrons which experience large resistance if their polarization direction is opposite to the magnetic moment of the layer.*

in figure 2.1.b), and therefore the total resistance is lower than in anti-parallel alignment. Of course this only applies to the case in which the electrons are able to move through all the layers, which means that the mean free paths of the electrons must be larger or in the order of the layer thicknesses.

A stack of two magnetic layers separated by a non-magnetic layer, which shows giant magnetoresistance effects, is often referred to as a spin-valve, as the structure acts as a kind of valve for spin-polarized electrons. Materials in which the magnetoresistance effect is found are for example Co/Cu/Co, NiFe/Cu/NiFe and Fe/Cr/Fe. Further we note that it is not necessary to have two antiferromagnetically coupled magnetic layers for a magnetoresistance effect. If we are able to achieve transition between parallel and anti-parallel alignment without coupling, also giant magnetoresistance effects are found. Other ways of obtaining anti-parallel alignment are discussed in chapter 5.2.

2.2 The origin of spin-dependent scattering

As already mentioned the giant magnetoresistance effect in spin-valves is related to spin-dependent scattering of electrons. In a simple picture one can say that resistivity of electrons in layered metal systems at low temperatures is a result of scattering at impurities and defects.

If we want to understand why this scattering may be spin-dependent, one has to consider the band structure of the ferromagnetic transition metals which are used in the spin-valves like Ni,Fe and Co. All these metals have in common that the spin-up and spin-down d-band are shifted with respect to each other, which results in a difference in occupation of the spin-up and spin-down band. This causes a net magnetic moment and therefore these metals are ferromagnetic. Figure 2.2 shows a schematic representation of the s- and d-band structure of a non-magnetic and magnetic metal. Scattering of electrons takes place near the Fermi-level. The scattering probability is therefore proportional to the density of states at the Fermi-level. As the resistivity is proportional to the scattering probability this results in the following relationship for the resistivity:

$$\rho \sim D(E_F). \tag{2.2}$$

As we can see in figure 2.2 the density of states at the Fermi-level in ferromagnetic materials

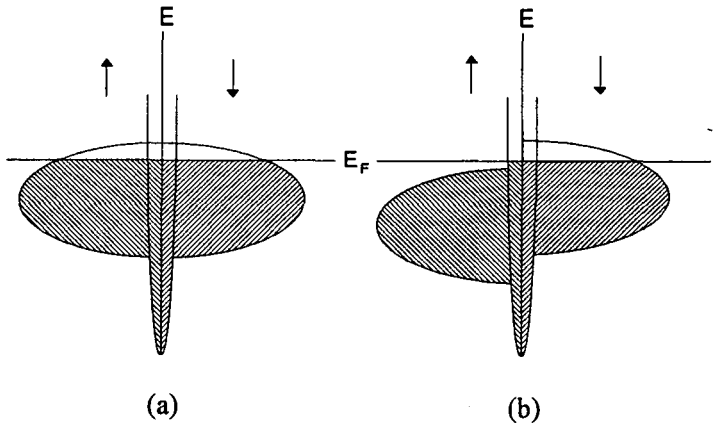

Figure 2.2: Simplified representation of the band structure of (a) a non-magnetic metal and (b) a magnetic metal. All bands are filled up to the fermi-level.

is different for spin-up and spin-down electrons. From this it follows that also the resistivity is spin-dependent.

Next to this bulk spin-dependent scattering, there also exists spin-dependent scattering localized around the interface. One may imagine that interdiffusion at the interfaces, which intermixes the elements within a region around each of the interfaces, causes spin-dependent impurity scattering around the interface. Another scattering mechanism at the interface is a result from the fact that electrons which cross an interface between two metals experience different (spin-dependent) potentials caused by differences in bandstructure between the two metals. This difference in potential between neighboring layers may results in coherent spin-dependent potential scattering at the interface.

2.2.1 The role of the interfaces

In the preceding section we have seen that both bulk spin-dependent scattering and interface spin-dependent scattering may contribute to the magnetoresistance effect.

However, the relative role of bulk and interface spin-dependent scattering in the magnetoresistance effect is not clear. In recent years many research has been done on the role of the interface in the magnetoresistance effect. It was found in general that the interface plays a key role in the magnetoresistance effect. Most of these studies are focussed on the effects of interfacial roughness on the magnetoresistance. In other studies the effects of adding a third element at the interface of magnetic and non-magnetic layers is investigated. In the next sections, a brief literature overview is given of some studies on the role of interfaces in the magnetoresistance effect.

The effects of interfacial roughness on the MagnetoResistance

Studies on Fe/Cr superlattices have shown that interfacial roughness can increase the magnetoresistance [Full92, Oguri92]. *Fullerton et al.* have varied the interface roughness of a sputtered Fe/Cr superlattice by varying three independent parameters in the sputtering process: the sputtering gas pressure, the sputter power, and the total thickness of the superlattice. Increasing sputtering Ar gas pressure from 4mTorr to 12mTorr increases interfacial roughness and enhances the MR from 6% to 11%. Decreasing the Fe target power has a similar effect on the interfacial roughness and the magnetoresistance. It is observed that the superlattice roughness increases cummulatively with increasing number of bilayers Fe/Cr. In conclusion, increasing roughness always resulted in enhanced magnetoresistance.

This result was confirmed by *Oguri et al.* [Oguri92], who studied the conductance in superlattices using the Landauer formula with transfer-matrix techniques to model a superlattice of Fe/Cr. He also concludes that increasing interfacial roughness enhances the magnetoresistance.

In general the enhancement of MR with increasing interface roughness in Fe/Cr superlattices is contributed to the increase in spin-dependent scattering at the Fe/Cr interface caused by strong spin-dependent Fe scatterers in Cr as pointed out by *Hall et al.* [Hall92]. He shows that vigorous annealing of Fe/Cr superlattices at high temperatures undermines the interface structure and therefore leads to strong spin-independent scattering and a decrease of the MR (see also [Petr93, Obi92]).

In a recent article by *Schad et al.* [Schad] magnetoresistance measurements on epitaxial(100) MBE-grown Fe/Cr superlattices are reported. The magnetoresistance as a function of growth temperature shows three distinct regimes. Above 300 °C interdiffusion of Fe and Cr produces a reduction in magnetoresistance. Between 50 °C and 300 °C an increased step density introduced by a Cr buffer layer enhances the magnetoresistance. Below 50 °C this enhancement vanishes. It is concluded that increased interface roughness in the form of an increased step density enhances the magnetoresistance and that interfacial roughness in the form of intermixing reduces the magnetoresistance. On the other hand, measurements by *Belien et al.* [Bel94] on polycrystalline Fe/Cr superlattices have shown that the highest magnetoresistance is obtained when the best layering quality is realised. However, they also conclude that a small amount of steps at the interface can enhance the magnetoresistance.

In contrast to Fe/Cr, *Hall* shows that annealing of a MBE-grown Co/Cu superlattice increases interfacial scattering independent of the spin direction of the conduction electrons. This leads to a significant decrease of the magnetoresistance. Other experiments by *Hall et al.* [Hall93] confirm the fact that increasing interface roughness in Co/Cu superlattices by annealing decreases the magnetoresistance. It is found that half (57%) of the additional scattering due to annealing arises from interface scattering and about half (43%) arises from bulk scattering. This result was obtained by using the ratio of change in bulk scattering to the change in interface scattering as a fitting parameter in the resistor model. Annealing at high temperature ranges (280-295 °C) undermines the structural integrity of the interface and leads to a dramatic decrease in magnetoresistance.

Suzuki et al. performed magnetoresistance measurements on Co/Cu superlattices with intentionally mixed interfaces [Suzuki93]. The interfacial mixed region was intentionally formed between the magnetron sputtered Co and Cu layers by codeposition of 0-0.15 nm of Co and Cu. The value of MR reduces with increasing mixing-region thickness from 27% to 4%. However, the decrease in MR might be contributed to the weakening of the AF-coupling as no significant change in topological roughness could be found using X-ray diffraction.

Willekens et al. have intentionally mixed the interfaces of uncoupled Co/Cu/Co spin-valves [Will95]. Mixing of Co and Cu was done by alternated sputtering of 1 Å Co and 1 Å Cu. The magnetoresistance shows a gradual decrease as the intentionally intermixed region is enlarged from 0 to 36 Å. There is no difference between mixing at one or at two Co/Cu interfaces in the spin-valves, which indicates that the electrons scattering in the intermixed region is predominantly spin-independent.

Annealing of NiFe/Cu/NiFe/FeMn spin-valve structures decreases the magnetoresistance [Huang93]. X-ray diffraction patterns show that annealing increases the thickness of a magnetically inactive layer NiFeCu at the NiFe/Cu interface. *Speriosu et al.* [Speriosu93] pointed out that the ultrathin intermixed regions NiFeCu are not ferromagnetic, and therefore centers of strong spin-independent scattering, which can account for the observed reduction in magnetoresistance.

Annealing of Co/Re superlattices causes a slight increase in interfacial mixing and contraction of lattice spacing owing to diffusion and structural relaxation [Huai93]. This increase in interfacial mixing causes an enhancement of the magnetoresistance as in Fe/Cr superlat-

tices. Vigorous annealing, though, at high temperatures destroys the interface structure and reduces the magnetoresistance.

However, annealing does not always lead to interfacial roughness and intermixing as was shown by *Tosin et al.* [Tos93]. They annealed Co/Ag multilayers and X-ray diffraction patterns show that annealing up to 360 °C leads to narrowing of the interface structure. This demixing of the Co/Ag multilayers is caused by an effective negative diffusion, since Co and Ag cannot form a solid solution. The sharpening of the interface leads to higher magnetoresistance.

NMR studies by *van Alphen* have shown that the microstructure of the Co layers in Co/Ag multilayers depends on the nominal Co thickness and on the annealing treatment [Alph95]. Changes in magnetoresistance upon annealing could be related to the demixing of the Co/Ag multilayers and a gradual change from continuous Co layers to a more granular system.

The effects of adding a third element at the interfaces of magnetic and non-magnetic layers

Another way to investigate the role of the interface with respect to the magnetoresistance is to put a third element at the interface of magnetic and non-magnetic layer.

Parkin [Par93] has investigated the effect of interface scattering in NiFe/Cu/NiFe spin valve systems by adding Co at the interface of NiFe and Cu. The magnetoresistance is found to increase fast with the thickness of the interface layer up to the value of Co/Cu/Co spin-valve systems. This shows, according to Parkin, that magnetoresistance in NiFe/Cu and Co/Cu spin-valves is mainly an interface effect. According to *Dieny* [Dien93], these experiments confirm his opinion that both interfacial and bulk spin-dependent scattering are important in Co/Cu multilayers. He came to this result by fitting Parkin's experimental data with the Camley-Barnas model.

Melo et al. have studied the effect of interface scattering in Co/Re multilayers by adding a third element (Fe,Ni,Co,Cr) at the interface of Co and Re [Melo93]. The magnetoresistance is found to decrease with decreasing interface layer thickness. While Cr and Mo kill the antiferromagnetic coupling, the data with Fe and Ni can be explained by a change of spin-dependent interface scattering.

Baumgart et al. introduced a third element in Fe/Cr multilayers at the Fe-Cr interface [Baum91]. He shows that inserting an element with a similar spin-dependent scattering behaviour as Cr in Fe, leads to a behaviour similar to that when Cr itself is added. This is the case for V and Mn. Adding In or Al at the interface quenches the magnetoresistance dramatically at low Ir and Al thicknesses. *Johnson and Camley* [John91] have made theoretical calculations based on the Boltzmann transport equation approach (Camley-Barnas model) which are appropriate for the experiments done by *Baumgarten et al.* They introduced in their model a thin region at the boundaries of Fe and Cr where Fe and Cr are intermixed. In addition they assumed bulk scattering in the mixed regions. The model is capable of reproducing theoretically all the major features of the Fe/Cr multilayer structures including the experiments done by *Baumgart et al.* of inserting a third element at the Fe-Cr interface.

Chapter 3

Theory

In this chapter the Camley-Barnas model for magnetoresistance is briefly outlined [Cam89]. We will focus on the approximations that are made and how spin-dependent scattering in the bulk and at the interfaces of the magnetic layers is modelled. The relevant parameters are listed, which we use in a computer program to calculate the magnetoresistance.

3.1 Boltzmann equation for a thin film

We compute the conductivity of our spin-valves using the Boltzmann transport equation. First consider the equilibrium Fermi-Dirac distribution

$$f^0(\vec{v}) = \frac{1}{exp\left(\frac{\epsilon_n(\vec{v})-\mu}{k_bT}\right)+1}, \tag{3.1}$$

with μ and T the local thermodynamic potential and temperature. Electrons are driven towards thermodynamic equilibrium by collisions. The general Boltzmann transport equation [Kit86] yields:

$$\frac{\partial f}{\partial t} + \vec{v}\cdot\frac{\partial f}{\partial \vec{r}} + \vec{a}\cdot\frac{\partial f}{\partial \vec{v}} = \left(\frac{\partial f}{\partial t}\right)_{scattering}. \tag{3.2}$$

In relaxation-time approximation the approximation is made that

$$\left(\frac{\partial f}{\partial t}\right)_{scattering} = -\frac{f-f^0}{\tau}, \tag{3.3}$$

in which τ is the relaxation time (mean time between collisions) and f^0 the equilibrium Fermi-Dirac distribution function. We only consider stationary solutions so that $\left(\frac{\partial f}{\partial t}\right) = 0$. The relationship between $\vec{a}$ and the applied external field is given by the Lorentz force

$$\vec{a} = -\frac{e}{m}(\vec{E} + \vec{v}\times\vec{B}). \tag{3.4}$$

We neglect terms in the Boltzmann equation which arise from magnetic fields, since for the size of the fields involved here, the resulting effects are much smaller than that discussed here. For the mass of the electrons the free electron mass is used, which is independent of spin direction.

The distribution function f is decomposed into two parts; the equilibrium distribution function in zero electrical field $f^0(\vec{v})$, and a small local contribution induced by external fields $g(\vec{v},\vec{r})$. Combining equation 3.2 and 3.3 gives the Boltzmann equation for a thin film

$$\frac{\partial g(z,\vec{v})}{\partial z} + \frac{g(z,\vec{v})}{\tau v_z} = \frac{eE_x}{mv_z}\cdot\frac{\partial f^0(\vec{v})}{\partial v_x}, \tag{3.5}$$

in case of the geometry of z perpendicular to the x-y film plane with an electrical field in x-direction.

3.2 The Camley-Barnas model for magnetoresistance

In this section the Camley-Barnas model is treated which makes use of equation 3.5 to calculate the conductivity in thin films and spin-valves. Figure 3.1 shows the geometry of our model spin-valve. The disturbance g from the equilibrium distribution function, must be split in

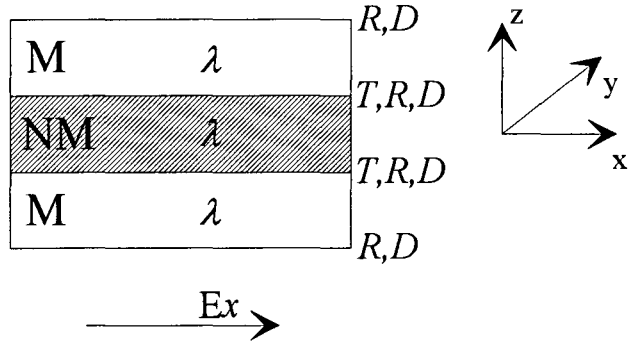

Figure 3.1: *Model spin-valve consisting of two magnetic layers M, separated by a non-magnetic spacer NM. Mean free paths λ, transmission probability T, reflection probability R and diffuse scattering probability D may be spin-dependent.*

$g^{\uparrow}$ and $g^{\downarrow}$, in accordance with the two current model which treats spin-up and spin-down electrons separately. We neglect magnon scattering which may cause electrons to change their spin direction leading to an effective spin-mixing relaxation time $\tau^{\uparrow\downarrow}$. Spin-up and spin-down are defined with respect to the magnetic moment in the magnetic layers. So in case of anti-parallel alignment of the two magnetic layers $g^{\uparrow}$ and $g^{\downarrow}$ have to interchange somewhere in the non-magnetic layer. Also a discrimination is made between electrons traveling upwards ($g_{+}^{\uparrow(\downarrow)}$) and downwards ($g_{-}^{\uparrow(\downarrow)}$) with respect to the z-axis.

The general solution of equation 3.5 for every layer of the spin-valve is

$$g_{\pm}^{\uparrow(\downarrow)}(z,\vec{v}) = e\tau^{\uparrow(\downarrow)}\,\vec{E}\cdot\vec{v}\,\frac{\partial f^0}{\partial \epsilon_n} \times \left[1 + F_{\pm}^{\uparrow(\downarrow)}(\vec{v}) \cdot exp\left(\frac{\mp z}{\tau^{\uparrow(\downarrow)} \mid v_z \mid}\right)\right]. \tag{3.6}$$

The spin-dependent relaxation times $\tau^{\uparrow(\downarrow)}$ are usually expressed in mean free paths using the free electron gas approximation:

$$\lambda^{\uparrow(\downarrow)} = v_F \cdot \tau^{\uparrow(\downarrow)}, \tag{3.7}$$

in which v_F represents the Fermi velocities, assumed equal in all layers. This also implies that diffraction effects that may occur at the interface of materials with different Fermi velocities are neglected. By introducing spin-dependent mean free paths bulk spin-dependent scattering is modelled. The coefficients F have to be determined from boundary conditions at the top and bottom of the total stack of layers and at the interfaces between the different layers. The boundary conditions at the top are

$$g_{-}^{\uparrow(\downarrow)} = R^{\uparrow(\downarrow)} g_{+}^{\uparrow(\downarrow)}, \tag{3.8}$$

and at the bottom

$$g_{+}^{\uparrow(\downarrow)} = R^{\uparrow(\downarrow)} g_{-}^{\uparrow(\downarrow)}, \tag{3.9}$$

with $R^{\uparrow(\downarrow)}$ the spin-dependent fraction of electrons reflecting at the outer interfaces. The fraction which is not reflected is diffusely scattering so that $R^{\uparrow(\downarrow)} + D^{\uparrow(\downarrow)} = 1$. At the interfaces between the layers the following boundary condition can be written for spin-up and spin-down electrons moving from layer B to A in direction $-$:

$$g_{A-}^{\uparrow(\downarrow)} = T^{\uparrow(\downarrow)} g_{B-}^{\uparrow(\downarrow)} + R^{\uparrow(\downarrow)} g_{A+}^{\uparrow(\downarrow)}, \tag{3.10}$$

and from A to B in the direction +:

$$g_{B+}^{\uparrow(\downarrow)} = T^{\uparrow(\downarrow)} g_{A+}^{\uparrow(\downarrow)} + R^{\uparrow(\downarrow)} g_{B-}^{\uparrow(\downarrow)}. \tag{3.11}$$

The fraction which is not reflected is diffusely scattered so that $T^{\uparrow(\downarrow)} + R^{\uparrow(\downarrow)} + D^{\uparrow(\downarrow)} = 1$. All coefficients T,R and D can be spin-dependent and different at all interfaces and boundaries. By introducing spin-dependent boundary conditions interfacial spin-dependent scattering is modelled. Any angular dependence of T and R is neglected.

After equation 3.6 is solved for all layers using the boundary conditions the current density in x-direction can be obtained by integrating the product of v_x and $g(z,\vec{v})$ to $\vec{v}$:

$$j_x(z) = -2e\left(\frac{m}{h}\right)^3 \cdot \sum_{\uparrow,\downarrow}\sum_{+,-} \int g_{\pm}^{\uparrow\downarrow}(z,\vec{v})\, v_x\, d^3v. \tag{3.12}$$

The local conductivity follows from Ohms law $\vec{j} = \sigma\vec{E}$. The sheetconductance G is obtained by integrating $\sigma(z)$ over z. Finally the magnetoresistance (in %) is calculated via

$$MR = 100 \cdot \frac{Gp - Gap}{Gap} = 100 \cdot \frac{Rap - Rp}{Rp}, \tag{3.13}$$

with Gp and Gap the sheet-conductances in case of parallel and anti-parallel alignment of the magnetic moments.

3.3 Camley-Barnas computer program

To calculate the magnetoresistance of spin-valves and multilayers a computer program is used [Heuvel]. This computer program has the following input parameters:

- Configuration of the spin-valve.
- Thicknesses of the different layers in the spin-valve.
- Spin-dependent mean free paths $\lambda^{\uparrow}$ and $\lambda^{\downarrow}$ for every magnetic material to model bulk spin-dependent scattering.
- Spin-independent mean free paths λ for every non-magnetic material.
- Spin-dependent reflection and transmission coefficients R and T at the interfaces of every magnetic/non-magnetic material to model spin-dependent scattering at the interfaces.
- Possibly also spin-independent reflection and transmission at the interfaces of every non-magnetic/non-magnetic material to model spin-independent scattering at the interfaces.

After inserting the configuration of the desired stack of layers this program automatically computes the magnetoresistance. Figures can be plotted of local conductivity $\sigma(z)$, Gp, Gap, ΔG=Gp-Gap and MR. It is also possible to vary the thickness of the different layers.

3.4 Falicov and Hood model for magnetoresistance

In a more realistic model by Falicov and Hood [Fal92], also reflection and transmission coefficients which result from coherent spin-dependent potential scattering are taken into account. Bandstructure and electron-density effects are included by means of constant spin-dependent potentials for each metal. Angular dependent reflection and transmission coefficients are calculated by quantum-mechanical matching of electron wave functions at the interfaces. Impurity scattering at the interfaces and interfacial roughness are also a source of spin-dependent

scattering, and they contribute to MR via a single spin-dependent parameter, in a similar way to that used by Camley and Barnas.

One important feature described by this model is total reflection. Consider the following stack of layers: I/M1/NM/M2/I, in which I is an insulating layer, M1 and M2 are two magnetic layers, and NM is a non-magnetic metal layer (figure 3.2).

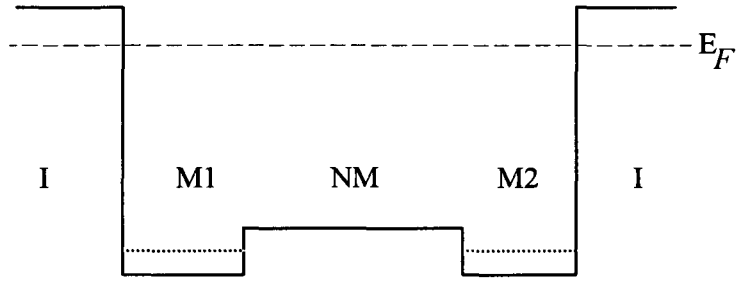

Figure 3.2: *Schematic representation of the potentials of a stack of layers consisting of I/M1/NM/M2/I, with I insulating layers, M1 and M2 ferromagnetic metals (spin-dependent potential = dotted and straight line) and NM a non-magnetic metal.*

Electrons travelling in M1 or M2 face an infinite high potential barrier at the interfaces with I. This results in this model in a reflection coefficient R=1 at this interface, which implies total reflection of electrons. Reflection of electrons may increase the magnetoresistance as we will see in chapter 8.

Chapter 4

Experimental

In this chapter the experimental setup is described. As the main objective of this report is magnetoresistance, the magnetoresistance equipment will be described most elaborated. Magnetization can be measured using a Squid magnetometer and MOKE equipment. A short discription of these techniques is given. X-ray diffraction studies give information about structure and texture of the samples, and therefore this technique is briefly outlined in the last section of this chapter.

4.1 Magnetoresistance measurements

All magnetoresistance measurements are performed with a standard four point contact method. The temperature can be varied standard between 10 K and 350 K using a flow cryostat. Liquid helium is used for cooling. In figure 4.1 a schematic overview of the measurement equipment is drawn. Magnetic fields up to 1.35 T can be applied.

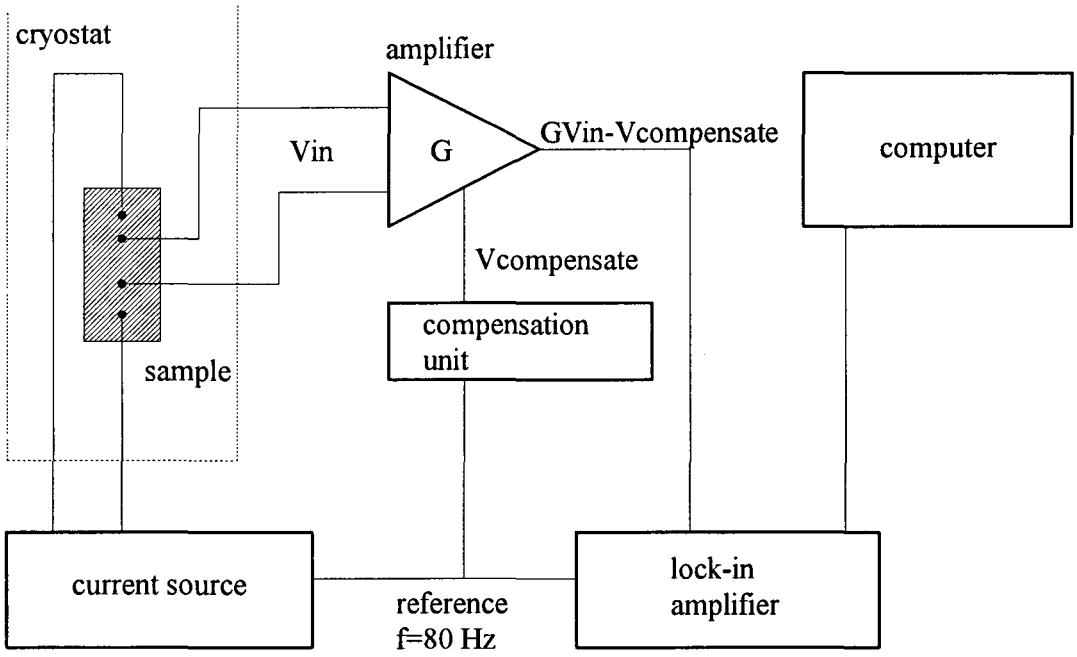

Figure 4.1: Schematic overview of the measurement equipment.

The equipment used to measure the resistance as a function of the applied magnetic field (magnetoresistance) works as follows. Two pressure contacts on the sample act as a current

lead, while two other contacts measure the voltage Vin. The resistance is simply determined by ohms law $R = Vin/I$. An alternating current (80 Hz) is used to measure Vin with a lock in amplifier to filter out unwanted noise. The measured alternating voltage is amplified (100 or 1000 times), and substracted with a compensation voltage with the same phase and frequency. The amplitude of the compensation voltage $V_{compensate}$ can be adjusted to the same amplitude as the measured voltage Vin, so that changes in resistance can be measured as a deviation from zero voltage. This makes it possible to operate the lock-in amplifier at a highly sensitive level.

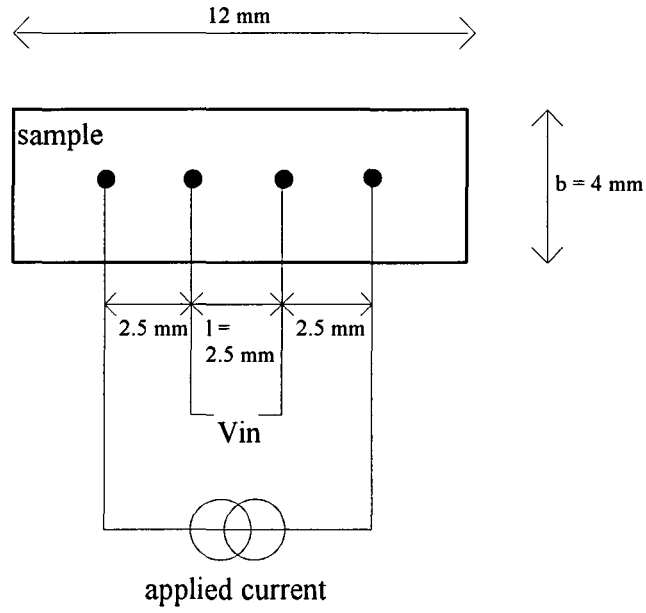

Figure 4.2: *Four point contact geometry used to apply a current and measure the voltage. The samples are rectangular (dimensions 12 × 4 mm²). The black dots represent four pressure contacts.*

Our four point pressure contacts have the geometry of figure 4.2. We have satisfied the conditions, which are required for this measuring geometry: The point contacts are far from any of the outer boundaries of the sample so that it may be considered to be an infinite area of uniform resistivity. The diameter of the contacts is small with respect to the distance between the contacts l.

In the limit of sample thickness much smaller than the distance between the contact ($h \ll l$), the sample may be considered as essentially two-dimensional [Wied79, Qian]. The relationship between conductivity σ and measured resistance R then reduces to

$$R = \frac{l}{bh\sigma}, \tag{4.1}$$

with l the distance between the two voltage contacts (2.5 mm), b the width of the sample (4 mm) and h the thickness of the sample. To allow comparison between measurements using different sample sizes or contact configurations, the measured resistance is normalized to the resistance that would be obtained for a square sample with a homegeneous current distribution. The so-called sheetresistance is defined as

$$R_s = \frac{b}{l} \cdot R = \frac{b}{l} \cdot \frac{l}{bh\sigma} = \frac{1}{h\sigma} = \frac{1}{G_s}, \tag{4.2}$$

with G_s the sheet conducitivity.

The magnetoresistance can be measured within certain accuracy limits which are determined by errors in the applied current, the measured voltage, the distance between contacts l and the temperature. We estimate the magnetoresistance to be accurate within 5%.

4.2 Magnetization measurements

For the magnetic characterization of our samples one of the tools we use, is measurement of the magnetization of the samples. Information can be obtained about the degree of anti-parallel alignment and the characteristic fields at which changes in alignment take place.

4.2.1 Squid measurements

A way of determining the magnetization of a stack of magnetic layers as a function of an applied magnetic field, is using a squid magnetometer. Squid stands for *superconducting quantum interference device*. The squid makes use of superconducting pick up coils to measure the total magnetic moment of a sample. In the Squid used in the cooperative phenomena group fields up to 5 Tesla can be applied to the sample. Measurements can be done at temperatures ranging from 1.7 K up to 400 K. For more information about the Squid magnetometer see [Bong95].

4.2.2 MOKE measurements

Another way to measure the magnetization of a stack of magnetic layers as a function of an applied field is MOKE. The Magneto Optical Kerr Effect (MOKE) is the effect that a linearly polarized laserbeam reflected of a magnetic material changes its polarization. This change in polarization is proportional to the magnetization of the material. The change in polarization can be a rotation of the polarization axis (kerr rotation) or a change from linearly to elliptically polarized (kerr ellipticity). As the spot of a laserbeam can be very small (typical 0.1 mm diameter), MOKE is a local technique. Information about magnetization is limited to the penetration depth of the laserbeam in the sample. For more information about the MOKE measurement apparatus in the cooperative phenomena group see [Haar94, Land95].

4.3 X-ray diffraction

The determine the texture of our samples we make use of X-ray diffraction measurements (XRD). The standard θ-2θ geometry of such a measurement is schematically drawn in figure

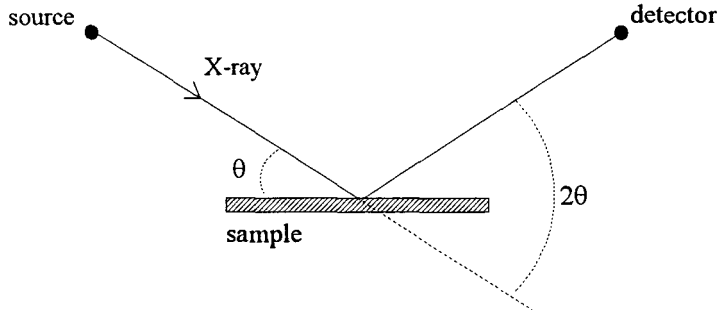

Figure 4.3: *Schematic representation of standard θ-2θ X-ray diffraction measurement.*

4.3. The sample is exposed to X-rays emitted by a Cu source (λ=1.541 and λ=1.544) under an angle θ. The reflected X-rays are detected under an angle 2θ with the incoming X-ray beam. Constructive interference takes place if x-rays, reflected at different crystal planes, at different layer interfaces or at the bottom and top of the sample, match the Bragg-rule [Kit86]

$$2d\,sin(\theta) = n\lambda \quad (n = 1, 2, 3, ...), \tag{4.3}$$

with d the distance between following crystal planes, interfaces or the thickness of the total sample. This constructive interference shows up as a peak in a θ-2θ scan. So information about crystal orientation, lattice constants, multilayer period and thickness of a sample can be obtained by analyzing peaks in a θ-2θ scan.

Another geometry with X-ray diffraction is to fix the source and detector at a certain angle at which constructive interference occurs at crystal planes. Then the sample is turned over a small angle Ω. The width of this so-called rocking-curve is a measure for spread in the orientation of the crystallites.

Chapter 5

Spin-valve design

In the first part of this chapter the sample preparation technique is discussed. The second part treats the general sample design, which we will use to obtain anti-parallel alignment of the layer magnetic moments in our spin-valves. Three ways of achieving anti-parallel alignment are discussed: antiferromagnetic coupling, coupling to a third magnetic layer and exchange biasing to an antiferromagnet together with an increase of coercive field.

5.1 HV magnetron sputtering

The samples described in this report are mainly produced using a technique called High Vacuum (HV) magnetron sputtering. In this sputtering process material is dislodged and ejected from a surface of a target due to bombardment by energetic particles. The material of the target evaporizes and condenses on a substrate (glass, Si, SiO_2), forming a thin film. The bombarding particles are ions of an inert gas (Ar) to avoid chemical reactions at target and substrate. The Ar plasma is confined above the target by a magnetic field and is generated by a large DC or AC voltage between the target and a nearby metallic plate (magnetron). Figure 5.1 shows a schematic representation of the main parts of the sputtering apparatus.

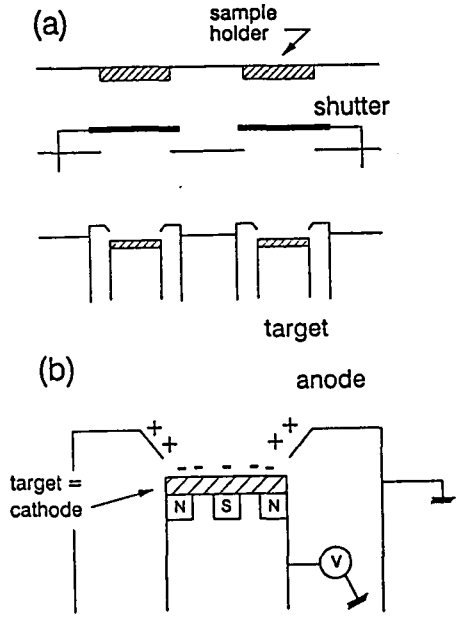

Figure 5.1: *Schematic representation of the main parts of the sputtering apparatus with (a) targets, shutters and sample holders , and (b) a detailed layout of the target (figure from [Bloem]).*

Our samples have been sputtered at Philips Research Laboratories in Eindhoven. The sputtering apparatus used has a background pressure in the order of 10^{-7} Torr, while the Ar pressure during deposition is in the order of 10^{-3} Torr. Growth rates are in the order of typical 1 or 2 Å/s. Samples are grown in deposition runs of 10 samples. The sputtering machine has three targets. Between targets and substrate computer controlled shutters are placed. These shutters determine which target material the substrate is exposed to. It is possible to apply a magnetic field during deposition, which however reduces the number of samples possible to grow in one run to 6 due to lack of space.

5.2 General sample design

The main sample design consists of two magnetic layers *M1* and *M2*, separated by a non-magnetic layer *NM*, which forms the spin-valve *M1/NM/M2* as schematically shown in figure 5.2. Next there must be some means to switch between anti-parallel and parallel alignment

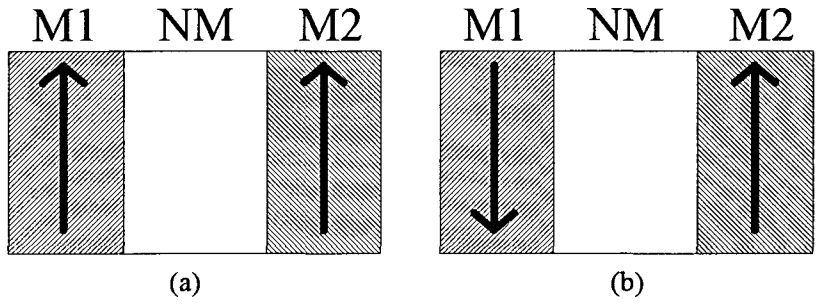

Figure 5.2: *Drawing of the main sample design. Two magnetic layers M1 and M2, separated by a non-magnetic layer NM in case of (a) parallel magnetic moments and (b) anti-parallel magnetic moments.*

of the magnetic moments of the layers *M1* and *M2*. This can be done in different ways, which we will discuss in the following sections. All manners have in common that we can switch between anti-parallel and parallel alignment by applying a magnetic field.

5.2.1 Antiferromagnetic coupling

A first way to achieve anti-parallel alignment of the two magnetic moments *M1* and *M2* is to make use of antiferromagnetic coupling between the two layers. In 1986 it was discovered that certain magnetic layers separated by a non-magnetic layer show antiferromagnetic coupling [Grün86]. This means that the two magnetic moments of the magnetic layers align anti-parallel at certain small thicknesses of the non-magnetic spacer layer. The coupling oscillates between antiferromagnetic and ferromagnetic as a function of the non-magnetic layer thickness. The antiferromagnetic coupling can be overcome by applying a magnetic field which will force the magnetic moments to align parallel. So by choosing an appropriate thickness of the non-magnetic spacer *NM*, the magnetic moments will align anti-parallel in zero field and parallel in an applied magnetic field. Figure 5.3 shows theoretical magnetization curves of two coupled magnetic layers. Layers which shows antiferromagnetic coupling are for example Co/Cu/Co, Co/Ru/Co and Fe/Cr/Fe. Detailed information about coupling can be found in [Bloem].

This way of achieving anti-parallel alignment has the disadvantage that any change of the structure (thickness of the layers, interface roughness) affects the anti-parallel alignment of the spin-valve.

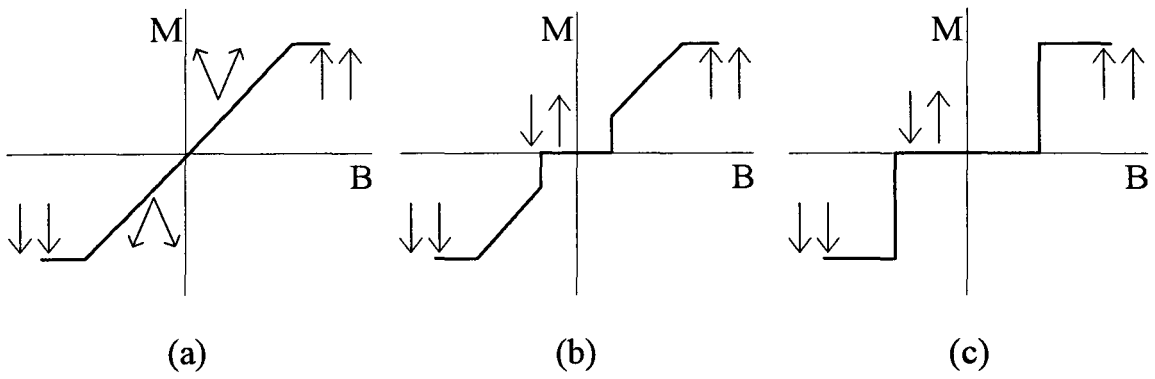

Figure 5.3: *Theoretical magnetization curves (minimum energy calculations) of two identical antiferromagnetically coupled layers having uniaxial anisotropy, which is (a) zero, (b) smaller than the coupling strength and (c) stronger than the coupling strength.*

5.2.2 Coupling to a third magnetic layer

Another manner to obtain anti-parallel alignment is to couple magnetic layer *M2* antiferromagnetically to a third magnetic layer *M3* with a larger magnetic moment (thicker layer). The stack of layers consists then basically of two parts. One part which is antiferromagnetically coupled, with the composition: *M3/NM*/M2*, and one part which is not coupled: *M2/NM/M1*. Figure 5.4 shows schematically the composition of such a stack of layers and a theoretical magnetization curve. The magnetization curve can be understood as follows.

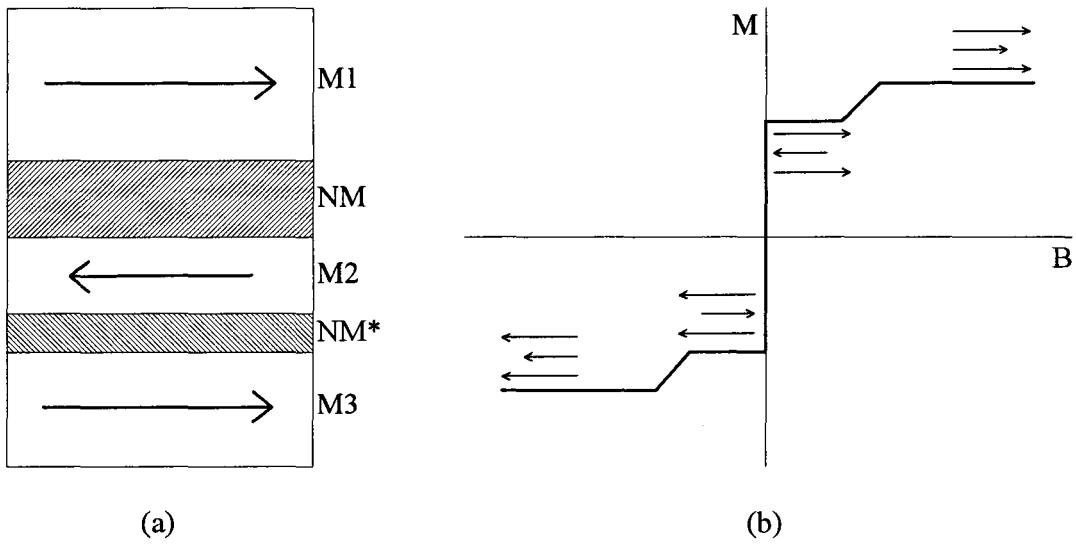

Figure 5.4: *(a) Stack of layers consisting of the spin-valve M1/NM/M2 in which anti-parallel alignment is obtained via coupling with M3. (b) theoretical magnetization curve of such a stack of layers.*

Layer *M1* is a free layer and will always align parallel to the applied field. Layer *M2* is antiferromagnetically coupled to layer *M3*, which causes layer *M2* to align opposite to layer *M3* in low fields. As layer *M3* has the larger moment of the *M2* and *M3*, this layer will align to the applied field. At higher fields the coupling strength is overcome and all magnetic moments will align parallel to the field.

A possible configuration for the stack of layers is Co/Ru/Co/Cu/Co. In this configuration Co/Ru/Co is the part in which the Co layers are coupled. Co/Ru/Co will also form a spin-valve but as the magnetoresistance of Co/Ru/Co is small (≈0.2%), this will be a constant and small background contribution. The actual spin-valve is Co/Cu/Co, with a large magnetoresistance (up to 6%). Now it is possible to change parts of the Co/Cu/Co spin-valve without affecting the coupling strength.

5.2.3 Exchange biasing and coercive field

A third manner to obtain antiferromagnetic orientation is exchange biasing. Exchange biasing is the effect that an antiferromagnetic layer, which adjoins a ferromagnetic layer, tends this ferromagnetic layer to align in one direction. This pinning of the ferromagnetic layer can be overcome by applying a magnetic field. The exchange biasing is often expressed in a exchange biasing field *Hex* over which the magnetization curve is shifted (see also figure 5.5). A spin-valve based on this effect may have the following composition: *AFM/M2/NM/M1*, in which *AFM* represents the antiferromagnetic layer. The exchange biasing effect induced by layer AFM is often accompanied by an increase in coercive field (*Hc*) of layer *M2*. This means that layer *M2* has a large hysteresis in magnetization when sweeping an applied field. Figure 5.5 shows the general structure of a spin-valve based on exchange biasing and its parts together with theoretical magnetization curves. As one can see in the figure both exchange biasing field *Hex* as coercive field *Hc* help to achieve anti-parallel alignment.

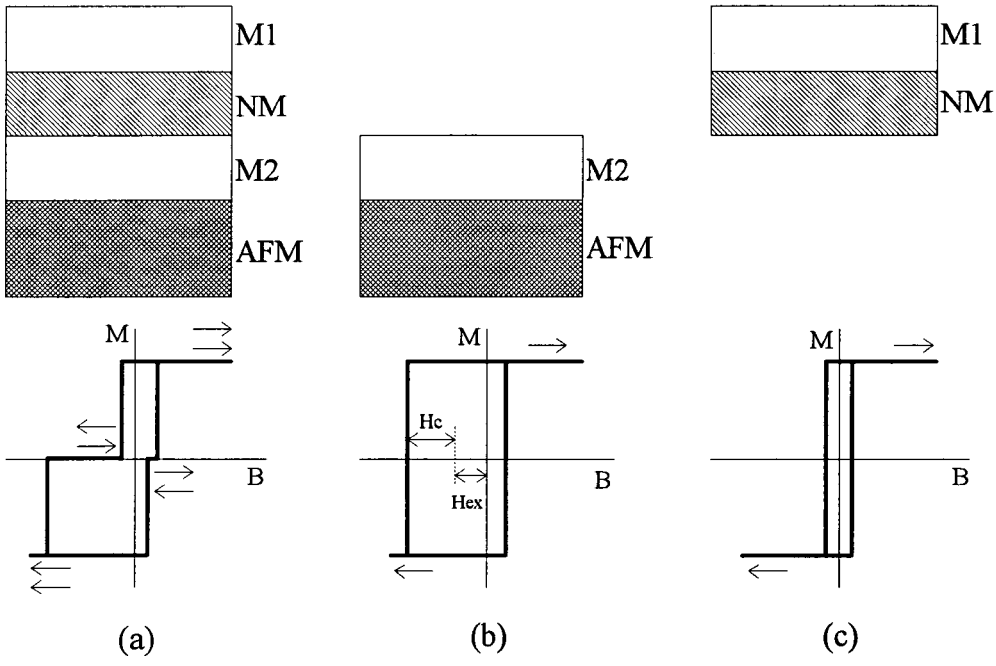

Figure 5.5: *Schematic representation and theoretical magnetization curves of (a) spin-valve AFM/M2/NM/M1, based on exchange biasing, and its individual parts (b) AFM/M2 and (c) M1. The coercive field and exchange biasing field are called Hc and Hex respectively.*

Antiferromagnets which are suitable for exchange biasing are for example *FeMn* and *NiO*. It is necessary to grow to spin-valve structure in a magnetic field to define the pinning direction. As the two magnetic layers *M1* and *M2* are not coupled, it is again possible to change parts of the spin-valve without affecting the degree of anti-parallel alignment.

Chapter 6

Co/Ru and Co/Cu interface scattering

In this chapter measurements are presented on Co/Cu-based spin-valves. We have changed the interfaces by adding thin Ru layers at the interfaces of Co and Cu in the spin-valve. This is done to investigate the role of the Co/Cu and Co/Ru interfaces in the magnetoresistance.

6.1 Motivation

To gain insight in the role and amount of interfacial spin-dependent scattering, a known strategy is to insert thin layers of a third material at the interfaces in ferromagnetic/non-magnetic/ ferromagnetic spin-valves or multilayers (see also section 2.2.1). Adding a third element at the interface changes the type of impurities localized around this interface, which might affect the size of spin-dependent interface impurity scattering.

In this contribution, we have inserted thin Ru layers at the interfaces of uncoupled Co/Cu/Co spin-valves. In contrary to other studies, we also introduced thin Ru layers in the middle of the Cu spacer layer to correct the measurements for the higher resisitivity of the Ru layers with respect to Cu and a larger thickness of the non-magnetic spacer layer. More precisely, we hope to gain insight in the role of the Co/Ru interfaces in the magnetoresistance with respect to Co/Cu interfaces.

6.2 Sample design

The reference sample consists of a SiO_2 substrate (dimensions : 12×4 mm^2) on top of which the following structure was deposited: 200 Å Ru + 75 Å Co + 6 Å Ru + 25 Å Co + 30 Å Cu + 100 Å Co + 10 Å Cu + 30 Å Ru. The 6 Å Ru layer antiferromagnetically couples the 75 Å Co layer to the 25 Å Co layer. The 30 Å thick Cu spacer layer is taken thick enough to ensure that there is no interlayer coupling between the 25 Å Co layer and the 100 Å Co layer. So anti-parallel alignment in the spin-valve is obtained as described in section 5.2.2. Now we have created a Co/Cu/Co spin-valve in which the anti-parallel orientation of the magnetizations does not depend on interlayer coupling across the Cu spacer layer. Spin-valves based on antiferromagnetically coupled layers are not suitable for investigation of the role of the interface in the magnetoresistance effect, because adding impurities at the interface will change the coupling strength which will affect the magnetoresistance as well [Hon94]. Further we note that the 75 Å Co + 6 Å Ru + 25 Å Co also forms a spin-valve. The magnetoresistance of this spin-valve however is small in comparison to the Co/Cu/Co spin-valve (see section 6.5).

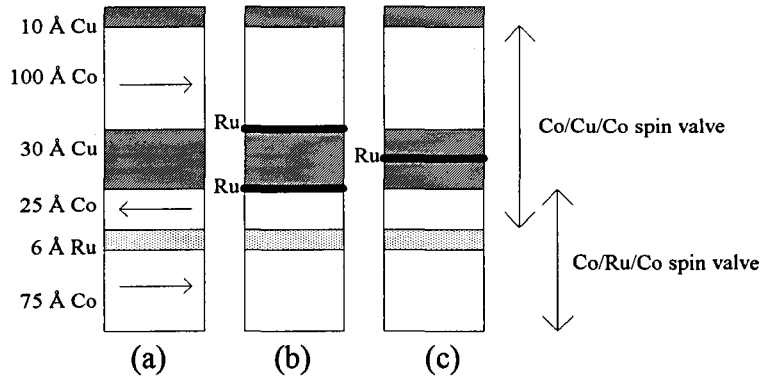

Figure 6.1: *Schematic representation of the samples. The 200 Å Ru base layer and the 30 Å top layer are not drawn. Drawing (a) shows the reference sample, (b) and (c) show the positions of the thin Ru layers at the Co/Cu interfaces and in the Cu spacer layer respectively.*

We will now investigate the influence of a thin Ru layer at the Co/Cu interface and in the Cu spacer layer. Figure 6.1 shows schematically the sample design. In appendix A a complete list of the samples is given. The sample numbers are 941095...9410101 and 9411177...9411186.

6.3 Magnetic characterization

As a difference in magnetic behaviour affects the magnetoresistance as well, we have measured the magnetization of two samples with Ru at the interface and in the middle of the Cu spacer layer. Figure 6.2 shows the magnetization curves of sample number 941097 and 9410100. Sample number 941097 has the configuration of figure 6.1.b with a Ru layer thickness of 4 Å. Sample number 9410100 has the configuration of figure 6.1.c with a Ru layer thickness of 8 Å. These magnetization measurements are obtained using the squid magnetometer.

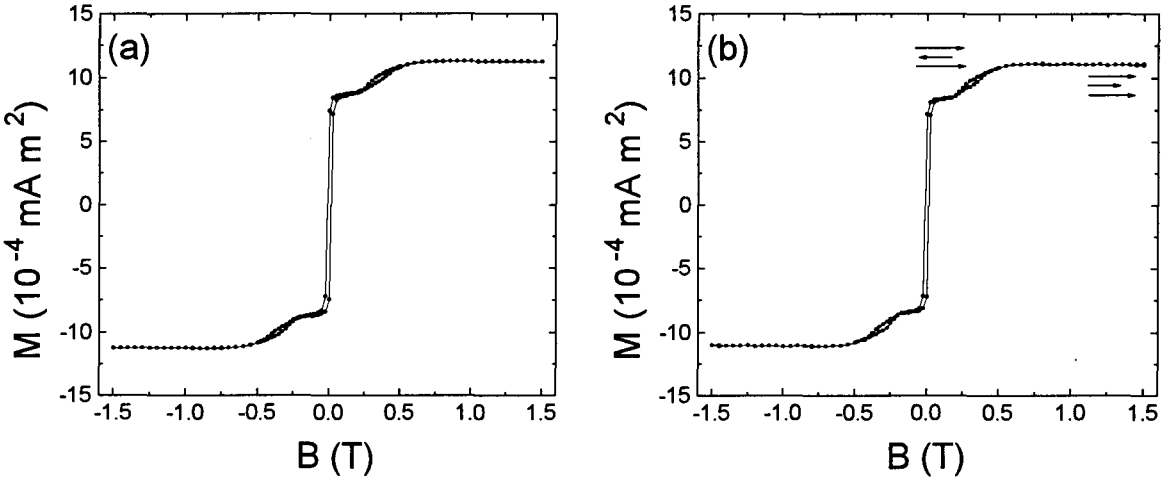

Figure 6.2: *Magnetization curves of (a) sample number 941097, and (b) sample number 9410100. The arrows indicate the directions of the three magnetic Co layers. The measurement temperature was T=10 K. The applied field was in the plane of the sample.*

Both magnetization curves are almost identical and in agreement with the theoretical curve as showed in figure 5.4. At fields between -0.25 T and 0.25 T the 25 Å Co layer is

aligned anti-parallel to the 75 Å Co and the 100 Å Co layer. At higher fields the field energy will overcome the coupling energy, so that at fields higher than 0.5 T and lower than -0.5 T all three magnetizations will align in the direction of the applied field. In the region between 0.25 T and 0.5 T, and in the region between -0.25 T and -0.5 T, a transition from an anti-parallel configuration to a parallel configuration occurs. The ratio of total magnetic moments in parallel and anti-parallel configuration is in proportion with the ratio of the corresponding Co layer thicknesses in parallel and anti-parallel configuration. This, together with a clear plateau in both magnetization curves, is an indication for a good and equal anti-parallel alignment of the magnetic moments in low fields.

6.4 X-ray diffraction measurements

Figure 6.3 shows the wide angle x-ray diffraction patterns of various samples with a thin Ru layer both in the Cu spacer layer and at the interface of the Cu spacer layer with the magnetic Co layers. All patterns are similar in peak position and in peak height. Two peaks can be

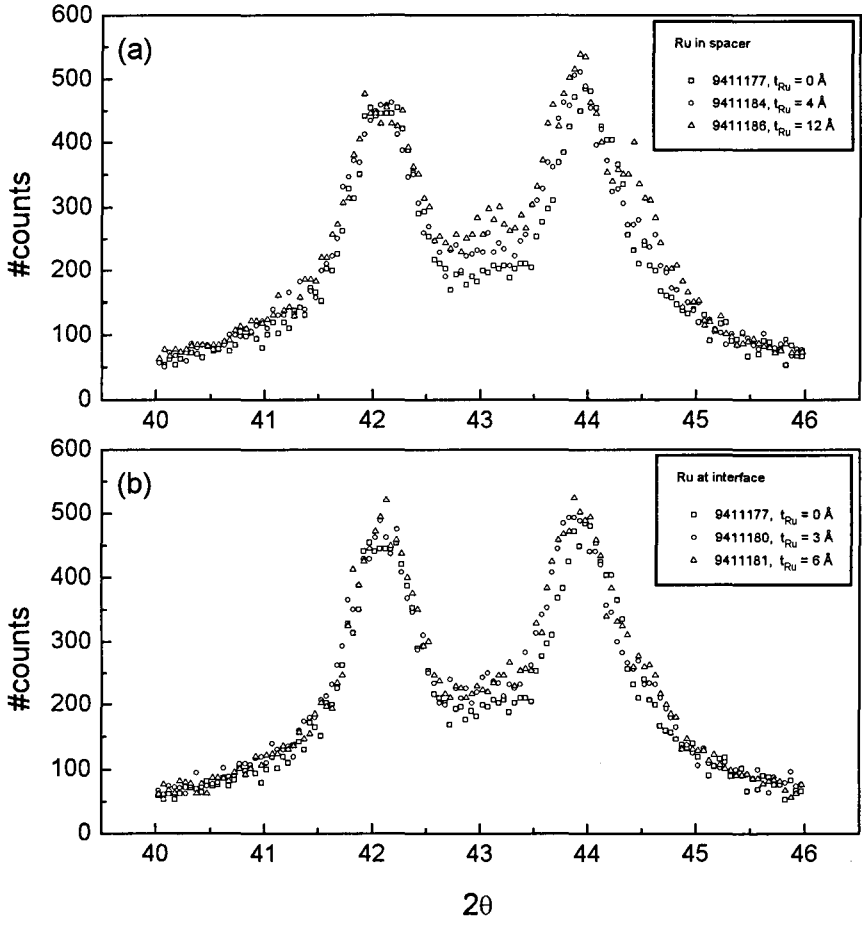

Figure 6.3: *Wide angle X-ray diffraction patterns of (a) sample numbers 9411177, 9411184 and 9411186 with t Å Ru in the Cu spacer layer, and (b) sample numbers 9411177,9411180 and 9411181 with t Å Ru at the two Co/Cu interfaces.*

distinguished. One peak at approximately 2θ=42°, which corresponds to Ru in the hcp phase in (002) direction with an expected peak position of 2θ=42.15°. As this peak also appears in sample number 9411177, in which only a Ru base layer and a Ru top layer is present, this peak can be attributed to this base layer and top layer. So it can be concluded that Ru mainly

grows in the hcp phase. A second peak appears at about 2θ=44°, which corresponds to Co in the fcc phase in (111) direction with an expected peak position of 2θ=44.1°. A third peak is expected at 2θ=43.2° corresponding to Cu in fcc growth in (111) direction. No clear peak at this position can be distinguished. However, this peak might be blurred by the broad Ru and Co peaks. Moreover, there's only 40 Å Cu in the layers in contrast to 200 Å Co and 236 Å Ru.

It can be concluded that thin Ru layers in the spin-valve structure do not influence the predominantly (111) texture of the spin-valve.

6.5 Magnetoresistance

The reference spin-valve system is known to have about 6% magnetoresistance. We have added thin Ru layers at the interfaces of Co and Cu (figure 6.1.b). As Ru is highly resistive this will automatically lead to a decrease in MR. To filter out the interface effect, the Ru layer is also introduced in the middle of the Cu spacer layer. The Ru in the spacer layer is twice as thick as the Ru at the interface, so that the total Ru thickness is the same. Then we hope it is possible to correct the measurements for the extra resistivity and spin-independent scattering at the Ru/Cu interfaces.

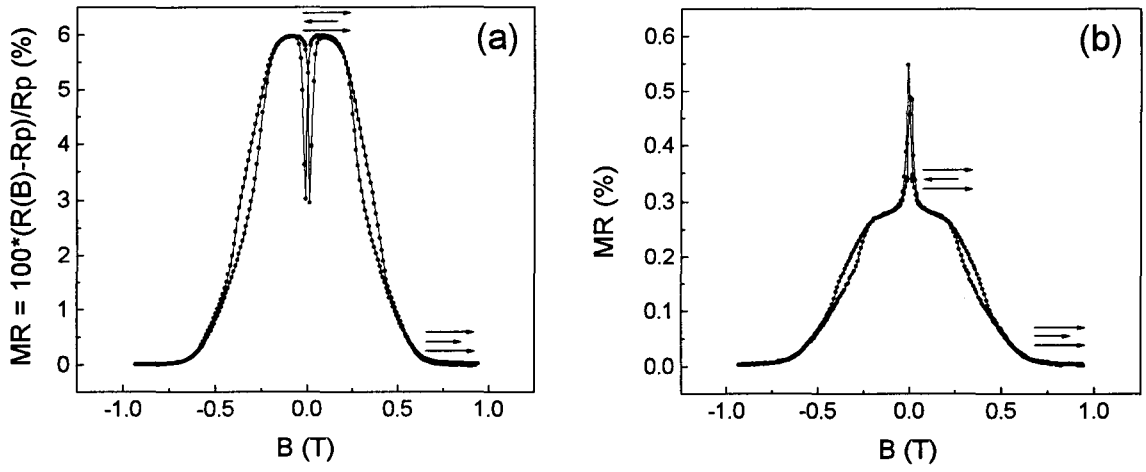

Figure 6.4: *Magnetoresistance as a function of the applied field of (a) sample number 9411177 and (b) sample number 9411178. The temperature during measurement was 10K. The relative orientation of the magnetic moments is indicated by arrows.*

Figure 6.4 shows the magnetoresistance of the reference sample (sample number 9411177) and sample number 9411178, which has the composition of figure 6.1.b with a Ru thickness of 1 Å. Reference sample number 9411177 has a magnetoresistance of 6%, as defined by the relative change in resistance between anti-parallel and parallel orientations of the magnetic moments in the spin-valve which show up as plateaus and are indicated by arrows in figure 6.4. Inserting a 1 Å thick Ru layer at the interface of Co and Cu results in a decrease in magnetoresistance to 0.28%.

As the magnetic moments change direction at zero applied field, two side effects influence the magnetoresistance versus field curve. At zero applied field there is no complete antiferromagnetic alignment, because no preferential direction is given by an applied field. This leads to a decrease in magnetoresistance. The second effect, is the anisotropic magnetoresistance: when magnetic moment and current through a magnetic layer are parallel the resistance is higher than when magnetic moment and current are perpendicular with respect

to each other. The magnetic moments of the Co layers are perpendicular to the current in high fields, but in reversing their direction they pass a state in which the magnetic moments are parallel to the current. This leads to an increase in magnetoresistance at zero applied field. The anisotropic magnetoresistance in Co is in the order of 1% [Viret]. In sample number 9411178 this anisotropic magnetoresistance effect dominates, leading to an increase in magnetoresistance at zero field (upwards peak). In sample number 9411177 the effect of incomplete antiferromagnetic alignment dominates the anisotropic magnetoresistance, which leads to a decrease in magnetoresistance at zero field (downwards peak).

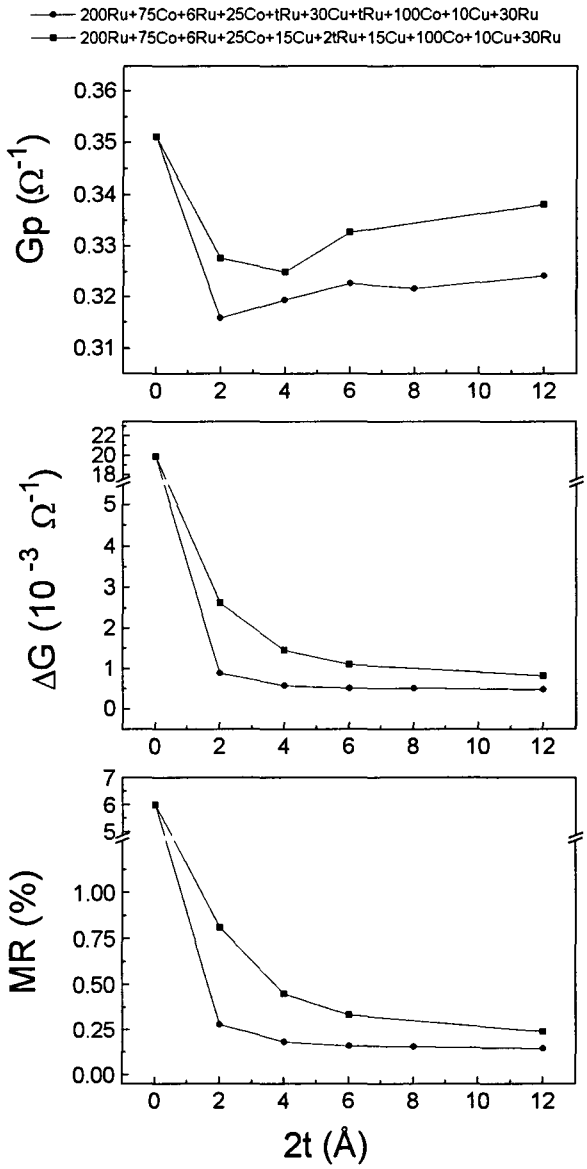

Figure 6.5: *MR, ΔG and Gp as a function of the total thickness of the inserted thin Ru layers. The sample numbers are 9411177...9411186.*

Now we concentrate again on the giant magnetoresistance effect which was defined as the relative resistance change between parallel and anti-parallel orientation (plateaus in MR versus field curves) of the magnetic moments in the spin-valve. Figure 6.5 shows the magnetoresistance, ΔG=Gp-Gap and Gp as a function of the total thickness of the thin inserted Ru layers both at the interface and in the middle of the spacer layer. Gp decreases about 10% when the Ru is introduced in the spin-valve. This can be explained by the fact that

electrons find their mean free path resticted by the resistive Ru layer. MR and ΔG decrease as a function of the Ru layer thickness. In the case of Ru in the spacer layer, however, the magnetoresistance and ΔG remain higher than in the case of Ru at the Co/Cu interfaces. A Ru layer thickness of 1 Å at both interfaces leads to a magnetoresistance of 0.28%, whereas a Ru layer thickness of 2 Å in the spacer layer leads to a magnetoresistance of 0.82%.

Summarizing the results as obtained so far, we have seen that adding Ru layers has no influence on the magnetic behaviour of the samples (section 6.3). Also, no change in structure or texture was observed in high angle x-ray diffraction measurements (section 6.4). We therefore search for an explanation of the magnetoresistance and ΔG behaviour in the resistivity of the extra Ru layers and the character of the Co/Ru and the Co/Cu interfaces.

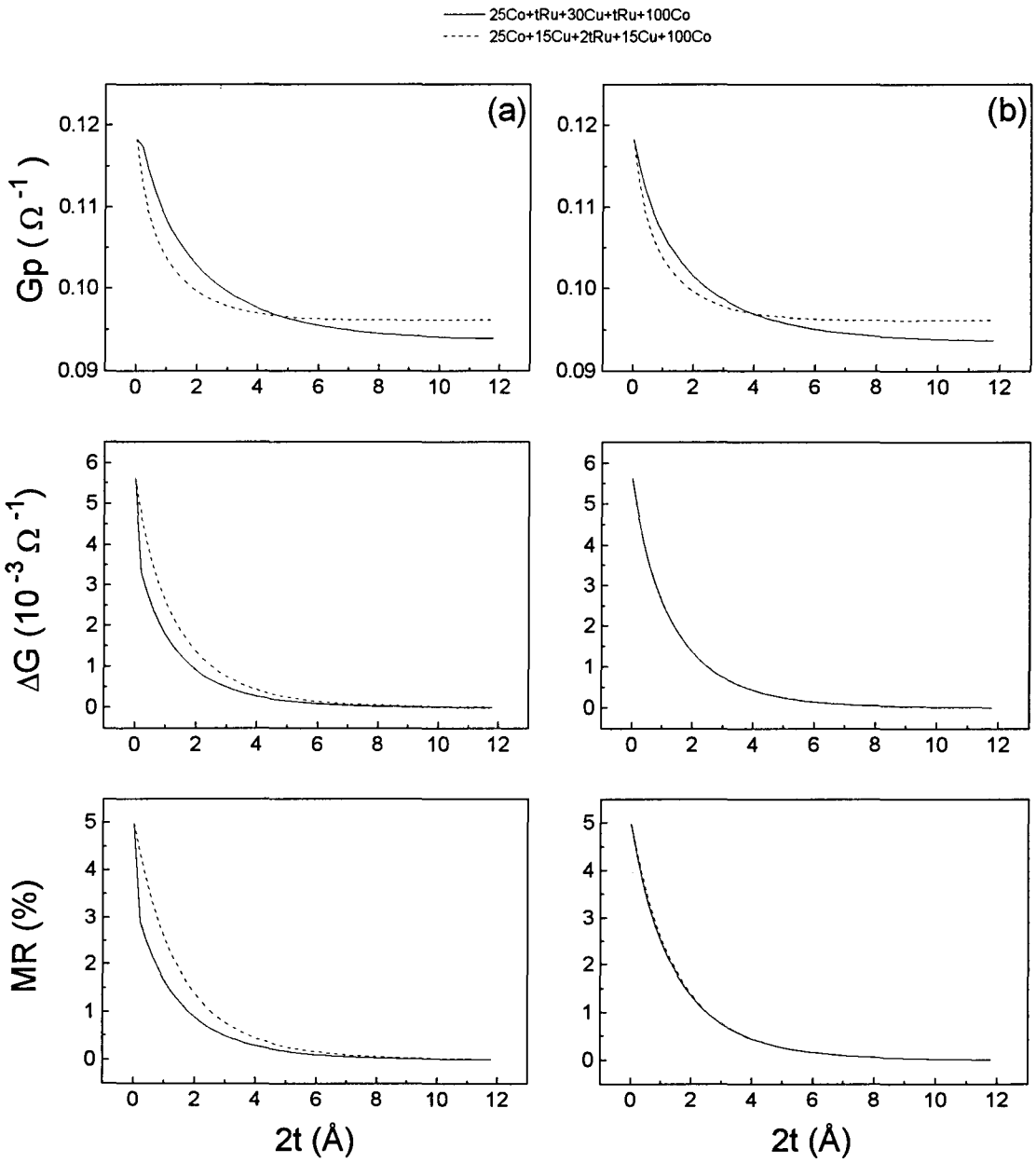

Figure 6.6: *Simulations of two model spin-valves with (a) no interface scattering at Co/Ru interfaces and (b) equal interface scattering assymetry at Co/Ru as at Co/Cu interfaces. The parameters used in the model are listed in the text.*

As Ru is highly resistive, adding Ru between the two Co layers makes it difficult for electrons to cross the spacer layer. The magnetoresistance drops, because in order to contribute to the magnetoresistance electrons must cross the spacer layer. We will see, however, in the following that this cannot explain the difference in MR between Ru at the interface and in the middle.

If we consider the number of interfaces in the reference sample as schematically drawn in figure 6.1.a, we see that there are two Co/Cu interfaces which are involved in the magnetoresistance. In the samples with Ru at these Co/Cu interfaces (figure 6.1.b), there are two Co/Ru and two Cu/Ru interfaces. In the samples with Ru in the middle of the Cu spacer layer (figure 6.1.c), there are two Co/Cu and two Cu/Ru interfaces involved in the magnetoresistance. So the difference between Ru at the interfaces or in the middle of the spacer layer is two Co/Ru interfaces instead of two Co/Cu interfaces. This proofs that the difference in magnetoresistance can be attributed to the different characteristics of a Co/Ru interface compared to a Co/Cu interface.

To substantiate this provisional conclusion we performed model calculations with the help of the Camley-Barnas theory of magnetoresistance. To make the interpretation more transparent, we used two simplified model spin-valves. The first was a spin-valve with Ru at the Co/Cu interface : 25 Å Co + t Ru + 30 Å Cu + t Ru + 100 Å Co. The second was a spin-valve with Ru in the spacer layer : 25 Å Co + 15 Å Cu + 2t Ru + 15 Å Cu + 100 Å Co. Our goal was not to make an exact fit of the measurements, but rather to gain insight in the role of the Co/Ru and Co/Cu interfaces. Therefore we inserted parameters in the model which seem to be reasonable from literature [Dien93, Frei93]. The parameters inserted in the model are: λ_{Cu}=200 Å, λ_{Ru}=3 Å, $\lambda^{\uparrow}_{Co}$=90 Å, $\lambda^{\downarrow}_{Co}$=10 Å, $T^{\uparrow}_{Co/Cu}$=1, and $T^{\downarrow}_{Co/Cu}$=0.2. Additionally we assumed a lower scattering assymetry for the Co/Ru interfaces than for the Co/Cu interfaces (for illustration the extreme values $T^{\uparrow}_{Co/Ru}$=1 and $T^{\downarrow}_{Co/Ru}$=1). The result of these calculations is shown in figure 6.6.a in which the dashed line represents Ru in the middle and the solid line Ru at the interfaces. In qualitative agreement with the measurements we see that Gp decreases as the Ru layer is introduced. Both ΔG and MR decrease and are higher in the case of Ru in the middle than with Ru at the interfaces, in agreement with the experiment.

To make clear that the difference in ΔG and MR is purely and interface effect and no consequence of the position of the Ru layers in the spacer, Gp, ΔG and MR are also calculated using $T^{\uparrow}_{Co/Ru}$=1 and $T^{\downarrow}_{Co/Ru}$=0.2, the same scattering assymetry as the Co/Cu interface. No difference in ΔG and MR is observed (figure 6.6.b). This also is a direct consequence of the equal total Ru thicknesses in both Ru at the interfaces and in the middle of the spacer layer.

6.6 Conclusions and discussion

We have added thin Ru layers in Co/Cu spin-valves at the Co/Cu interfaces and in the middle of the Cu spacer layer as schematically drawn in figure 6.1. Adding thin Ru layers has no influence on the degree of anti-parallel alignment of the Co layers in the spin-valve. No change in structure or texture could be observed in high angle x-ray diffraction measurements.

Adding 1 Å Ru at the interface of Co and Cu reduces the magnetoresistance from 6% to 0.28%. From this abrupt decrease it directly follows that the Co/Cu interfaces play a key role in the magnetoresistance effect in Co/Cu spin-valves and must have a significant scattering assymetry.

The magnetoresistance with Ru at the interfaces is lower than with Ru in the middle of the spacer layer. This difference observed, can be described qualitatively using the Camley-Barnas model in which it is assumed that a Co/Ru interface has a lower scattering assymetry ($T^{\uparrow}/T^{\downarrow}$) than a Co/Cu interface. This seems to be at variance with the reported ratio of the subband resistivities $\rho^{\downarrow}/\rho^{\uparrow}$=0.22 for Ru impurities in Co [Fert82], which is often used as a

measure for the scattering assymetry at the interface (see chapter 2). The relation between magnetoresistance and the ratio of the subband resistivities, however, is not fully understood and must therefore be investigated both theoretically and experimentally in future.

A possible explanation for a low or negligible scattering assymetry might be a reduced moment of Co, which is probably intermixed with Ru at the interfaces. Bloemen reported strongly reduced moments of Co at Co/Ru interfaces [Bloem]. Moreover, from the Co-Ru phase diagram it is clear that above 34% Ru, Co looses its moment.

The relative large lattice mismatch between Co and Ru ($\approx$ 8%) may also cause extra spin-independent scattering ($T^{\uparrow}_{Co/Ru}$ and $T^{\downarrow}_{Co/Ru} < 1$), which might further lower the magnetoresistance in the case of Ru at the interfaces.

Chapter 7

Determination of scattering lengths in Co and Cu

*In this chapter calculations and measurements are presented on Co/Cu/**Co** and Co/Cu/Co/**Cu** spin-valves with a Ru barrier layer shifted through **Co** and **Cu** respectively. We calculated under what condition these experiments can be used to extract the longest of the mean free paths in **Co** and **Cu**. Finally, λ^{long} is compared with the conductivity to see if decisive evidence about the role of bulk spin-dependent scattering can be found.*

7.1 Introduction

The research on giant magnetoresistance in magnetic metallic multilayers is to a great extend devoted to the origin of spin-dependent scattering, in the bulk or at the interfaces of the magnetic layers. Recently, it was suggested that the shift of a highly resistive thin Ru barrier layer through one of the magnetic consistuents of a spin-valve sandwich creates a flexible tool to extract the longest of the mean free path ($\lambda^{long} = \lambda^{\uparrow}$) within the magnetic layer [Par94]. In the next sections we present calculations and measurements on Co/Cu/**Co** spin-valves with a Ru layer shifted through **Co** and Co/Cu/Co/**Cu** spin-valves with a Ru layer shifted through **Cu**. Calculations with the Camley-Barnas model are focused on the conditions under which these experiments can be used to extract λ^{long} of Co and Cu respectively. Magnetoresistance measurements are done at seven different temperatures, ranging from 10 K to 300 K, from which λ^{long} could be extracted. Finally we compare λ^{long} with the bulk conductivity for both Co and Cu ($\propto \lambda^{long} + \lambda^{short}$) to see if decisive evidence for bulk spin-dependent scattering can be found.

7.2 Long scattering lengths in Co

7.2.1 Spin-valve design

The samples we have used to determine the long scattering lengths in Co have the following composition: 200 Å Ru + 75 Å Co + 6 Å Ru + 25 Å Co + 30 Å Cu + t Co + 2 Å Ru + (250-t) Co + 30 Å Ru. The position of the 2 Å Ru layer t ranges between 0 and 250 Å. Anti-parallel alignment of the Co/Cu spin-valve is obtained via antiferromagnetic coupling of the 25 Å Co layer across 6 Å Ru, as described in section 5.2. A schematic view of the samples used is given in figure 7.1. The free Co layer of the Co/Cu spin-valve is 250 Å thick, but divided in two parts by a 2 Å Ru barrier layer. As no antiferromagnetic coupling occurs across this 2 Å Ru layer the two parts of the Co layer act equally. The goal of this 2 Å Ru layer is to divide the sample in an active part and an inactive part with respect to the magnetoresistance. We have

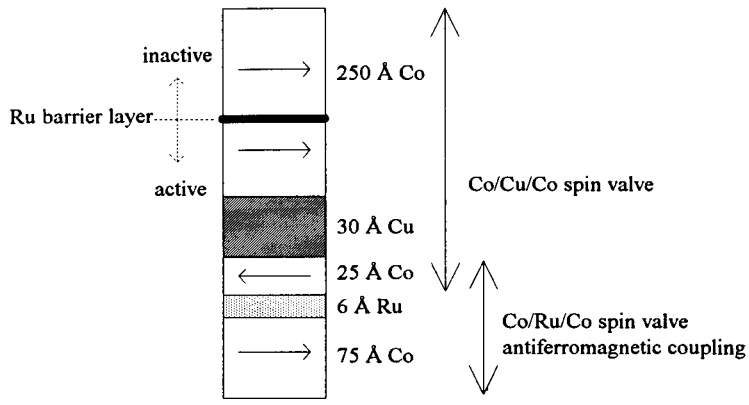

Figure 7.1: *Schematic representation of the samples used for determining the scattering length in Co. A 200 Å Ru base layer and a 30 Å Ru top layer are not drawn.*

seen in chapter 6 that Ru is effective in blocking electrons, as adding thin Ru layers abruptly decreases the magnetoresistance. The active part of the spin-valve is 25 Å Co + 30 Å Cu + t Co and the inactive part is the remainder of the Co layer ((250-t) Co).

7.2.2 Interpretation of the measurements

As the active part of the spin-valve increases in thickness, ΔG is expected to increase exponentially and finally saturate at a certain value of t. This can be understood as follows. When the active part of the spin-valve is small, scattering is dominated by spin-independent scattering at the Ru barrier layer of the spin-valve. An increase of the active part by shifting the Ru barrier layer, increases the relative importance of spin-dependent scattering in the bulk and/or at the interfaces of the Co layers. The exponential behaviour is directly related to the Boltzmann transport equation and its solution (equation 3.6). The increase of ΔG=Gp-Gap saturates when the thickness of the active Co layer is in the order of the longest of the mean free path of electrons in Co, as then spin-dependent scattering has come to its full potential.

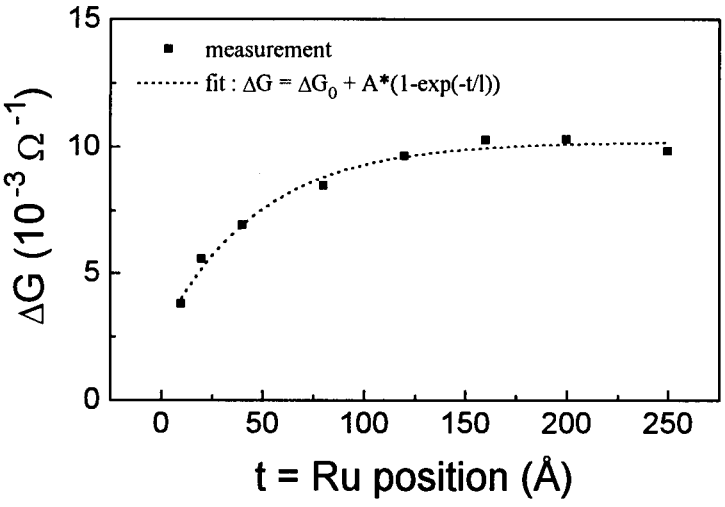

Figure 7.2: ΔG *as a function of the position of the 2 Å Ru barrier layer at a temperature of 300K.*

Figure 7.2 presents a measurement of ΔG as a function of the Ru position at a temperature of 300K, illustrating the exponential behaviour. An exponential relationship was suggested before by Parkin [Par94] although not in ΔG but in MR. However, MR reduces at higher Ru position, due to a small but noticable increase in conductivity as the Ru layer approaches the outer boundary and the probability to scatter diffusively at the barrier becomes minimal. Therefore, we did not try to fit MR with an exponential function, but rather ΔG. We will illustrate this in the presentation of the experimental data.

We will now try to find a relationship between the parameter l and the mean free path λ_{Co} (which might be spin-dependent) via the exponential fit

$$\Delta G = \Delta G_0 + A \cdot (1 - exp(-\frac{t}{l})). \tag{7.1}$$

To do this we use the Camley-Barnas model for magnetoresistance as described in section 3.2. We do not fit our measured data directly with the Camley-Barnas model, because we only want to use the qualitative behaviour of ΔG to extract λ_{Co}. Fitting of magnetoresistance data both qualitative and quantitative with the Camley-Barnas model is complicated due to the large number of fitting parameters. To make our interpretations more transparant all calculations will be performed on a model spin-valve with the following composition: 25 Å Co + 30 Å Cu + t Co + 2 Å Ru + (250-t) Co. First we consider the ideal situation in which

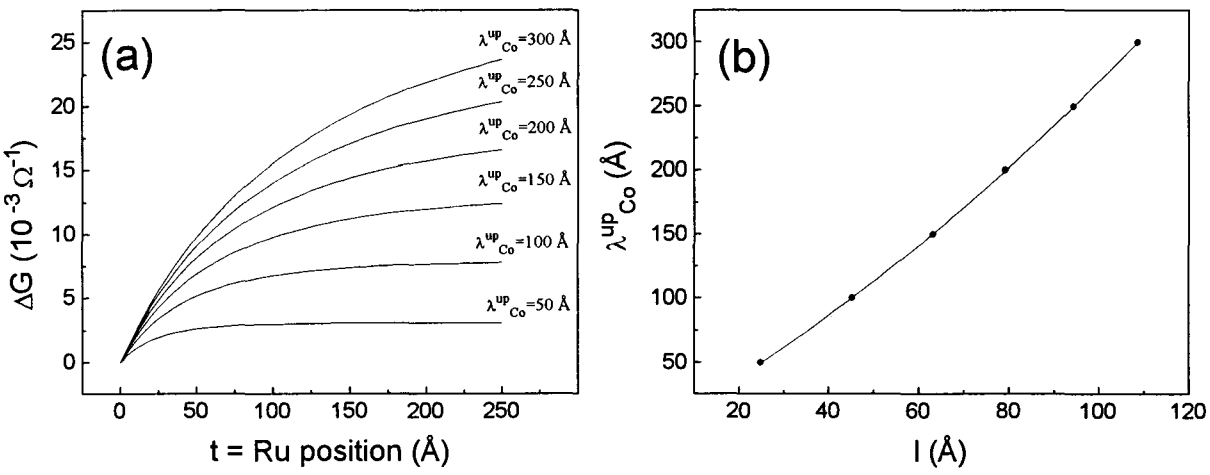

Figure 7.3: *ΔG as a function of the position of the 2 Å Ru for a number of mean free paths $\lambda^{\uparrow}_{Co}$ calculated with the Camley-Barnas model (a) and $\lambda^{\uparrow}_{Co}$ as a function of the fitting parameter l (b).*

λ_{Ru}=0, this means that the Ru layer is a perfect barrier, and $\lambda^{\downarrow}_{Co}$=0. Figure 7.3.a shows the Camley-Barnas calculation of ΔG as a function of the Ru position t for a number of mean free paths $\lambda^{\uparrow}_{Co}$. ΔG saturates if $\lambda^{\uparrow}_{Co}$ is small with respect to the 250 Å Co layer. If $\lambda^{\uparrow}_{Co}$ is in the order or larger than 250 Å, ΔG does not saturate but is still exponential in form. All curves can be fitted with equation 7.1, and the results of the fits are presented in figure 7.3.b in which $\lambda^{\uparrow}_{Co}$ as a function of l is plotted. Now we have found a relation between l and $\lambda^{\uparrow}_{Co}$, we might think that we have the tool to extract $\lambda^{\uparrow}_{Co}$ from the experimental data.

However, we have inserted in the model λ_{Cu}=200 Å, $T^{\uparrow}_{Co/Cu}$=1 and $T^{\downarrow}_{Co/Cu}$=0.2. These are parameters which seem reasonable from literature [Dien93, Frei93] and have proved to describe our sputtered Co/Cu spin-valves reasonably [Roer94]. But these mean free paths and scattering coefficients do not have to apply for these specific spin-valves. Most important it is that we have assumed $\lambda^{\downarrow}_{Co}$=0 Å. This means that bulk spin-dependent scattering plays an

important role in our calculations. Experimental investigation did not yet reveal if bulk spin-dependent scattering plays an important role in Co/Cu spin-valves. Experiments by Parkin [Par93] suggest that the main cause of magnetoresistance in Co/Cu spin-valves is interface spin-dependent scattering, but his measurements are also subject to different interpretations [Dien93].

So next we try to calculate what influence a change of the parameters inserted in the model has on the relationship between $\lambda^{\uparrow}_{Co}$ and l. Figures 7.4.a...e show the influence of a change of λ_{Cu}, $\lambda^{\downarrow}_{Co}$, $T^{\downarrow}_{Co/Cu}$ and λ_{Ru} on the characteristic length l. In all calculations $\lambda^{\uparrow}_{Co}$ is taken 100 Å, which corresponds to l=45.3 Å in the ideal case (dotted lines figure 7.4.a...e).

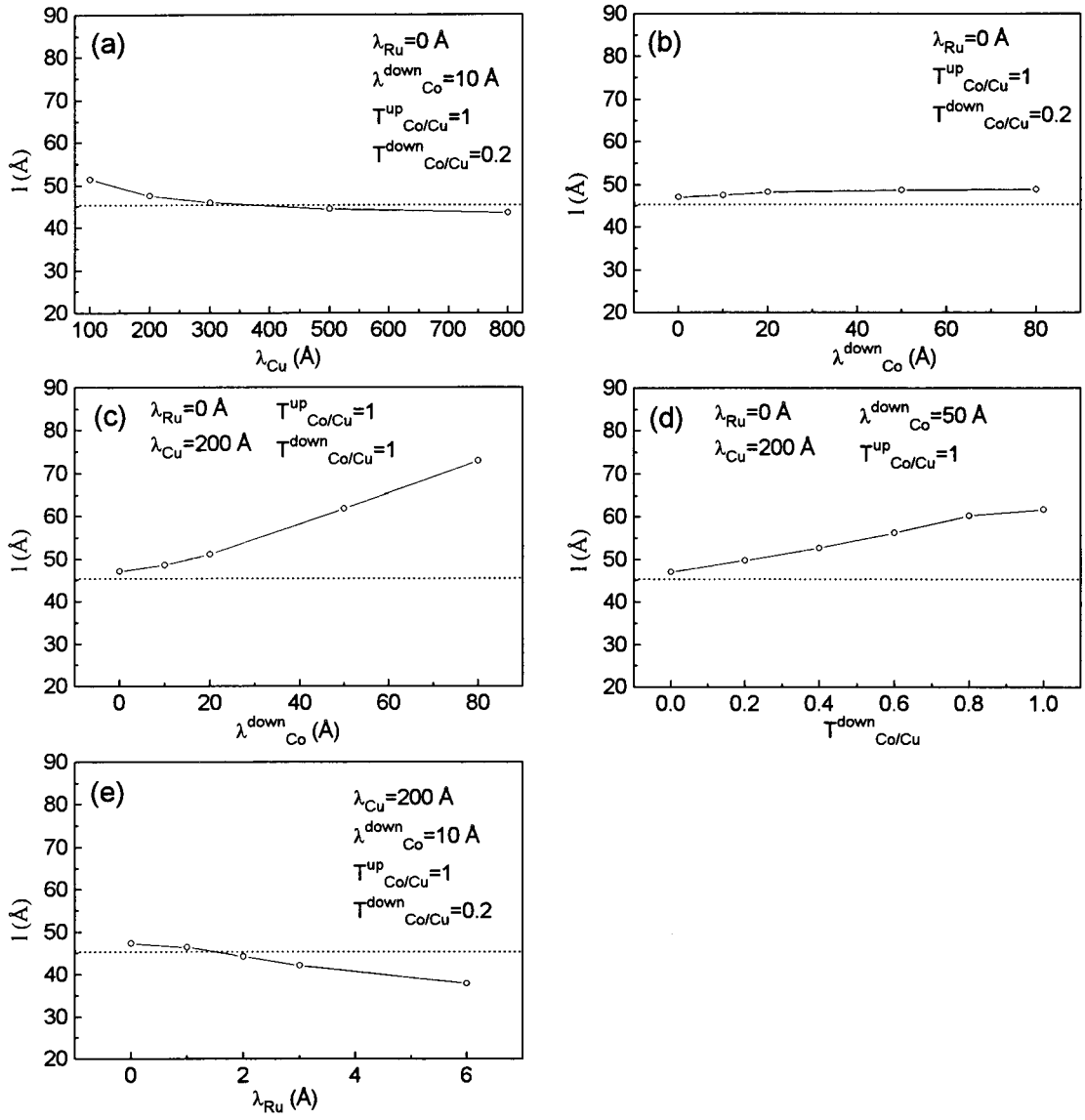

Figure 7.4: *Influence of different parameters calculated with the Camley-Barnas model on the fitting parameter l. In all calculations* $\lambda^{\uparrow}_{Co}$*=100 Å and the dotted line represents l in the ideal situation (see text).*

Influence of λ_{Cu}:

In figure 7.4.a it is shown that an increase of λ_{Cu} from 100 to 800 Å results in a minor change of l. This can be understood if one realizes that the Cu spacer layer in the Co/Cu spin-valve

is 30 Å thick. Electrons are not disturbed in crossing the spacer layer because of the long scattering length of electrons in Cu. This does not significantly change if λ_{Cu} is increased from 100 to 800 Å.

Influence of $\lambda^{\downarrow}_{Co}$ ($T^{\downarrow}_{Co/Cu}$=0.2):

In figure 7.4.b l is presented for $\lambda^{\downarrow}_{Co}$ varying between 0 and 80 Å. We have assumed significant spin-dependent interface scattering via the parameters $T^{\uparrow}_{Co/Cu}$=1 and $T^{\downarrow}_{Co/Cu}$=0.2 . The fitting parameter l stays almost equal for all $\lambda^{\downarrow}_{Co}$. So in case of significant interface scattering l is independent of $\lambda^{\downarrow}_{Co}$. The explanation for this is that in case of sufficient interface scattering all spin-down electrons are filtered out at the interface, after which they cannot contribute anymore to the characteristic length l.

Influence of $\lambda^{\downarrow}_{Co}$ ($T^{\downarrow}_{Co/Cu}$=1):

In the case of no interface scattering $\lambda^{\downarrow}_{Co}$ has a strong influence on the characteristic length l as can be seen in figure 7.4.c. An increase of $\lambda^{\downarrow}_{Co}$ from 0 to 50 Å results in a change of l from 47 to 62. As the spin-down electrons are not filtered at the interface they contribute to the characteristic length l.

Influence of $T^{\downarrow}_{Co/Cu}$ ($\lambda^{\downarrow}_{Co}$=50 Å):

A change of $T^{\downarrow}_{Co/Cu}$ from 0 to 1 has also a strong influence on l as is demonstrated in figure 7.4.d, in which is assumed that $\lambda^{\downarrow}_{Co}$=50 Å.

Influence of λ_{Ru}:

The last parameter we have varied is λ_{Ru}. From earlier experiments (chapter 6) we have shown that Ru is very effective in blocking electrons, which we have demonstrated by putting Ru in the middle of the Cu spacer layer in Co/Cu spin-valves. Nevertheless λ_{Ru} is varied between 0 and 6 Å and the influence on l is presented in figure 7.4.e . The fitting parameter l decreases slightly in raising λ_{Ru}.

The precise values of $T^{\downarrow}_{Co/Cu}$ and $\lambda^{\downarrow}_{Co}$ are not known, and we have seen that these parameters have serious influence on the interpretation of the data. Note that a non-effective blocking of spin-down electrons at the interface ($T^{\downarrow}_{Co/Cu} > 0$ and/or $\lambda^{\downarrow}_{Co} > 0$) leads to a larger l and therefore an overestimation of $\lambda^{\uparrow}_{Co}$. Although this seems a serious problem one has to realize that in order to gain sufficient magnetoresistance (up to 5% at T=10K) either $\lambda^{\downarrow}_{Co}$ or $T^{\downarrow}_{Co/Cu}$ (or both) must be small. We have seen in chapter 6, as mentioned before, that adding a 1 Å thick Ru layer at the interfaces of a Co/Cu spin-valve almost completely destroys the magnetoresistance, what is an indication for a significant interface contribution to the magnetoresistance. Although the before mentioned experiments by Parkin [Par93] do not rule out bulk spin-dependent scattering they proof the existence of significant interface scattering for Co/Cu interfaces. A significant interface contribution to the magnetoresistance is therefore not an unreasonable assumption.

The conclusion from varying the different parameters is that, presumed there is a large interface scattering assymetry or $\lambda^{\downarrow}_{Co}$ is small, it is possible to connect l to $\lambda^{\uparrow}_{Co}$ using figure 7.3. This relation can be fitted into the equation

$$\lambda^{\uparrow}_{Co} = 0.86128 + 1.83861 \cdot l + 0.0091 \cdot l^2. \tag{7.2}$$

7.2.3 Magnetoresistance results

In figure 7.5 Gp, ΔG and MR measurement data are presented for sample numbers 950184...950193 at 7 different temperatures ranging from 10K to 300K. Gp increases with decreasing temperature which is in agreement with increasing mean free paths in the different materials due to less magnon and phonon scattering. As a function of the Ru position Gp first decreases and after reaching a minimum at about 80 Å, Gp increases again. This finds its explanation in the fact that electrons find their mean free paths restricted by the borders of

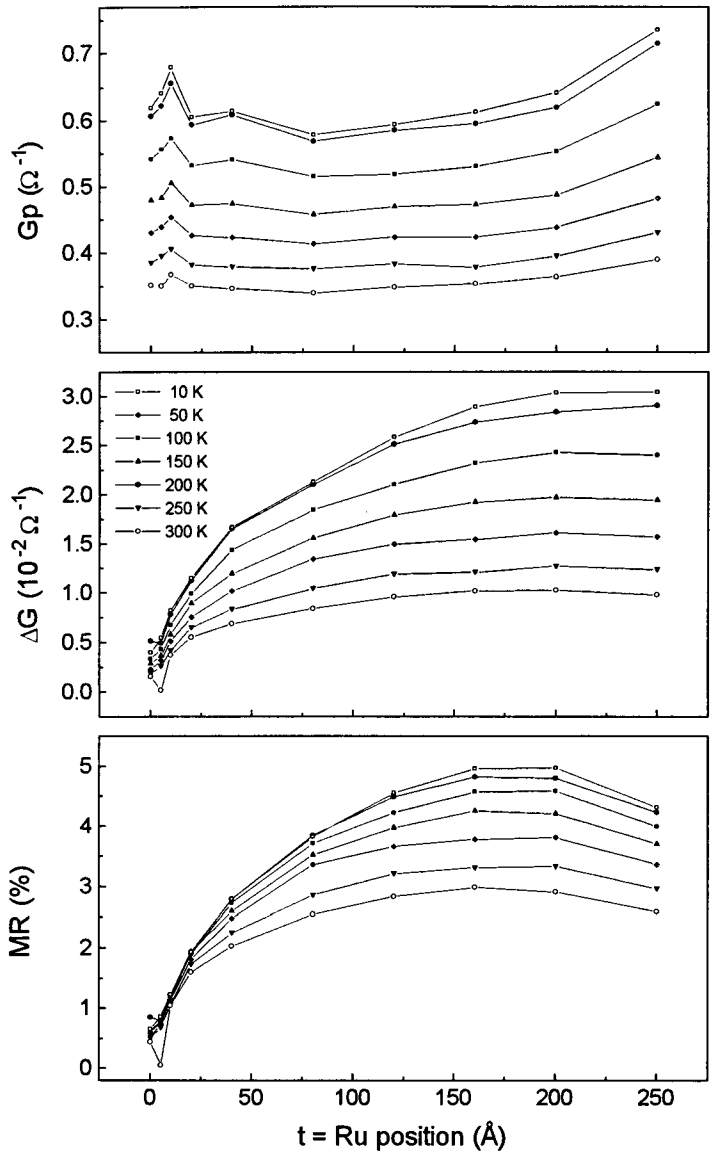

Figure 7.5: *MR, ΔG and Gp as a function of the Ru barrier layer position for temperatures between 10K and 300K.*

the active and the inactive-part of the samples which are separated by the Ru layer. A small Ru position leads to an increased conductivity in the inactive part of the Co/Cu spin-valve and a high Ru position leads to increased conductivity in the active part of the spin-valve between which a minimum is situated.

ΔG shows exponential behaviour, except for small t. This is probably caused by the fact that at small t the Co layer is not well defined, maybe granular, and therefore not acts as a uniform ferromagnetic layer. At high temperatures ΔG is saturated at lower Ru position than at low temperatures, which is in agreement with a smaller mean free path in Co at high temperatures (see figure 7.3).

The next step is to determine the long scattering length of Co by fitting the ΔG data with equation 7.1 and then connect the fitting parameter l with $\lambda^{\uparrow}_{Co}$ via equation 7.2. This is done in figure 7.6, in which ΔG is plotted again for seven temperatures and fitted with equation 7.1. In every ΔG versus t plot an estimation of $\lambda^{\uparrow}_{Co}$ is shown, which is calculated using equation 7.2. In section 7.4 we will further analyse these data in relation to λ_{Cu} and the conductivity.

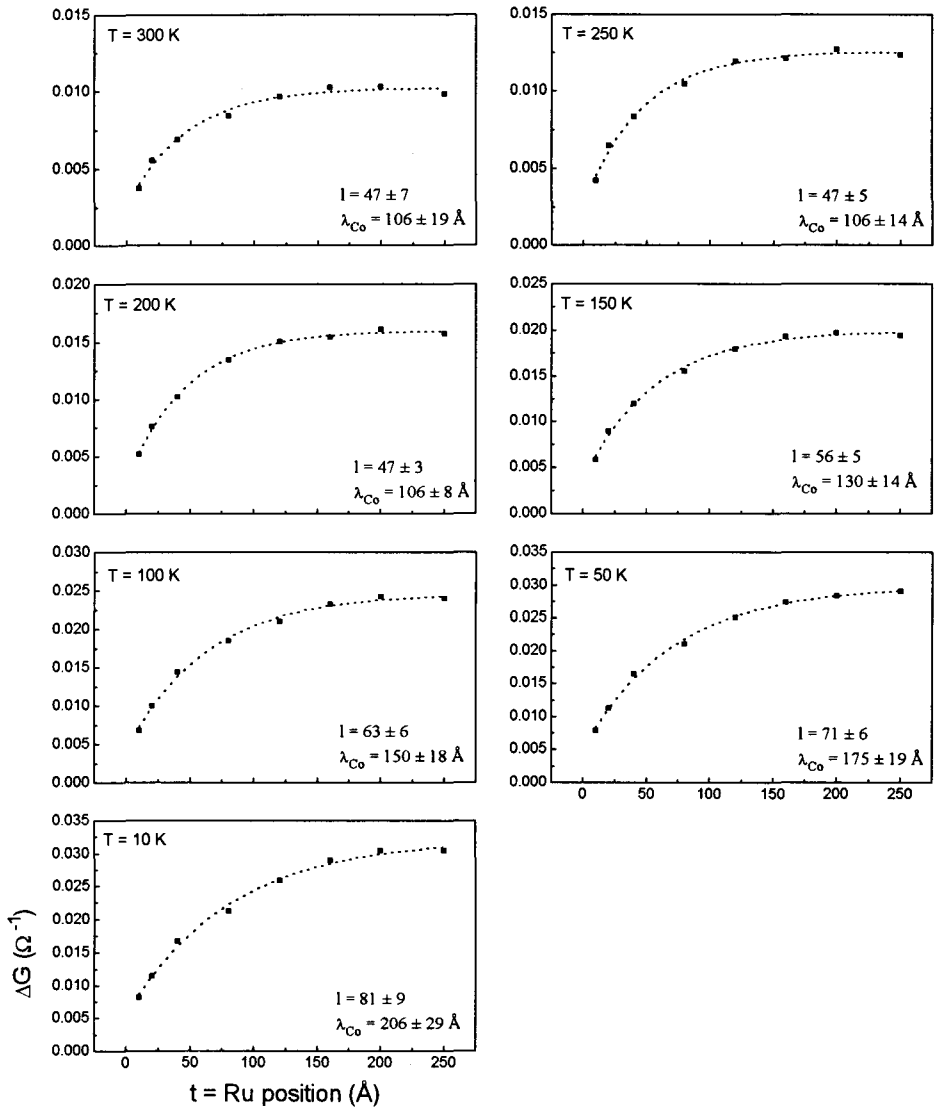

Figure 7.6: ΔG *as a function of the Ru barrier layer position for temperatures between 10K and 300K. The solid squares are the measurements and the dotted lines are the exponential fits of the data. In every figure* l *and the estimated* $\lambda^{\uparrow}_{Co}$ *are shown.*

7.3 Long scattering lengths in Cu

7.3.1 Spin-valve design

The samples we have used in an attempt to determine the long scattering lengths in Cu have the following composition: 200 Å Ru + 75 Å Co + 6 Å Ru + 25 Å Co + 30 Å Cu + 25 Å Co + t Cu + 5 Å Ru + (300-t) Cu + 30 Å Ru, with t ranging from 0 to 300 Å. We have used a 25 Å Co filter layer with the purpose to filter out spin-down electrons. The Cu back layer is 300 Å thick. Figure 7.7 shows a schematic representation of the samples. (sample numbers are 950194...9501103). The spin-valve is divided in an active and non-active part with a highly resistive 5 Å Ru barrier layer.

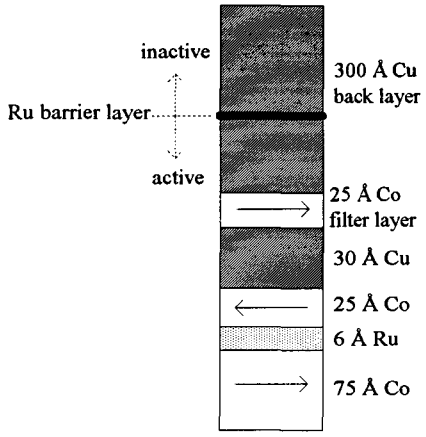

Figure 7.7: *Schematic representation of the samples used for determining the scattering length in Cu. A 200 Å Ru base layer and a 30 Å Ru top layer are not drawn.*

This principle of a filter and back layer (without Ru barrier layer) was used before by Gurney [Gurn93]. He measured ΔG of NiFe/Cu/Nife/**X** spin-valves as a function of the thickness of the back layer **X** (**X** = Co, Fe, NiFe and Cu). The exponential behaviour of ΔG as a function of the back layer thickness was directly related to the longest of the mean free paths of electrons in material **X**. However, no careful analysis with the help of the Camley-Barnas model was performed. Therefore, we will not compare our measurements with the results as obtained by Gurney.

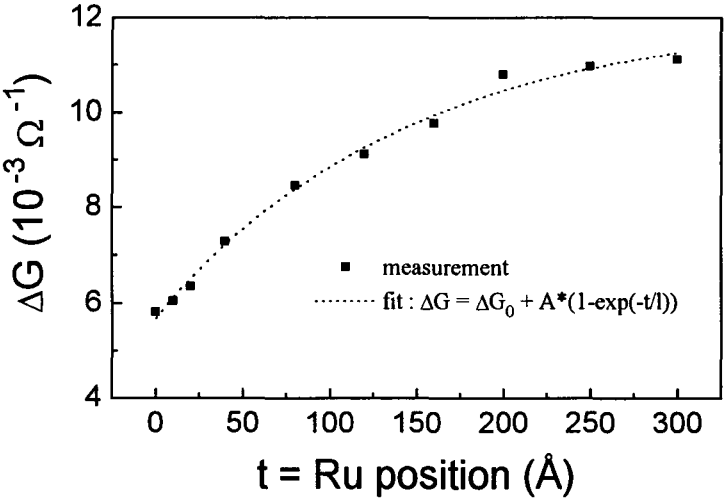

Figure 7.8: *Room temperature ΔG as a function of the position of the 5 Å Ru barrier layer.*

7.3.2 Interpretation of the measurements

In a similar way as in section 7.2 for Co we will determine whether the expected exponential behaviour of ΔG as a function of the Ru barrier layer in Cu, is a good measure for λ_{Cu}. In figure 7.8 room temperature ΔG as a function of the position of the 5 Å Ru barrier in the Cu back layer is presented. ΔG is fitted with equation 7.1 and we see that, although ΔG is not saturated at t=300 Å, reasonable agreement with this exponential function is obtained.

We now have calculated ΔG with the Camley-Barnas model for a number of mean free paths λ_{Cu} (figure 7.9) for the model spin-valve: 25 Å Co + 30 Å Cu + 25 Å Co + t Cu + 5 Å Ru + 300 Å Cu. We have calculated the ideal situation, in which $\lambda^{\downarrow}_{Co}$=0 and λ_{Ru}=0. The

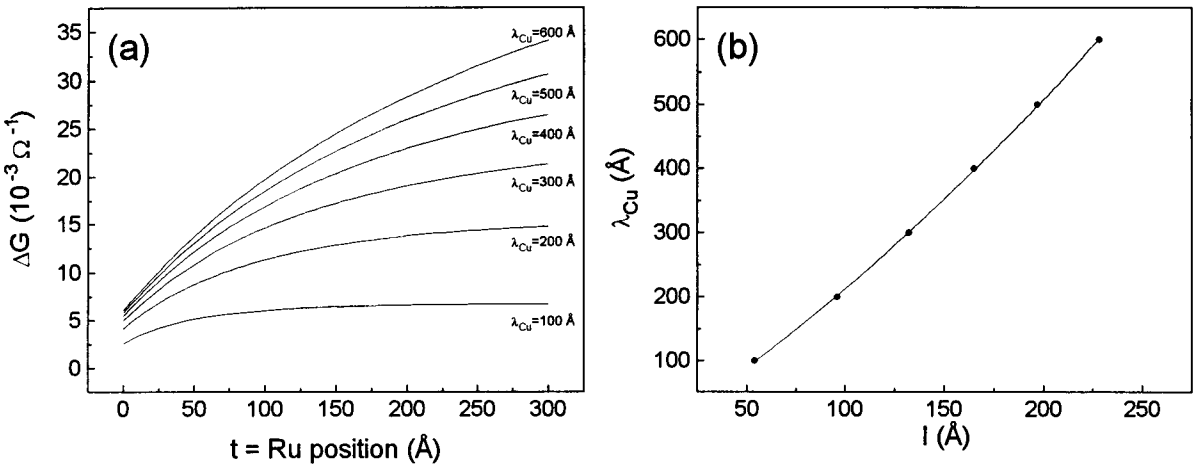

Figure 7.9: *ΔG as a function of the position of the 5 Å Ru for a number of mean free paths λ_{Cu} calculated with the Camley-Barnas model (a) and λ_{Cu} as a function of the fitting parameter l (b).*

mean free path for electrons in Co was $\lambda^{\uparrow}_{Co}$=150 Å, in agreement with the mean free paths as measured in section 7.2. Interface spin-dependent scattering coefficients at the Co/Cu interfaces were $T^{\uparrow}$=1 and $T^{\downarrow}$=0.2.

Because we do not know the exact values, we have varied the parameters $\lambda^{\uparrow}_{Co}$, $\lambda^{\downarrow}_{Co}$, λ_{Ru} and $T^{\downarrow}$ to investigate what influence a change of any of these parameters has on our interpretation of *l* being a measure for λ_{Cu}. In all calculations λ_{Cu} is taken 350 Å which corresponds to *l*=149 Å (dotted lines in figure 7.10).

Influence of $\lambda^{\uparrow}_{Co}$:

Figure 7.10.a shows that a change of $\lambda^{\uparrow}_{Co}$ from 50 to 300 Å has a significant effect on our fitting parameter l. This means that although our intention was to probe the mean free path of electron in the Cu back layer, we also probe, at least partly, $\lambda^{\uparrow}_{Co}$. Even within the range of the estimated $\lambda^{\uparrow}_{Co}$ in the previous sections (100 Å at room temperature to 200 Å at 10K), *l* changes significantly from 160 to 140 Å. This will make any further interpretation difficult.

Influence of $\lambda^{\downarrow}_{Co}$ ($T^{\downarrow}_{Co/Cu}$=0.2):

In case of transmission coefficients at the Co/Cu interface $T^{\uparrow}_{Co/Cu}$=1 and $T^{\downarrow}_{Co/Cu}$=0.2, a change of $\lambda^{\downarrow}_{Co}$ has almost no influence on the fitting parameter l. This means that spin-down electrons are sufficiently filtered at the interface of the filter layer to make sure that we only probe spin-up electrons.

Influence of $\lambda^{\downarrow}_{Co}$ ($T^{\downarrow}_{Co/Cu}$=1):

In case of no spin-dependent scattering at the Co/Cu interfaces, a change of $\lambda^{\downarrow}_{Co}$ from 0 to 100 Å results in a change of *l* from 150 to 100 Å. This means that without sufficient filtering

of spin-down electrons in the filter layer, also spin-down electrons are probed.

Influence of $T^{\downarrow}_{Co/Cu}$:

In case of bulk scattering in Co ($\lambda^{\uparrow}_{Co}$=150 Å and $\lambda^{\downarrow}_{Co}$=10 Å), a change of $T^{\downarrow}_{Co/Cu}$ from 0 to 1 has no significant influence on *l*.

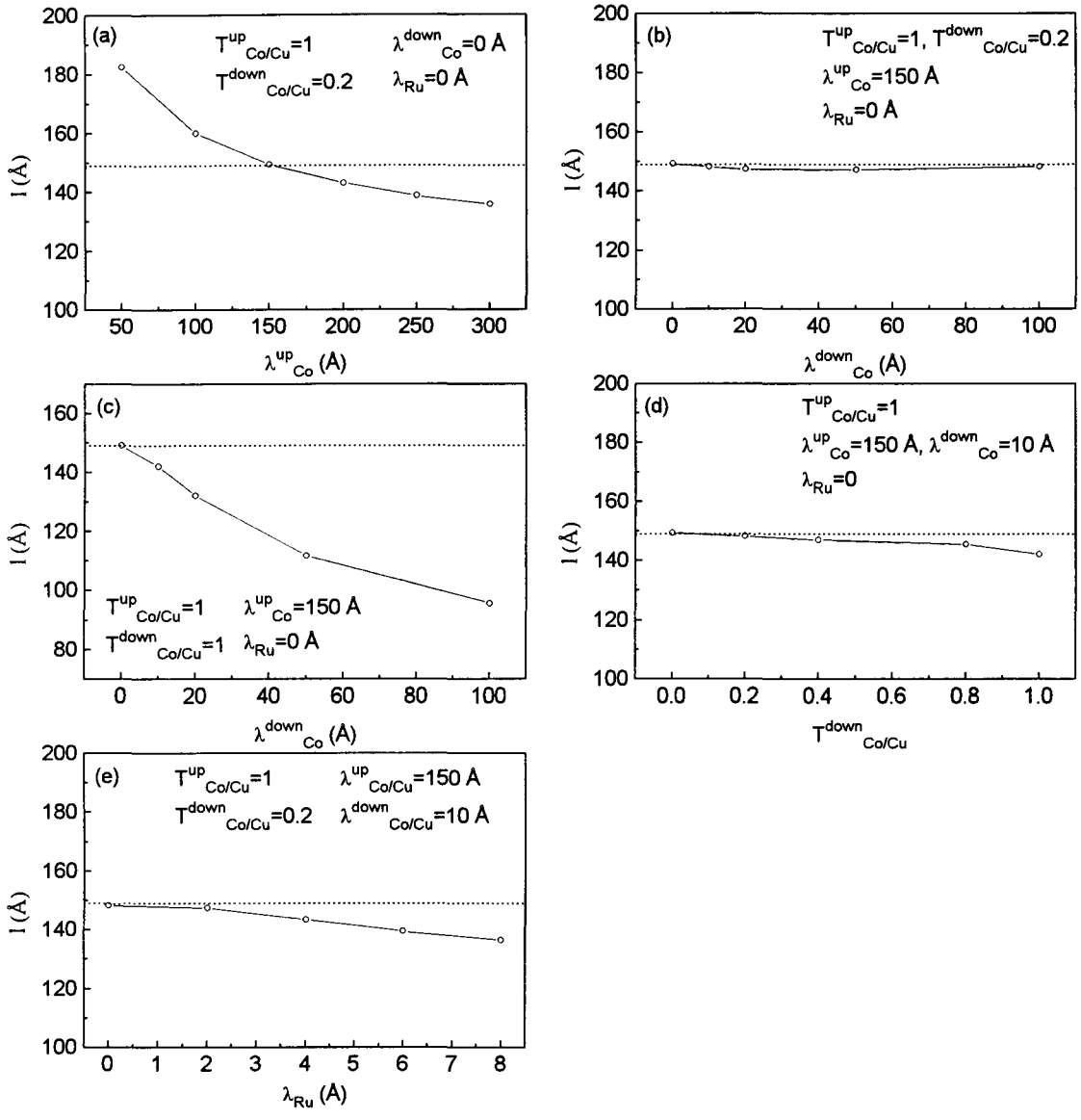

Figure 7.10: *Influence of different parameters calculated with the Camley-Barnas model on the fitting parameter l for the model spin-valve 25 Å Co + 30 Å Cu + 25 Å Co + t Cu + 5 Å Ru + (300-t) Cu. The dotted lines are l in the ideal case (see text).*

Influence of λ_{Ru}:

A change of λ_{Ru} from 0 to 8 Å has no significant influence on the fitting parameter l.

The conclusion from varying the different parameters is that, in case of sufficient filtering of spin-down electrons in the filter layer, what we assume to be the case, *l* is a constant measure. This filtering can be both spin-dependent scattering at the interface or in the bulk of the Co filter layer. However, next to λ_{Cu} also $\lambda^{\uparrow}_{Co}$ has an influence on the fitting parameter l, so that no unique relationship between λ_{Cu} and *l* exists. From figure 7.10.a we conclude that within the range of $\lambda^{\uparrow}_{Co}$, as measured in section 7.2, about 15% variation in *l* can occur.

7.3.3 Magnetoresistance results

In figure 7.11 Gp, ΔG and MR are presented of sample number 950194...9501103, measured at seven temperatures ranging from 10K to 300K. Gp increases with decreasing temperature in

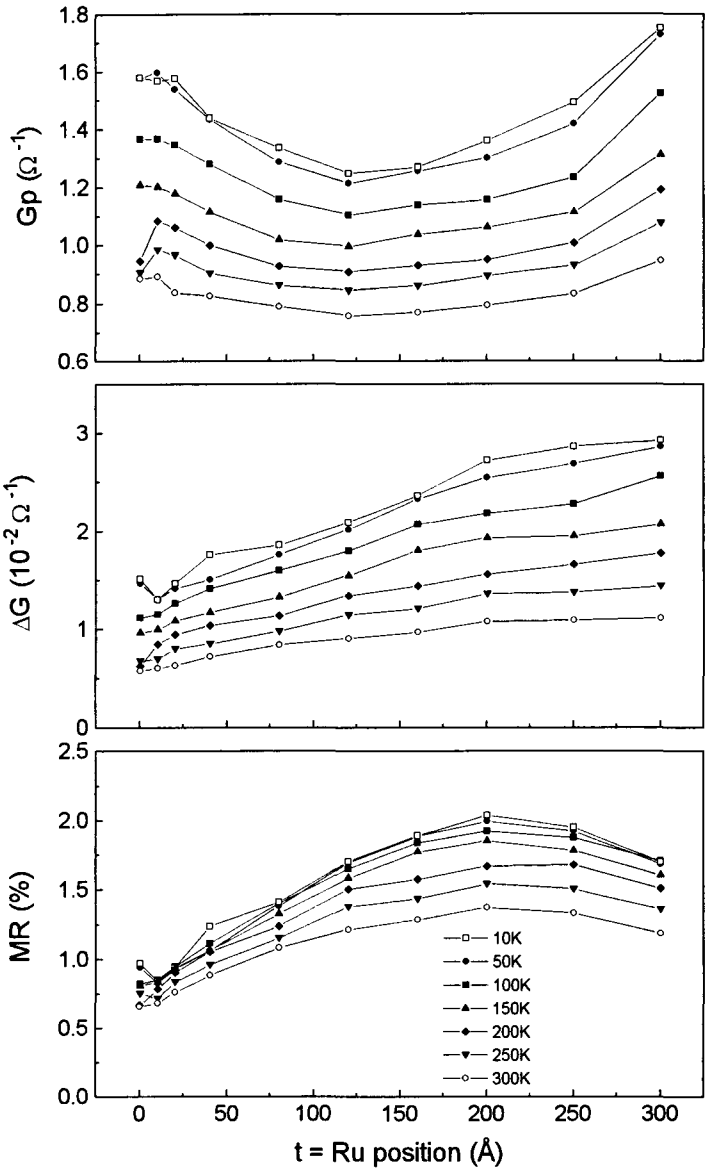

Figure 7.11: *MR, ΔG and Gp as a function of the Ru barrier layer position for temperatures between 10K and 300K.*

accordance with a larger mean free path for electrons at lower temperature. Again a mimimum can be observed in Gp as a function of the Ru barrier layer position similar to Gp for the Ru barrier layer in Co. Also in this case, the minimum can be explained by the restriction of the mean free paths by the borders of the active and inactive part of the structure, which is least effective for low and high Ru positions. ΔG increases with increasing Ru barrier layer position t, but shows in general no clear exponential behaviour. This might be due to the fact that the back layer is too thin, in comparison to the mean free path of electrons in Cu, to saturate ΔG. We cannot, however, make the Cu layer much thicker, because the relative change in conductivity ΔG becomes then smaller with respect to the conductivity. This would introduce larger errors in the measurements. The magnetoresistance increases with increasing t and decreases at high t, due to increasing conductivity.

We will only analyze ΔG for T=250K and T=300K, because for all the other temperatures fitting of ΔG with the exponential equation 7.1 resulted in errors of the fitting parameters l in the order of their value. From an analysis of ΔG at T=250K and T=300K and figure 7.9 we have estimated λ_{Cu} to be 441±117 Å and 362±147 Å respectively. In the next section we will further analyse these data in relation to $\lambda^{\uparrow}_{Co}$ and the conductivity.

7.4 Mean free paths and conductivity

In figure 7.12 $\lambda^{\uparrow}_{Co}$ is presented as a function of temperature. As mentioned before, Parkin performed measurements in similar structures before and determined the mean free path in Co [Par94] by assuming that the fitting parameter l (equation 7.1) is equal to the longest of the mean free paths in Co. We have however re-examined his data with the Camley-Barnas model (figure 7.3) from which follows that he underestimated λ_{Co} by about a factor 2. The corrected value for the mean free path as obtained by Parkin is plotted in figure 7.12 (black square). Dieny et al. studied the magnetoresistance of spin-valves with the basic structure : 50 Å NiFe + 22 Å Cu + t Co [Dien92]. He introduced an effective thickness t_0, which is proportional to the Co mean free path, to take into account that only part of the ferromagnetic layer (t Co) effectively contributes to the magnetoresistance. As suggested by Dieny recently [Dien93], this value t_0 has to be multiplied by a factor 2 to obtain the correct value for the Co mean free path, because of the fact that electrons travel at various angles θ with respect to the plane of the layers, and thus effectively experience a smaller thickness. The mean free path for Co and its temperature dependence as obtained by Dieny are also plotted in figure 7.12 (solid circles). In comparison with both studies we have obtained similar temperature

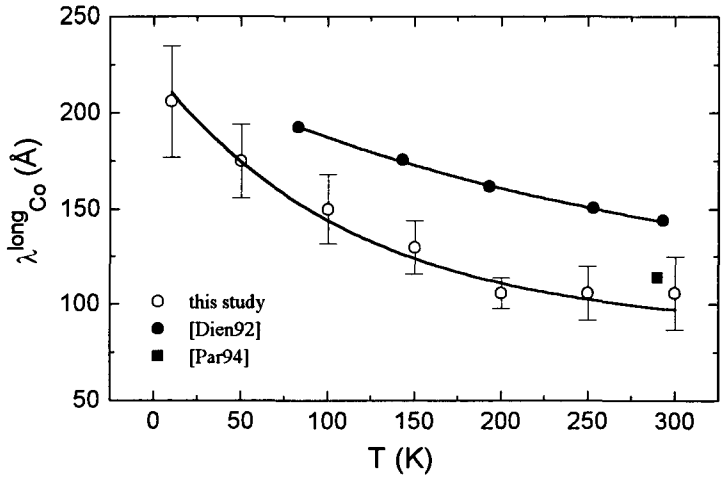

Figure 7.12: *Longest of the Co mean free paths ($\lambda^{long}_{Co}=\lambda^{\uparrow}_{Co}$) from our analysis of ΔG (open circles) and re-examined data on similar structures (solid square) and on exchange biased 50 Å NiFe + 22 Å Cu + t Co (solid circles). The lines are guides to the eye.*

behaviour and comparable values for the mean free paths in Co.

In the previous sections we have measured $\lambda^{\uparrow}_{Co}$ for several temperatures and we made an estimation for $\lambda^{\uparrow}_{Cu}$ (T=250K and T=300K). As Cu is a non-magnetic material we may assume that $\lambda^{\uparrow}_{Cu}=\lambda^{\downarrow}_{Cu}$. For Co, however, it is not clear to what extent $\lambda^{\uparrow}_{Co}$ differs from $\lambda^{\downarrow}_{Co}$. Therefore, we have measured the conductivity of single Co layers and Cu layers (sample numbers 9503122...9503131 and 950403...950412). We assume a conduction band for Co and Cu to be free electron like. This is well known for Cu, and although Co possesses a more complicated band structure, transport in Co is also dominated by free-electron-like behaviour

as well [Mott64, Pap86]. Then the conductivity is proportional to the sum of $\lambda^{\uparrow}$ and $\lambda^{\downarrow}$ via Drude's equation [Kit86]

$$\sigma = (\lambda^{\uparrow} + \lambda^{\downarrow}) \cdot \frac{ne^2}{2mv_f}, \tag{7.3}$$

with n the total free electron density (n_{Cu}=8.45×10^{22} cm^{-3}), e the electron charge, m the electron mass and v_f the Fermi-velocity ($v_{f(Cu)}$=1.57×10^{8} cm s^{-1}). Thus for Co the conductivity can be written as

$$\sigma_{Co} \propto \lambda^{\uparrow} + \lambda^{\downarrow} \begin{cases} = 2\lambda^{\uparrow} & \text{if } \lambda^{\downarrow} = \lambda^{\uparrow} \\ < 2\lambda^{\uparrow} & \text{if } \lambda^{\downarrow} < \lambda^{\uparrow} \end{cases} \tag{7.4}$$

and for Cu

$$\sigma_{Cu} \propto \lambda^{\uparrow} + \lambda^{\downarrow} = 2\lambda^{\uparrow}. \tag{7.5}$$

Thus, if $\lambda^{\uparrow}_{Co} \neq \lambda^{\downarrow}_{Co}$, which in fact is representing the presence of bulk spin-dependent scattering, then a plot of $\lambda^{\uparrow}$ for Co and Cu versus σ does not yield a straight line. In contrast, when no bulk spin-dependent scattering would be present ($\lambda^{\uparrow}_{Co} = \lambda^{\downarrow}_{Co}$), we expect $\lambda^{\uparrow}$ for Co and Cu versus σ to lie on one straight line.

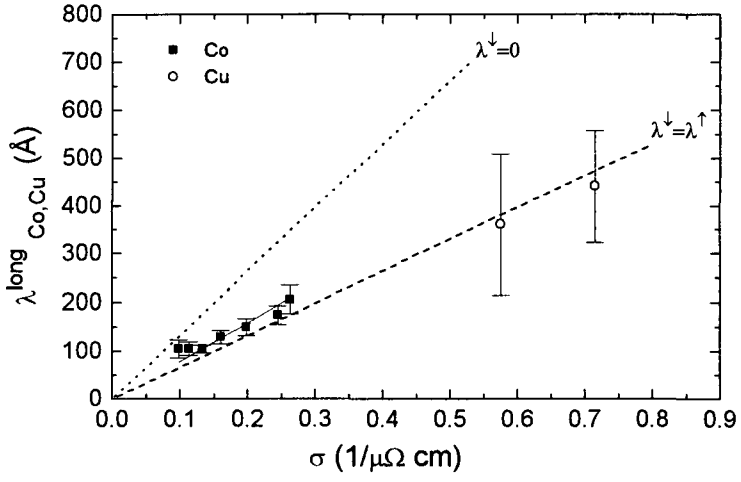

Figure 7.13: *The longest of the mean free paths ($\lambda^{long} = \lambda^{\uparrow}$) as measured with a Ru barrier layer for Co (solid squares) and Cu (open circle) as a function of the conductivity σ. The dashed line and dotted line are plots of equation 7.3 with $\lambda^{\downarrow} = \lambda^{\uparrow}$ and $\lambda^{\downarrow}$=0 respectively.*

Figure 7.13 shows the measured $\lambda^{long} = \lambda^{\uparrow}$ for Co and Cu as a function of the conductivity. The measured mean free paths versus conductivity for Cu are in agreement with equation 7.3, with $\lambda^{\uparrow}_{Cu}$=$\lambda^{\downarrow}_{Cu}$ (dashed line in figure 7.13). The dotted line in figure 7.13 is equation 7.3 with $\lambda^{\downarrow}$=0. The longest of the mean free paths versus conductivity of Co fitted with equation 7.3 yields $\lambda^{\uparrow}_{Co}/\lambda^{\downarrow}_{Co}$=1.5±0.2 (solid line in figure 7.13). However, in Drude's equation we have made assumptions for the Fermi-velocity, the electron density and the electron mass, which are probably not correct for our specific structures. Therefore, the conclusion is that within the experimental accuracy $\lambda^{\uparrow}$ for Co and Cu versus σ lie on one line, which implies the absence of significant bulk spin-dependent scatttering in Co.

For completeness we present the results of the Ru barrier layer experiments by Parkin [Par94]. In figure 7.14 room temperature λ^{long} as a function of the conductivity for various magnetic and non-magnetic materials is shown. Parkin performed no analysis with the Camley-Barnas model and the fitting parameter l (equation 7.1) was assumed equal to λ^{long}. Nevertheless he obtaines perfect agreement with the Drude equation for $\lambda^{\uparrow} = \lambda^{\downarrow}$. But as mentioned before we make assumptions in the Drude equation which may not count for the considered materials. Therefore the main result is that magnetic ($Ni_{59}Fe_{41}$, $Ni_{81}Fe_{19}$, $Ni_{50}Co_{50}$,

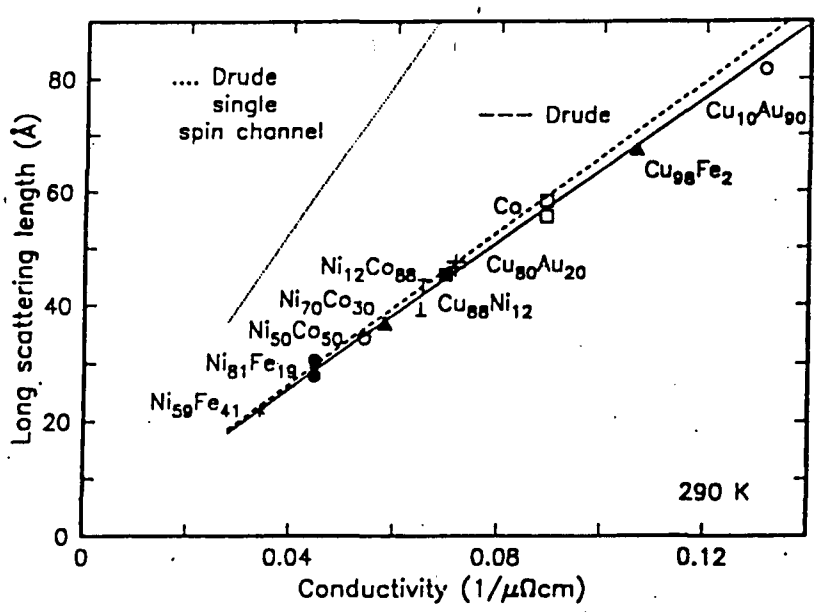

Figure 7.14: *The longest of the mean free paths versus conductivity determined by Ru barrier layer experiments at room temperature. The dashed line and dotted line are plots of equation 7.3 with* $\lambda^{\downarrow} = \lambda^{\uparrow}$ *and* $\lambda^{\downarrow}=0$ *respectively (figure from [Par94]).*

$Ni_{70}Co_{30}, Ni_{12}Co_{88}, Co$) as well as non-magnetic materials ($Cu_{88}Ni_{12}, Cu_{80}Au_{20}, Cu_{10}Au_{90}$, $Cu_{98}Fe_2$) lie on one line. Thus Parkin found no evidence for the existence of significant bulk spin-dependent scattering in Co, in agreement with our experiments.

7.5 Conclusions

We have measured the magnetoresistance of Co/Cu/**Co** spin-valves with a Ru barrier layer shifted through **Co**. Camley-Barnas calculations have shown that the exponential behaviour of ΔG as a function of the Ru position is a good measure for the longest of the mean free paths in Co ($\lambda_{Co}^{long} = \lambda_{Co}^{\uparrow}$). ΔG as a function of the Ru barrier layer position has been measured and connected to $\lambda_{Co}^{\uparrow}$ for seven temperatures ranging from 10K to 300K .

Second we have measured the magnetoresistance of Co/Cu/Co/**Cu** spin-valves with a Ru barrier layer shifted through **Cu**. Although Camley-Barnas calculations showed that the exponential behaviour of ΔG as a function of the Ru barrier layer is not only related to λ_{Cu} but also to λ_{Co}, we were able to extract λ_{Cu} for T=250K and T=300K, albeit not as accurate as $\lambda_{Co}^{\uparrow}$.

From comparison of λ^{long} for Co and Cu with the conductivity $\sigma_{Co,Cu}$ ($\propto \lambda^{\uparrow} + \lambda^{\downarrow}$) we have found no indication for the existence of significant bulk spin-dependent scattering in Co.

Chapter 8

NiO based spin-valves

In this chapter measurements are presented on Co/Cu/Co and $Ni_{80}Fe_{20}$/Cu/ $Ni_{80}Fe_{20}$ spin-valves sandwiched between NiO. One of the magnetic layers of the spin-valves is exchange biased with NiO. Effects on the magnetoresistance of the insulating NiO layers are investigated.

8.1 Introduction

Giant magnetoresistance in sandwiches consisting of two ferromagnetic layers separated by a non-magnetic layer is facilitated by exchange-biasing one of the magnetic layers to an anti-ferromagnet (see section 5.2). Exchange biasing to an antiferromagnet is one way to achieve anti-parallel alignment of the two ferromagnetic layers (see also section 5.2). Compared to coupled sandwiches, the main advantage of the exchange-biased systems is the high potential for application in e.g. MR heads for magnetic recording, as well as the possibility to create full anti-parallel alignment of the magnetic layers, which permits unambigous measurement and analysis of the intrinsic sheet conductance in the parallel and anti-parallel state.

Experiments so far were mostly focused on the elucidation of the spatial origin of spin-dependent scattering, in the bulk or at the interface of magnetic layers. Nevertheless, the role of electron channeling and reflection or confinement due to e.g. potential steps at the interfacial regions of the consistuents, has not been addressed experimentally. Effects of potential steps might be most predominant at the interfaces of noninsulating and insulating layers as electrons face an infinite potential wall at such an interface. Therefore we have investigated exchange biased spin-valves of Co/Cu/Co and $Ni_{80}Fe_{20}$/Cu/$Ni_{80}Fe_{20}$ sandwiched between insulating NiO.

8.2 NiO based Co/Cu/Co

8.2.1 Investigation of exchange biasing

To study the exchange biasing between Co and NiO, we investigated a number of samples consisting basically of a single Co layer exchange biased to a NiO layer. Our goal is to construct a Co layer, exchange biased to NiO, which has a high exchange biasing field Hex to obtain good anti-parallel alignment in a possible spin-valve. For comparison, exchange coupling fields up to 20 Oe ($\approx$ 1.6 kA/m) have been found in exchange biased $Ni_{81}Fe_{19}$/NiO films [Soe93] for a 400 Å thick $Ni_{81}Fe_{19}$ film.

MOKE measurements at room temperature are done to determine the exchange biasing field *Hex* and coercive field *Hc* of NiO exchange biased Co layers. Figure 8.1 shows a typical MOKE curve of sample number 941289, which consists of 500 Å NiO + 30 Å Co + 30 Å Cu. The 30 Å Cu layer prevents the 30 Å Co layer from oxidation.

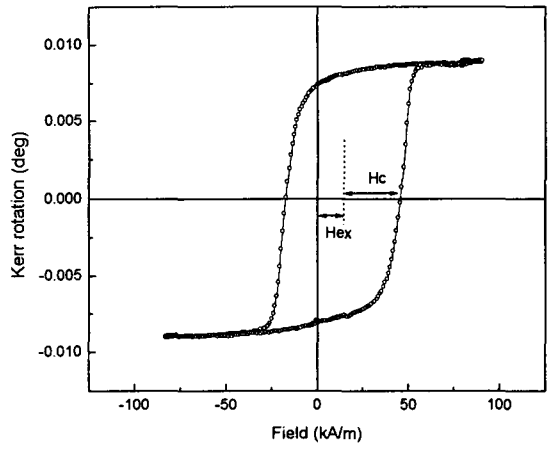

Figure 8.1: *Kerr rotation as a function of the applied field of 500 Å NiO + 30 Å Co + 30 Å Cu. Exchange biasing field and coercive field are denoted with Hex and Hc respectively.*

We investigated the influence of the thickness of the NiO layer by determining Hex and Hc of t NiO + 30 Å Co + 30 Å Cu (sample numbers 941286...941291), with t ranging from 50 Å to 2000 Å. In figure 8.2 we present Hex and Hc as a function of the NiO layer thickness. Hc increases with increasing NiO layer thickness and Hex shows a sharp increase in the

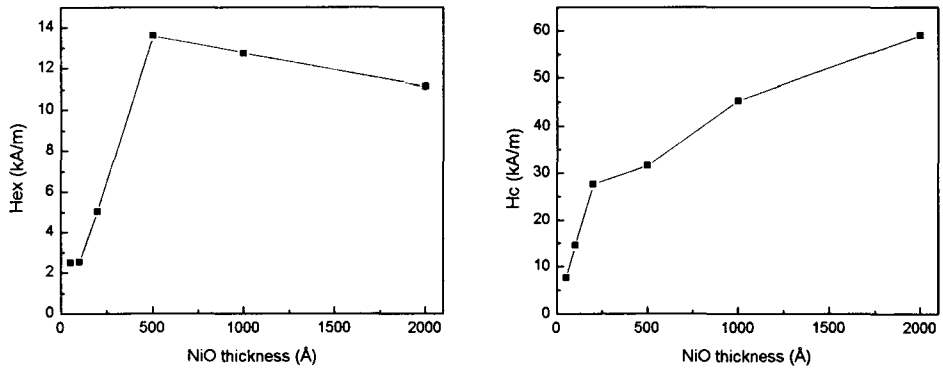

Figure 8.2: *Hex and Hc as a function of the NiO layer thickness of t NiO + 30 Å Co + 30 Å Cu.*

range t is 50 Å to 500 Å and then slowly decreases when the NiO layer thickness is further increased. From this it can be concluded that a NiO layer thickness of 500 Å results in the largest exchange biasing field of approximate 13.5 kA/m. For comparison, in Molecular-Beam-Epitaxy grown NiFe/FeMn bilayers maximum exchange biasing fields up to 25 kA/m are obtained [Jung94].

Next we investigate the influence of the Co layer thickness on Hc and Hex. MOKE measurements are done on 500 Å NiO + t Co + 30 Å Cu (sample numbers 941280...941285), with t ranging from 10 Å to 80 Å. Figure 8.3 shows Hex and Hc as a function of the Co layer thickness. Hc has a maximum (60 kA/m) at t=15 Å and Hex decreases with increasing Co layer thickness. The sharp increase of Hc at low Co thicknesses has been related to island shape growth of the Co layer at small thicknesses. These islands decrease the polydomain behaviour of the Co, which increases Hc, controlled by the anisotropy present [Lub61, Jung94]. From figure 8.3.b we estimate that at thicknesses below about 15 Å the Co layer grows in islands. The decrease of Hex as a function of the Co layer thickness is proportional to 1/t,

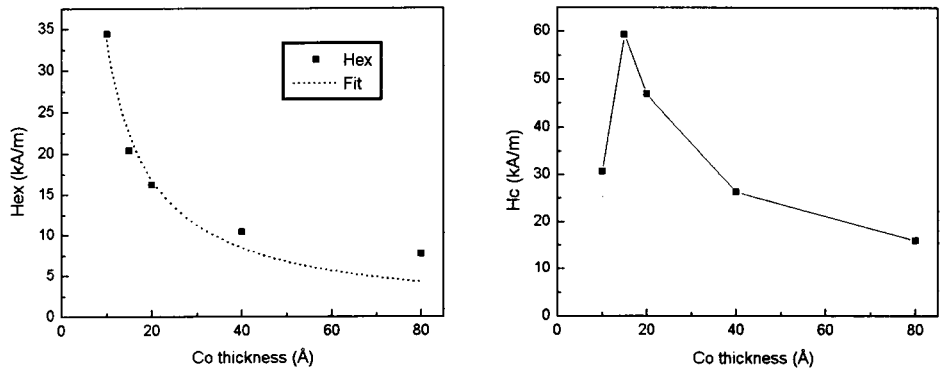

Figure 8.3: *Hex and Hc as a function of the Co layer thickness of 500 Å NiO + t Co + 30 Å Cu. Hex is fitted proportionally to 1/t.*

in agreement with FeMn exchange biased layers as reported in literature [Jung94]. This 1/t behaviour is usually related to interfacial nature of the exchange biasing interaction effect.

Finally the exchange biasing of Co layers with NiO layer on top was investigated. The NiO layer on top has to be grown at room temperature to prevent interdiffusion in the Co layer, in contrast to NiO on bottom, which can be grown at 200 °C to obtain a better quality layer (section 8.2.2). In figure 8.4 Hex and Hc is shown as a function of the NiO layer thickness of the structure: 30 Å Co + t NiO (sample numbers 941292...941297), with t ranging from 50 Å to 2000 Å. Hex shows similar behaviour as with NiO on bottom, but has a higher maximum

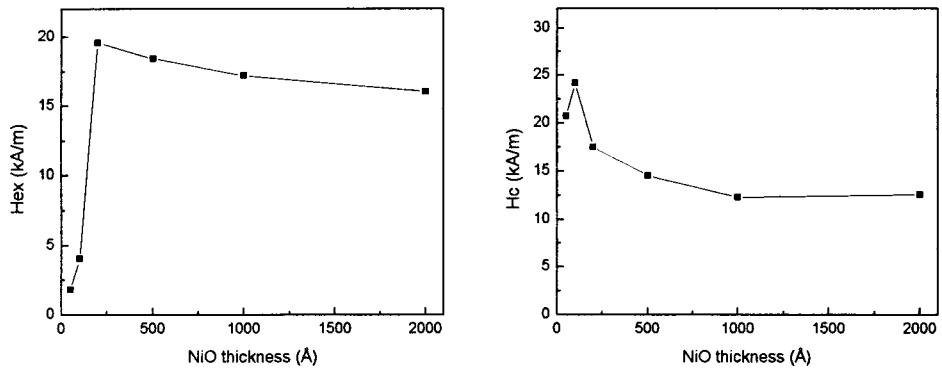

Figure 8.4: *Hex and Hc as a function of the NiO layer thickness of 30 Å Co + t NiO.*

(about 19 kA/m) at a lower NiO layer thickness (200 Å). However, Hc is significantly lower than in the case of NiO on bottom and decreases with increasing NiO layer thickness.

Although Hex has the highest value (19 kA/m) for NiO on top, we choose to construct our spin-valves with NiO on bottom. This has several reasons. As NiO is an insulator, a thick NiO top layer might prevent us from measuring the resistance of an underlying structure, as we do these measurements with point contacts on top of the samples. Although Hex has the highest value for NiO on top, Hc is significantly lower with NiO on top. This high Hc will proof to be our main source for anti-parallel alignment. We therefore have constructed spin-valves with basically the following structure: 500 Å NiO + 20 Å Co + 20 Å Cu + t Co. The exchange biased Co layer is 20 Å thick to obtain maximum Hc and Hex, but to be outside the island-shape Co regime, which was estimated 15 Å thick.

8.2.2 X-ray diffraction

To investigate the structure and texture of our spin-valves with NiO we performed X-ray diffraction measurements on three samples with sample number 941268, 941297 and 941291.

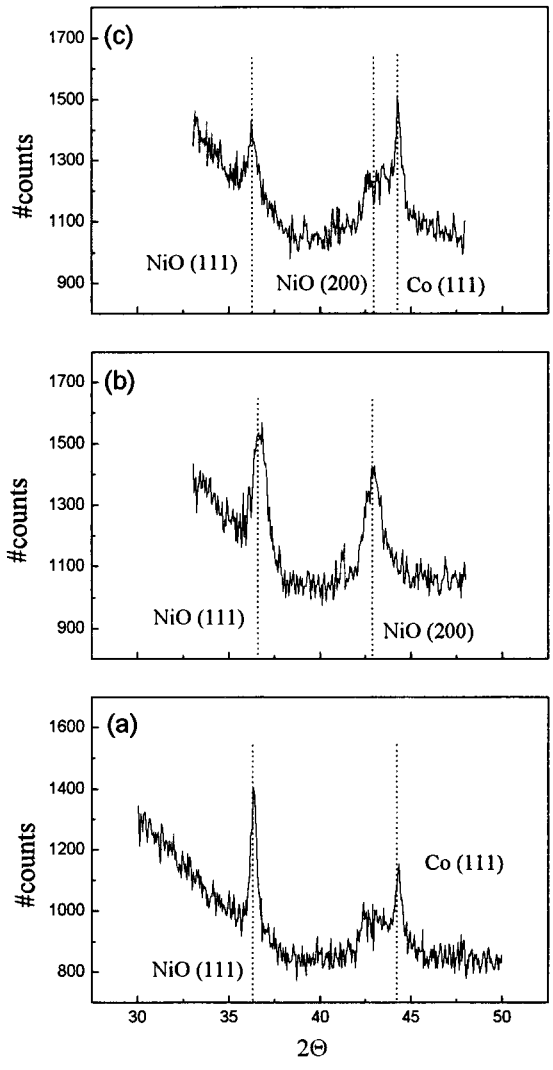

Figure 8.5: High angle θ-2θ X-ray diffraction measurements of sample number (a) 941291, (b) 941297 and (c) 941268.

As we are basically interested in the NiO layer we have grown thick NiO layers (2000 Å). Figure 8.5.a shows the high angle X-ray measurement of sample 941291, with the composition 2000 Å NiO + 30 Å Co + 30 Å Cu. The 2000 Å NiO layer was grown at 200 °C. The peak at 2θ=36.3° corresponds with an interatomic distance d=2.475 Å. This is probably NiO in (111) texture with an expected interatomic distance d=2.410 Å. Rocking curves on this peak position are very broad (more than 10 degrees), and this is an indication for large spread in orientation of the crystallites. A second clear peak shows up at 2θ=44° which corresponds to Co in (111) texture, although this peak also might result from Cu in (111) texture.

In figure 8.5.b the high angle X-ray diffraction pattern of sample 941297 is presented, which has the following composition: 30 Å Co + 2000 Å NiO. The 2000 Å NiO layer was grown at room temperature. The peak which corresponds to NiO in (111) texture is also present in this sample but the peak is broader than in sample 941291. A second peak shows up at about 43°, which corresponds to NiO (200). This indicates that NiO grown at room

temperature has at least two crystalline orientations.

Finally the X-ray diffraction pattern of sample 941268 is shown in figure 8.5.c, which is a complete spin-valve with the composition: 500 Å NiO + 30 Å Co + 20 Å Cu + 30 Å Co + 12 Å Cu + 100 Å NiO. Both NiO(111) and Co(111) peak show up in this pattern.

8.2.3 Spin-valve design

Basically, the samples have the following composition: 500 Å NiO + t1 Co + 20 Å Cu + t2 Co + 12 Å Cu + 100 Å NiO (t1=5...30 Å and t2=15...300 Å). The substrate on top of which this stucture is deposited is glass (dimensions: 12 × 4 mm^2). The samples were grown in a field to achieve exchange biasing between the 500 Å NiO layer and the t1 Å Co layer. Between the Co layer t2 and the top 100 Å NiO layer a 12 Å thin Cu layer is grown to prevent exchange biasing of the Co layer with the top NiO layer. A Cu layer thickness of 12 Å (5 monolayers) proved to be thick enough to ensure that there is no exchange biasing between Co layer t2 and the 100 Å NiO layer. The bottom 500 Å NiO layer was grown at 200°C to obtain good layer quality. The rest of the structure, including the top NiO layer was grown at room temperature to prevent interdiffusion.

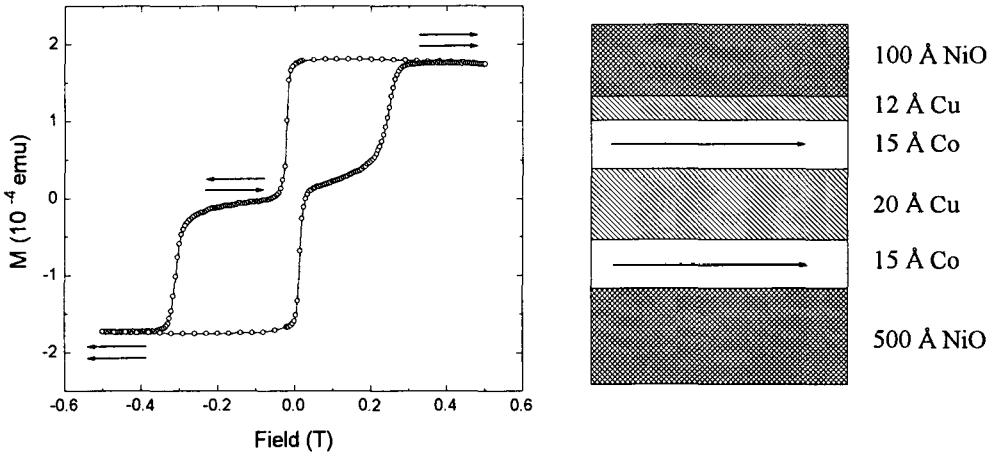

Figure 8.6: *Squid magnetization measurement of sample number 9410207, schematically drawn on the right. The alignment of the two Co layers is denoted with arrows. The temperature during measurement was 10K. The field was applied along the bias direction.*

Figure 8.6 shows the magnetization curve of sample 9410207 with the composition 500 Å NiO + 15 Å Co + 20 Å Cu + 15 Å Co + 12 Å Cu + 100 Å NiO. The magnetization curve is in agreement with the theoretical loop as described in figure 5.5.a and reflects an anti-parallel state at negative fields.

8.2.4 Magnetoresistance

In figure 8.7 we present a typical magnetoresistance curve of a Co/Cu/Co spin-valve exchange biased to NiO. The sample has the following composition: 500 Å NiO + 20 Å Co + 20 Å Cu + t Co + 12 Å Cu + 100 Å NiO, with t=25 Å (sample number 950288).

The giant magnetoresistance of this sample is 22.5%. This is very high as compared to literature. For example in FeMn exchange biased Co/Cu/Co spin-valves a maximum magnetoresistance is obtained of about 12% at low temperature for an exchange biased Co layer thicknesses of 50 Å and a free Co layer thickness of 80 Å [Sour94]. In chapter 6 we obtained 6% magnetoresistance at low temperature for a Co/Cu/Co spin-valve with Co layer thicknesses of 25 Å and 100 Å. Dieny reported up to 9.5% magnetoresistance at room temperature for FeMn

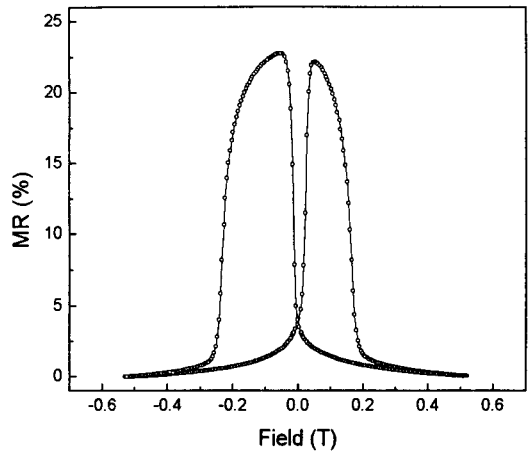

Figure 8.7: *Typical magnetoresistance curve for Co/Cu/Co spin-valves with NiO. The measurement temperature was 10K and the sample number 950288.*

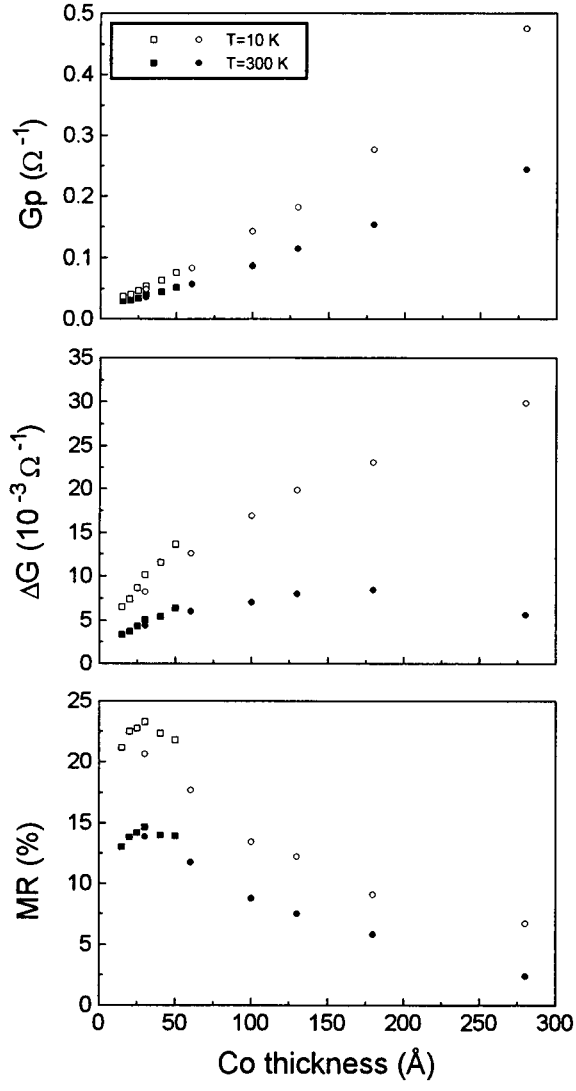

Figure 8.8: *Gp, ΔG and MR as a function of the free Co layer thickness of sample numbers 950286...950291 (squares) and 9503217... 9503222 (circles).*

exchange biased Co/Cu/Co [Dien93]. Upon variation of the free Co layer thickness t between 15 Å and 280 Å, the magnetoresistance has a maximum at t≈30 (figure 8.8). The differential conductivity increases exponentially with increasing free layer thickness t. The conductivity in parallel alignment also increases with increasing free layer thickness t. The most prominent feature, however, is the magnitude of the MR ratio as compared to, for example, the MR of FeMn exchange biased spin-valves [Sour94].

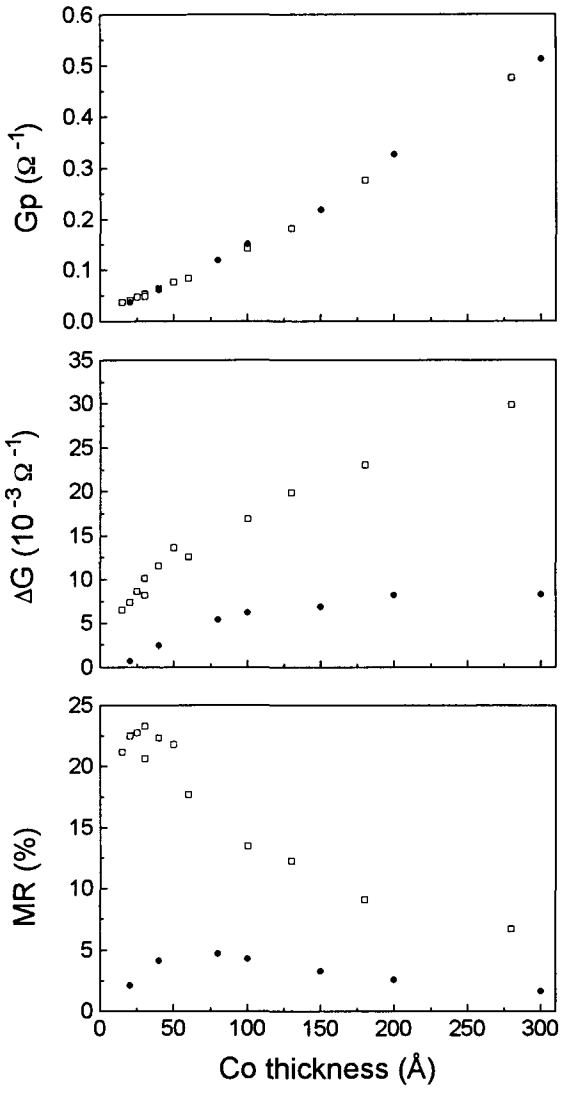

Figure 8.9: *Gp, ΔG and MR as a function of the free Co layer thickness t of 500 Å NiO + 20 Å Co + 20 Å Cu + t Co + 12 Å Cu + 100 Å NiO at 10K (open squares) and 30 Å Ta + t Co + 30 Å Cu + 20 Å Co + 100 Å FeMn + 20 Å Ta at 5K (solid circles, data from [Sour94]).*

To illustrate this we compare in figure 8.9 Gp, ΔG and MR of our NiO exchange biased Co/Cu spin-valves with measurements by Sour on FeMn exchange biased Co/Cu spin-valves. These FeMn exchange biased spin-valves have the following structure: 30 Å Ta + t Co + 30 Å Cu + 20 Å Co + 100 Å FeMn + 20 Å Ta (with t=0...300 Å). The magnitude and Co free layer thickness dependence of Gp is equal for both FeMn and NiO spin-valves. However, as for the FeMn exchange biased Co/Cu/Co spin-valves the non-magnetic Cu layer is 30 Å thick as compared to 20 Å for the NiO based spin-valves, the fact that FeMn is no insulator in contrast to NiO and the measurements are done at 5 K instead of 10 K, we can say that the conductivity of the NiO based spin-valves is slightly higher under equal conditions than for the

FeMn biased spin-valves. Both ΔG and MR are much higher for the NiO biased spin-valves than for the FeMn biased spin-valves. The maximum MR for the FeMn biased spin-valves is reached at about a free Co layer thickness of 80 Å, while for the NiO biased spin-valves the maximum is reached at about 30 Å.

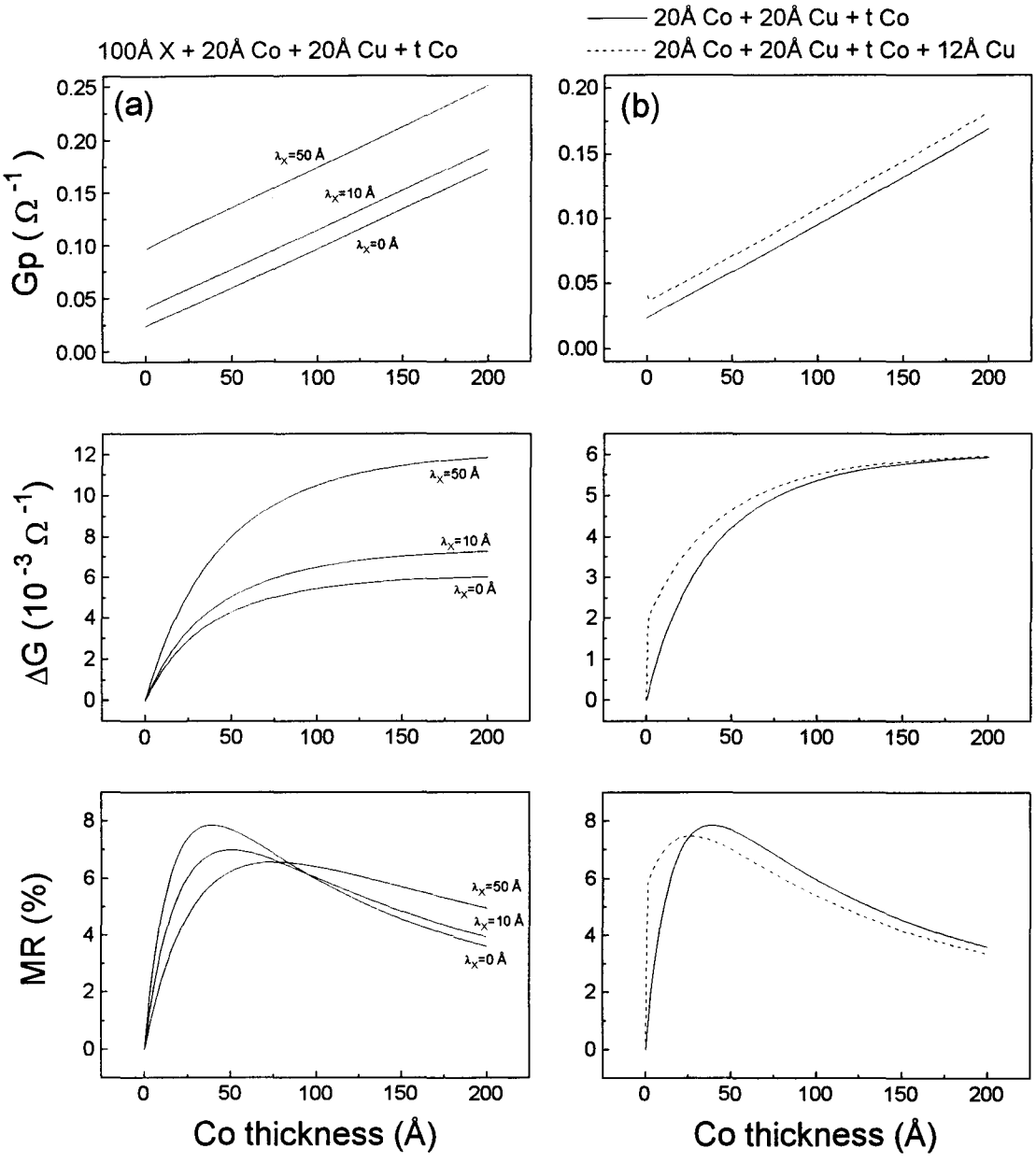

Figure 8.10: *Camley-Barnas model calculations to gain insight in (a) the effect of an extra non-insulating layer and (b) the effect of the 12 Å Cu layer.*

We will try to understand the physical mechanism behind this unusually large MR. First, NiO is an insulator. So electrons are not allowed to leave the spin-valve via e.g. a non-insulating antiferromagnetic bias layer, which may lead to a shunting effect. Shunting is the effect that part of the current flows through regions of the sample which do not contribute to the magnetoresistance effect. As the relative change in conductivity is lower than without shunting the magnetoresistance decreases.

In figure 8.10.a we have calculated a model spin-valve to gain insight in the effect of an extra non-insulating antiferromagnetic bias layer on Gp, ΔG and MR. The model spin-valve

has the composition: 100 Å X + 20 Å Co + 20 Å Cu + t Co. Mean free paths are used of $\lambda^{\uparrow}_{Co}$=90 Å, $\lambda^{\downarrow}_{Co}$=10 Å and λ_{Cu}=200 Å. The interface spin-dependent transmission coefficients at the Co/Cu interface are taken $T^{\uparrow}$=1 and $T^{\downarrow}$=0.2. We do not claim that these are the exact values for mean free paths and transmission coefficients in the bulk and at the interfaces of Co and Cu, but we only want to gain insight in the shunting effect. Therefore we have used mean free paths and transmission coefficients which seem to be in agreement with literature [Dien93]. The transmission coefficients at the X/Co interface were taken spin-independent and unity. At the outer boundaries of the stack of layers total diffusive scattering was assumed. The mean free path of the imaginary material X is taken 0, 10 and 50 Å. The conductivity

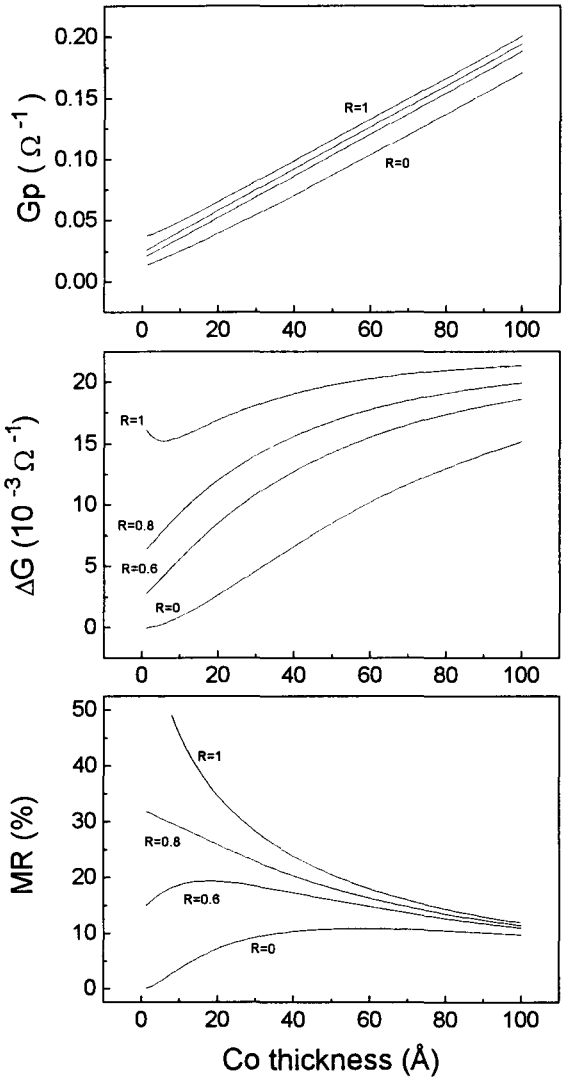

Figure 8.11: *Camley-Barnas calculation of the spin-valve 20 Å Co + 20 Å Cu + t Co with a nonzero reflection coefficient R at the outer boundaries ranging from 0 to 1.*

Gp increases with increasing mean free path of material X. The differential conductivity ΔG also increases with increasing mean free path of material X, due to an effective larger area where a difference in Gp and Gap takes place. The maximum of the magnetoresistance ratio MR moves to lower Co thickness with increasing mean free path λ_X. This may explain at least partly why the maximum magnetoresistance in this study occurs at about 30 Å, while in the FeMn/Co/Cu/Co system the maximum occurs at 80 Å. FeMn was estimated to have a mean free path $\lambda \approx$10 Å [Sour94], and this nonzero mean free path moves the maximum

magnetoresistance to higher Co thicknesses. The decrease of λ_X from 10 Å to 0 Å increases the maximum MR from 7% to 8%. So the insulating character of NiO increases MR not enough to explain the high magnetoresistance ratios obtained as measured in these spin-valves.

Second we have calculated the influence of the 12 Å Cu layer in the spin-valve. Figure 8.10.b shows the Camley-Barnas calculation for the spin-valve 20 Å Co + 20 Å Cu + t Co with (solid) and without (dashed) a top 12 Å Cu layer. Spin-dependent mean free paths and transmission coefficient were taken as before (figure 8.10.a). At small Co thicknesses t, the 12 Å Cu layer effectively enlarges the area where a difference in Gp and Gap takes place. This results in a maximum MR at lower Co thickness than without the Cu layer. The maximum MR, however, is almost equal with and without Cu top layer. So the 12 Å Cu layer also cannot explain the large magnetoresistance.

Third we will consider the influence of reflections at the NiO interface, which we might expect because of the insulating character of NiO (see also section 3.4). Introducing reflections of electrons at NiO interfaces, increases both MR and ΔG significantly as can be seen in figure 8.11. In this figure a calculation is shown of the spin-valve 20 Å Co + 20 Å Cu + t Co + 12 Å Cu. We have chosen $\lambda^{\uparrow}_{Co}$=100 Å, $\lambda^{\downarrow}_{Co}$=10 Å, λ_{Cu}=200 Å and spin-dependent transmission coefficients $T^{\uparrow}$=1 and $T^{\downarrow}$=0.2 at the Co/Cu interface. Spin-independent reflection coefficients R at the outer boundaries of the spin-valve range from 0 to 1.

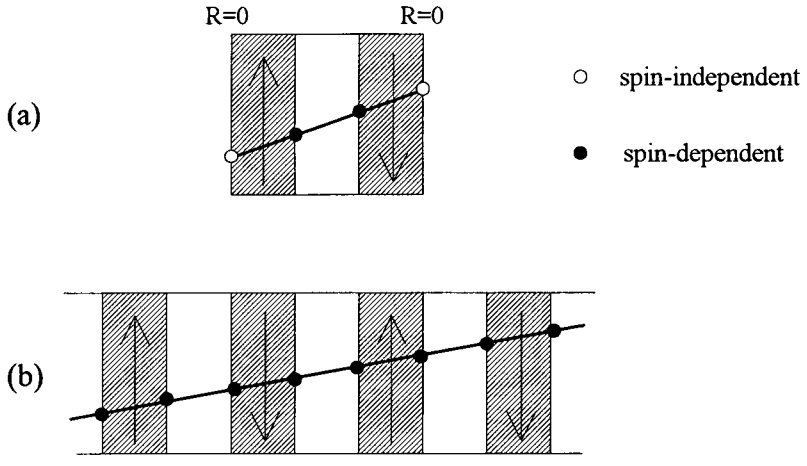

Figure 8.12: *Schematic representation of a Spin-valve (a) and a multilayer (b). The solid lines represent imaginary paths electrons, which can scatter spin-dependent or spin-independent.*

The increase in ΔG and MR can be understood as follows. By introducing a reflection coefficient R=1 at the outer boundaries of the spin-valve, the trilayer structure is effectively reflected at the boundaries until infinity. The magnetoresistance of such a structure is the same as an infinite multilayer of repeating ferromagnetic/non-magnetic layers, which is markedly different from that of a spin-valve structure.

Figure 8.12 shows schematically a spin-valve and a multilayer. In case of a spin-valve the effect of spin-dependent scattering at the interfaces or in the bulk of the magnetic layers (represented by solid circles) is decreased by the relative important spin-independent scattering at the outer boundaries of the spin-valve (represented by open circles). On going from a spin-valve to a multilayer the spin-independent scattering boundary is replaced by a spin-dependent scattering interface. And thus spin-dependent scattering becomes more important and this effectively increases the magnetoresistance ratio.

But as only the fact that the magnetoresistance is higher is no direct proof for the existence of reflections at the NiO interface, we will try to establish in a direct way via experiments if reflections at NiO/metal interfaces occur.

8.2.5 Investigation of reflections

Single Co layers

The resistivity of a metal is inverse proportional to the mean free path of the electrons in the material. The mean free path is limited by scattering at impurities, defects, phonons and magnons. For a thin film the mean free path is also restricted by the dimensions of the film due to diffuse scattering at the outer boundaries of the film. This means that when the thickness of a Co layer is in the order of or less than the mean free path of the electrons, it has a higher resistivity than bulk Co.

When the thin film is sandwiched between a material which induces reflections at the interfaces, the mean free path of electrons is not restricted by film dimensions. Electrons reflect specular at the interfaces and have bulk mean free paths, and thus the film has bulk resistivity.

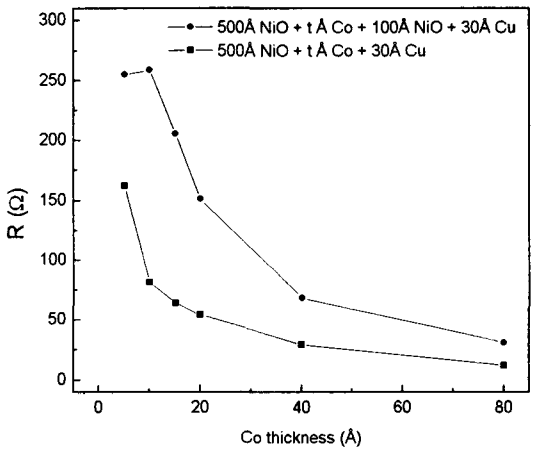

Figure 8.13: *Sheetresistance of a single Co layer sandwiched between two NiO layers (circles) and of a single Co layer grown on NiO and not covered with NiO (squares).*

To investigate if NiO/Co interfaces reflect electrons specular we measured the resistivity of two sets of samples. One set with a Co layer sandwiched between two NiO layers with the following composition: 500 Å NiO + t Co + 100 Å NiO + 30 Å Cu (sample numbers 941274...941279), with t=5...80 Å. The second set of samples consists of 500 Å NiO + t Co + 30 Å Cu (sample numbers 941280...941285), with t=5...80 Å. The 30 Å Cu layer is grown on top to prevent oxidation of the Co layer. Figure 8.13 shows the resistance as a function of t for both series of samples. Measurements are done at 10 K in a 1.35 T field to ensure equal alignment of the Co layers during every measurement. The sheet resistance of the Co layers sandwiched between two NiO layers is higher than the sheet resistance of the Co layers not covered with NiO, in contrast with what one would expect with reflections of electrons at the NiO interfaces.

However, these experiments don't rule out reflections only at the bottom 500 Å NiO layer, because this would result in similar behaviour of the resistivity as with no reflections. As the 500 Å NiO layer was grown at 200° C, this layer is expected to have the best interface quality, in contrast to the 100 Å NiO layer which was grown at room temperature.

Spin-valve without top NiO layer

In the preceding experiment on single Co layers we have seen that no traceable reflections occur at the top NiO layer. Therefore we have measured the magnetoresistance of two sets of spin-valves. One set with the composition 500 Å NiO + t Co + 20 Å Cu + t Co + 12

Å Cu + 100 Å NiO (sample numbers 950274...950279), and a serie with no 100 Å top layer with the composition 500 Å NiO + t Co + 20 Å Cu + t Co + 12 Å Cu (sample number 950280...950285). The Co thickness t was varied between 20 Å and 100 Å. Samples were not grown in field what resulted in poor anti-parallel alignment of the Co layers. In figure 8.14 we

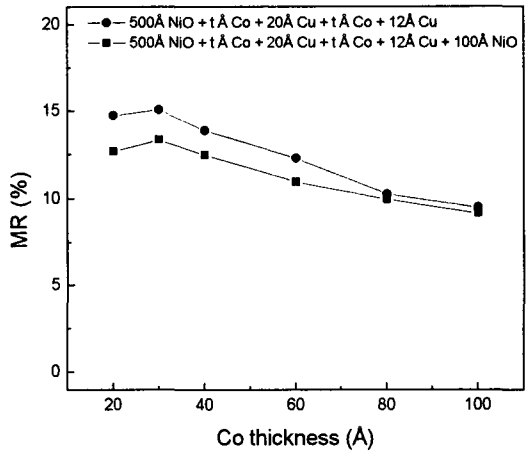

Figure 8.14: *Magnetoresistance of NiO/Co/Cu/Co as a function of the Co layer thickness with (squares) and without (circles) a NiO top layer. Measurements are done at 300K.*

present the magnetoresistance of the two series as a function of the Co layer thickness. The Magnetoresistance is little higher without a NiO top layer than with a NiO top layer. This proofs that the top NiO layer is not responsible for the high values of the magnetoresistance as obtained in the NiO biased spin-valves. As reflections at the bottom NiO layer are not excluded in the experiments on the single Co layers, the influence of the bottom NiO layer requires more investigation.

Influence of bottom NiO layer on the magnetoresistance

The bottom NiO layer is important for the degree of anti-parallel alignment of the total spin-valve. Any change of this layer influences the exchange biasing with the Co layer and therefore also the magnetoresistance. Nevertheless, we have tried to change the interface structure of the bottom NiO layer. A serie of 2 × 3 samples has been prepared consisting of 500 Å NiO + 20 Å Co + 20 Å Cu + t Co + 12 Å Cu + 100 Å NiO, with t=20,40 and 60 Å (sample numbers 950301...950306). For three samples the 500 Å NiO was grown at 200° and for three samples this layer was grown at room temperature. Although we have no means to determine the interface quality, we expect the NiO interface structure to become worse when the layer is grown at room temperature, because thicker NiO layers are visibly of poor structural quality when grown at room temperature. In section 8.2.2 X-ray measurements have been discussed which show that the texture of NiO grown at 200° C differs from NiO grown at room temperature.

Figure 8.15 shows the magnetoresistance for the samples 950301...950306. There is no reduction of the magnetoresistance in case of a NiO base layer grown at room temperature. Magnetoresistance is even slightly higher in the case of NiO grown at room temperature. As we have no check for the quality of the interface, it is difficult to draw any further conlusions from this experiment.

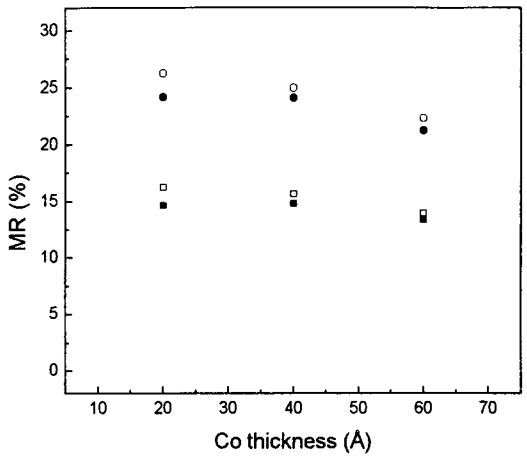

Figure 8.15: *Magnetoresistance as a function of the Co layer thickness for sample number 950301...950306. Both room temperature (squares) and 10K measurements (circles) are shown. The solid points are the samples with a NiO layer grown at 200°C and the open points are those with a NiO layer grown at room temperature.*

8.2.6 Conclusions

Magnetoresistance ratios up to 24% at low temperatures have been found in exchange biased Co/Cu/Co spin-valves sandwiched between NiO. This is a considerable increase with respect to stacks containing for example FeMn. Camley-Barnas calculations have shown that this high value for the magnetoresistance may be explained with specular reflections of electrons at NiO/Co interfaces, due to potential scattering at the impenetrable NiO.

However, no direct proof for reflections has been found in comparing single Co layers sandwiched between NiO and single Co layers without a top NiO layer. Spin-valves NiO/Co/Cu/Co with and without a top NiO layer showed comparable magnetoresistance ratios, which proofs that the top NiO layer is not responsible for high magnetoresistance ratios. However, these experiments leave open the possibility of reflections at the bottom NiO interface.

To summarize, we may conclude that no direct proof for reflections at NiO/metal interfaces has been found. We were not able to explain the high magnetoresistance ratios as compared to other systems in terms of reflections at the impenetrable NiO.

8.2.7 Future plans

As we were not able to show any reflections which may account for the observed magnetoresistance ratios, we must search for another explanation for the high magnetoresistance ratios. A few aspects of the spin-valves were not investigated thouroughly.

First we have not investigated the role of spin-dependent scattering or reflection at the NiO interface and in particular the NiO/Co interface which is an antiferromagnetic/ferromagnetic interface. This can be investigated by using other insulators than NiO. MgO for example is an insulator but no antiferromagnet, and therefore suitable for comparing with NiO. Also CoO can may be interesting in this respect, because CoO is an antiferromagnet with a Néel temperature close to roomtemperature. This enables a measurement of the magnetoresistance below and above the Néel temperature.

Second we have not studied on the role of interface roughness. As we have seen in chapter 2 interface roughness may enhance the magnetoresistance as well. A study of molecular-beam-epitaxy grown NiO/Co/Cu/Co spin-valves with sharper interfaces may be usefull.

8.3 NiO exchange biased $Ni_{80}Fe_{20}/Cu/Ni_{80}Fe_{20}$

From a technological point of view $Ni_{80}Fe_{20}/Cu/Ni_{80}Fe_{20}$ spin-valves are interesting for application in GMR heads for magnetic recording. As a single $Ni_{80}Fe_{20}$ layer has low coercive fields, changes in alignment of the magnetic layers of the spin-valve can be obtained at very low fields. In this respect the sensitivity, defined as the change in magnetoresistance per change in field (sensitivity = $\Delta MR/\Delta H$) is an important parameter.

In the previous sections we have seen that in Co/Cu/Co spin-valves the magnetoresistance ratio is enhanced by a factor 2 when exchange biased with NiO. Therefore, we have measured the magnetoresistance of NiO exchange biased $Ni_{80}Fe_{20}/Cu/Ni_{80}Fe_{20}$ spin-valves to investigate the effect of NiO in these kind of spin-valves. The measurements and discussion are far from conclusive and therefore we will focus on the results as obtained and we will give some suggestions for further research concerning these kind of spin-valves.

8.3.1 Sample design

The samples have basically the following composition: 500 Å NiO + 20 Å $Ni_{80}Fe_{20}$ + 20 Å Cu + t $Ni_{80}Fe_{20}$ + 12 Å Cu + 100 Å NiO. This composition proved to give high magnetoresistance ratios for Co/Cu in section 8.2. Therefore we adopted this composition for $Ni_{80}Fe_{20}$ also. The thickness of the free $Ni_{80}Fe_{20}$ layer t varies between 15 and 300 Å. Figure 8.16 shows a representative MOKE measurement at room temperature. The low anisotropy of the $Ni_{80}Fe_{20}$

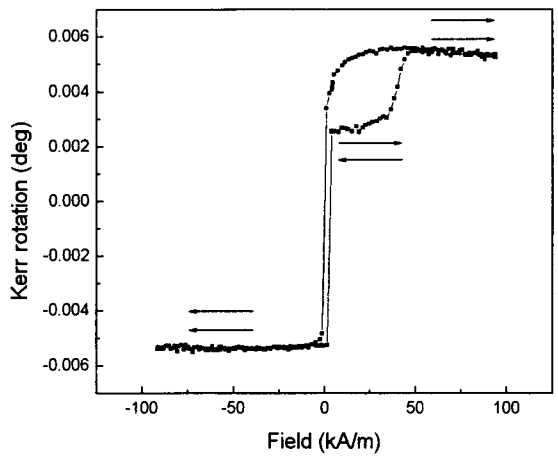

Figure 8.16: *MOKE measurement at room temperature for sample number 9502174 with a free $Ni_{80}Fe_{20}$ layer thickness t=30 Å. Arrows denote the relative orientation of the magnetic layers.*

layer is reflected by a sharp flip of the free $Ni_{80}Fe_{20}$ layer at zero field. The plateau between 0 and 50 kA/m of the anti-parallel state is not fully horizontal what implies that no full anti-parallel state of the magnetic moments of the layers is obtained.

8.3.2 Magnetoresistance results

In figure 8.17 we present a representative 10K magnetoresistance curve of sample number 9502174. This sample has the composition: 500 Å NiO + 20 Å $Ni_{80}Fe_{20}$ + 20 Å Cu + 30 Å $Ni_{80}Fe_{20}$ + 12 Å Cu + 100 Å NiO. No horizontal plateau is obtained in the magnetoresistance which can be related to an incomplete parallel alignment of the magnetic moments.

Figure 8.18 shows the magnetoresistance as a function of the $Ni_{80}Fe_{20}$ free layer thickness t for temperatures of 10K and 300K. The magnetoresistance at low temperatures has a

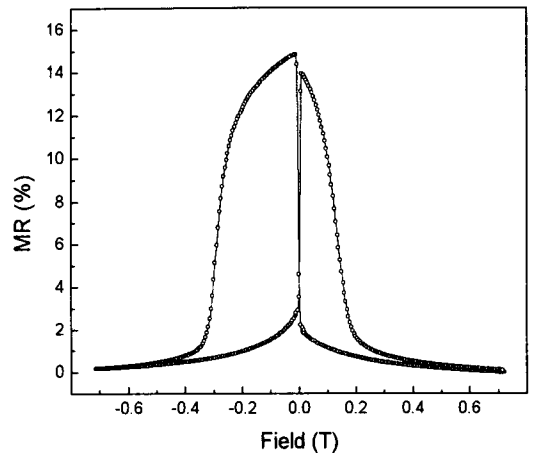

Figure 8.17: *10K magnetoresistance measurement of sample number 9502174, with a free $Ni_{80}Fe_{20}$ layer thickness of 30 Å.*

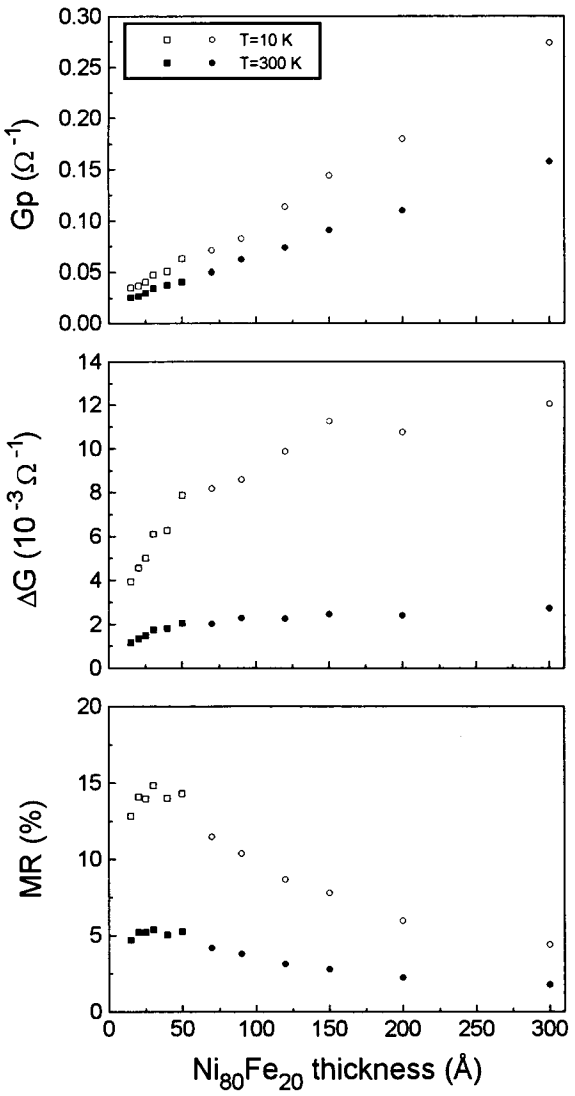

Figure 8.18: *Gp, ΔG and MR as a function of the free $Ni_{80}Fe_{20}$ layer thickness of sample numbers 9502171...9502176 (squares) and 9502177...9502182 (circles).*

maximum at about t=30 Å of 15%.

In FeMn exchange biased spin-valves magnetoresistance ratios of about 9% at 5K are obtained at NiFe free layer thicknesses of approximately 80 Å [Sour94]. Dieny reported magnetoresistance ratios for FeMn exchange biased $Ni_{80}Fe_{20}/Cu/Ni_{80}Fe_{20}$ of maximum 5% at roomtemperature [Dien93]. The enhancement is not as dramatic as for the NiO/Co/Cu/Co spin-valves (compared to FeMn/Co/Cu/Co). As we have performed no systematic research yet to investigate the role of reflections at the $NiO/Ni_{80}Fe_{20}$ interfaces, no conclusions about the role of reflections for the magnitude of the magnetoresistance can be drawn. The position of the maximum magnetoresistance at 30 Å $Ni_{80}Fe_{20}$, compared to FeMn biased at 80 Å is an effect of the 12 Å Cu layer and the insulating character of the NiO layer in a similar way as was demonstrated in section 8.2.4 and figure 8.10 for Co/Cu.

8.3.3 Sensitivity

An important parameter for magnetic sensors is the sensitivity, which is defined as the change in magnetoresistance per change in field:

$$S = \frac{\Delta MR}{\Delta H}. \tag{8.1}$$

This change in resistivity is the highest at the onset between parallel and anti-parallel alignment of the magnetic moments of the two magnetic layers. For sample number 9502172 with the composition 500 Å NiO + 20 Å $Ni_{80}Fe_{20}$ + 20 Å Cu + 20 $Ni_{80}Fe_{20}$ + 12 Å Cu + 100 Å NiO, a sensitivity of 0.17 %/Oe has been obtained at room temperature. Dieny reported a sensitivity of 2 %/Oe for FeMn exchange biased NiFe/Cu/NiFe [Dien93].

8.3.4 Conclusions and discussion

We have obtained a magnetoresistance ratio of 15% at 10K for the following structure: 500 Å NiO + 20 Å $Ni_{80}Fe_{20}$ + 20 Å Cu + t $Ni_{80}Fe_{20}$ + 12 Å Cu + 100 Å NiO, with t=30 Å. As a function of the free layer thickness t, the magnetoresistance at 10K has a maximum of 15% for t=30 Å after which it decreases to 5% for t=300 Å. Room temperature magnetoresistance ratios of maximum 5% are obtained, which is comparable to values as reported by Dieny [Dien93]. We have obtained a sensitivity of 0.17 %/Oe for t=20 Å at room temperature.

MOKE measurements show that no complete anti-parallel alignment of the magnetic layers is obtained, which might have a negative (lowering) effect on the magnetoresistance. Therefore a systematical investigation of the exchange biasing and the coercive fields in this NiO/NiFe system has to be performed in order to improve the antiparallel alignment.

Spin-valves must be able to endure high temperatures (typical up to 150°C) in connection with a possible application for NiO exchange biased spin-valves in magnetic sensors. This temperature endurance has to be tested by heating up the sample in air for a certain time interval (typical 2 min) and then measure the magnetoresistance at room temperature. First results obtained recently indicate that heating to about 180°C does not lead to a drastic reduction of the magnetoresistance ratio at room temperature.

Appendix A

List of samples

In this appendix a list of all the samples is given. The layer thicknesses are given in Å=10^{-10}m. Layer thicknesses were calculated from the sputter deposition rate and the sputtering time. The sputter deposition rate was determined by low angle X-ray diffraction measurements on a single film. Deviations up to 5% can be expected in the layer thicknesses. The samplenumbers are chronologically listed on preparation date. Sample number 941082 indicates that this sample was the 82nd sample sputtered in november 1994.

substrate : SiO_2, baselayer : 200Ru, toplayer : 30Ru base pressure : $5{\cdot}10^{-7}$ Torr, sputter pressure : $7{\cdot}10^{-3}$ Torr sputter deposition rate (Å/s) : Ru=1, Cu=2, Co=2	
sample number	composition
941082	75Co+6Ru+25Co+30Ru+100Co+10Cu
941083	75Co+6Ru+25Co+2Cu+30Ru+2Cu+100Co+10Cu
941084	75Co+6Ru+25Co+4Cu+30Ru+4Cu+100Co+10Cu
941085	75Co+6Ru+25Co+6Cu+30Ru+6Cu+100Co+10Cu
941086	75Co+6Ru+25Co+15Ru+4Cu+15Ru+100Co+10Cu
941087	75Co+6Ru+25Co+15Ru+8Cu+15Ru+100Co+10Cu
941088	75Co+6Ru+25Co+15Ru+12Cu+15Ru+100Co+10Cu
941089	75Co+6Ru+15Co+2Cu+10Co+30Ru+10Co+2Cu+90Co+10Cu
941090	75Co+6Ru+15Co+4Cu+10Co+30Ru+10Co+4Cu+90Co+10Cu
941091	75Co+6Ru+15Co+6Cu+10Co+30Ru+10Co+6Cu+90Co+10Cu

substrate : SiO_2, baselayer : 200Ru, toplayer : 30Ru base pressure : $5{\cdot}10^{-7}$ Torr, sputter pressure : $7{\cdot}10^{-3}$ Torr sputter deposition rate (Å/s) : Ru=1, Cu=2, Co=2	
sample number	composition
941095	75Co+6Ru+25Co+30Cu+100Co+10Cu
941096	75Co+6Ru+25Co+2Ru+30Cu+2Ru+100Co+10Cu
941097	75Co+6Ru+25Co+4Ru+30Cu+4Ru+100Co+10Cu
941098	75Co+6Ru+25Co+6Ru+30Cu+6Ru+100Co+10Cu
941099	75Co+6Ru+25Co+15Cu+4Ru+15Cu+100Co+10Cu
9410100	75Co+6Ru+25Co+15Cu+8Ru+15Cu+100Co+10Cu
9410101	75Co+6Ru+25Co+15Cu+12Ru+15Cu+100Co+10Cu
9410102	75Co+6Ru+15Co+1Ru+10Co+30Cu+10Co+1Ru+90Co+10Cu
9410103	75Co+6Ru+15Co+2Ru+10Co+30Cu+10Co+2Ru+90Co+10Cu
9410104	75Co+6Ru+15Co+3Ru+10Co+30Cu+10Co+3Ru+90Co+10Cu

substrate : SiO_2, baselayer : 200Ru, toplayer : 30Ru
base pressure : $4 \cdot 10^{-7}$ Torr, sputter pressure : $7 \cdot 10^{-3}$ Torr
sputter deposition rate (Å/s) : Ru=1, Cu=2, Co=2

sample number	composition
9410105	75Co+6Ru+25Co+30Cu+100Co+10Cu
9410105	75Co+6Ru+25Co+30Cu+10Co+2Cu+90Co+10Cu
9410105	75Co+6Ru+25Co+30Cu+10Co+4Cu+90Co+10Cu
9410105	75Co+6Ru+25Co+30Cu+10Co+6Cu+90Co+10Cu
9410105	75Co+6Ru+25Co+30Cu+10Co+2Cu+10Co+2Cu+80Co+10Cu
9410105	75Co+6Ru+25Co+30Cu+10Co+4Cu+10Co+4Cu+80Co+10Cu
9410105	75Co+6Ru+25Co+30Cu+10Co+6Cu+10Co+6Cu+80Co+10Cu
9410105	75Co+6Ru+25Co+30Cu+10Co+2Cu+10Co+2Cu+10Co+2Cu+70Co+10Cu
9410105	75Co+6Ru+25Co+30Cu+10Co+4Cu+10Co+4Cu+10Co+4Cu+70Co+10Cu
9410105	75Co+6Ru+25Co+30Cu+10Co+6Cu+10Co+6Cu+10Co+6Cu+70Co+10Cu

substrate : glass, grown in field
base pressure : $7 \cdot 10^{-7}$ Torr, sputter pressure Co and Cu: $7 \cdot 10^{-3}$ Torr, T=RT
sputter pressure 200NiO and 500NiO: $1 \cdot 10^{-3}$ Torr, T=200°C
sputter pressure 100NiO : $1 \cdot 10^{-3}$ Torr, T=RT
sputter deposition rate (Å/s) : Cu=2, NiO=0.5, Co=2

sample number	composition
9410204	200NiO+15Co+20Cu+15Co+4Cu+100NiO
9410205	200NiO+15Co+20Cu+15Co+8Cu+100NiO
9410206	200NiO+15Co+20Cu+15Co+12Cu+100NiO
9410207	500NiO+15Co+20Cu+15Co+12Cu+100NiO
9410208	200NiO+15Co+15Cu+15Co+8Cu+100NiO
9410209	200NiO+15Co+10Cu+15Co+8Cu+100NiO

substrate : glass
base pressure : $3 \cdot 10^{-7}$ Torr, sputter pressure Fe and Cr: $7 \cdot 10^{-3}$ Torr, T=RT
sputter pressure 200NiO : $1 \cdot 10^{-3}$ Torr, T=200°C
sputter pressure 50NiO : $1 \cdot 10^{-3}$ Torr, T=RT
sputter deposition rate (Å/s) : Fe=2, NiO=0.5, Cr=2

sample number	composition
941114	200NiO+8Fe+9Cr+8Fe+50NiO+100Cr
941115	200NiO+10Fe+9Cr+10Fe+50NiO+100Cr
941116	200NiO+12Fe+9Cr+12Fe+50NiO+100Cr
941117	200NiO+14Fe+9Cr+14Fe+50NiO+100Cr
941118	200NiO+16Fe+9Cr+16Fe+50NiO+100Cr
941119	200NiO+18Fe+9Cr+18Fe+50NiO+100Cr
941120	200NiO+20Fe+9Cr+20Fe+50NiO+100Cr
941121	200NiO+22Fe+9Cr+22Fe+50NiO+100Cr
941122	200NiO+24Fe+9Cr+24Fe+50NiO+100Cr
941123	200NiO+26Fe+9Cr+26Fe+50NiO+100Cr

substrate : glass base pressure : $4 \cdot 10^{-7}$ Torr, sputter pressure Fe and Cr: $7 \cdot 10^{-3}$ Torr, T=RT sputter pressure 200NiO : $1 \cdot 10^{-3}$ Torr, T=200°C sputter pressure 50NiO : $1 \cdot 10^{-3}$ Torr, T=RT sputter deposition rate (Å/s) : Fe=2, NiO=0.5, Cr=2	
sample number	composition
941128	200NiO+50Cr+8Fe+9Cr+8Fe++50Cr+50NiO
941129	200NiO+50Cr+10Fe+9Cr+10Fe+50Cr+50NiO
941130	200NiO+50Cr+12Fe+9Cr+12Fe+50Cr+50NiO
941131	200NiO+50Cr+14Fe+9Cr+14Fe+50Cr+50NiO
941132	200NiO+50Cr+16Fe+9Cr+16Fe+50Cr+50NiO
941133	200NiO+50Cr+18Fe+9Cr+18Fe+50Cr+50NiO
941134	200NiO+50Cr+20Fe+9Cr+20Fe+50Cr+50NiO
941135	200NiO+50Cr+22Fe+9Cr+22Fe+50Cr+50NiO
941136	200NiO+50Cr+24Fe+9Cr+24Fe+50Cr+50NiO
941137	200NiO+50Cr+26Fe+9Cr+26Fe+50Cr+50NiO

substrate : SiO_2, baselayer : 200Ru, toplayer : 30Ru base pressure : $6 \cdot 10^{-7}$ Torr, sputter pressure : $7 \cdot 10^{-3}$ Torr sputter deposition rate (Å/s) : Ru=1, Cu=2, Co=2	
sample number	composition
9411177	75Co+6Ru+25Co+30Cu+100Co+10Cu
9411178	75Co+6Ru+25Co+1Ru+30Cu+1Ru+100Co+10Cu
9411179	75Co+6Ru+25Co+2Ru+30Cu+2Ru+100Co+10Cu
9411180	75Co+6Ru+25Co+3Ru+30Cu+3Ru+100Co+10Cu
9411181	75Co+6Ru+25Co+4Ru+30Cu+4Ru+100Co+10Cu
9411182	75Co+6Ru+25Co+6Ru+30Cu+6Ru+100Co+10Cu
9411183	75Co+6Ru+25Co+15Cu+2Ru+15Cu+100Co+10Cu
9411184	75Co+6Ru+25Co+15Cu+4Ru+15Cu+100Co+10Cu
9411185	75Co+6Ru+25Co+15Cu+6Ru+15Cu+100Co+10Cu
9411186	75Co+6Ru+25Co+15Cu+12Ru+15Cu+100Co+10Cu

substrate : SiO_2, baselayer : 200Ru, toplayer : 30Ru base pressure : $5 \cdot 10^{-7}$ Torr, sputter pressure : $7 \cdot 10^{-3}$ Torr sputter deposition rate (Å/s) : Ru=1, Cu=2, Co=2	
sample number	composition
9411190	75Co+6Ru+25Co+30Cu+100Co+10Cu
9411191	75Co+6Ru+25Co+30Cu+2Ru+100Co+10Cu
9411192	75Co+6Ru+25Co+30Cu+2Co+2Ru+98Co+10Cu
9411193	75Co+6Ru+25Co+30Cu+4Co+2Ru+96Co+10Cu
9411194	75Co+6Ru+25Co+30Cu+6Co+2Ru+94Co+10Cu
9411195	75Co+6Ru+25Co+30Cu+10Co+2Ru+90Co+10Cu
9411196	75Co+6Ru+25Co+30Cu+20Co+2Ru+80Co+10Cu
9411197	75Co+6Ru+25Co+30Cu+40Co+2Ru+60Co+10Cu
9411198	75Co+6Ru+25Co+30Cu+60Co+2Ru+40Co+10Cu
9411199	75Co+6Ru+25Co+30Cu+80Co+2Ru+20Co+10Cu

substrate : glass, grown in field base pressure : $3 \cdot 10^{-7}$ Torr, sputter pressure Co and Cu: $7 \cdot 10^{-3}$ Torr, T=RT sputter pressure 500NiO : $1 \cdot 10^{-3}$ Torr, T=200°C sputter pressure 100NiO : $1 \cdot 10^{-3}$ Torr, T=RT sputter deposition rate (Å/s) : Cu=2, NiO=0.5, Co=2	
sample number	composition
941268	500NiO+30Co+20Cu+30Co+12Cu+100NiO
941269	500NiO+25Co+20Cu+25Co+12Cu+100NiO
941270	500NiO+20Co+20Cu+20Co+12Cu+100NiO
941271	500NiO+15Co+20Cu+15Co+12Cu+100NiO
941272	500NiO+10Co+20Cu+10Co+12Cu+100NiO
941273	500NiO+5Co+20Cu+5Co+12Cu+100NiO

substrate : glass, grown in field base pressure : $4 \cdot 10^{-7}$ Torr, sputter pressure Co and Cu: $7 \cdot 10^{-3}$ Torr, T=RT sputter pressure 500NiO : $1 \cdot 10^{-3}$ Torr, T=200°C sputter pressure 100NiO : $1 \cdot 10^{-3}$ Torr, T=RT sputter deposition rate (Å/s) : Cu=2, NiO=0.5, Co=2	
sample number	composition
941274	500NiO+5Co+100NiO+30Cu
941275	500NiO+10Co+100NiO+30Cu
941276	500NiO+15Co+100NiO+30Cu
941277	500NiO+20Co+100NiO+30Cu
941278	500NiO+40Co+100NiO+30Cu
941279	500NiO+80Co+100NiO+30Cu

substrate : glass, grown in field base pressure : $4 \cdot 10^{-7}$ Torr, sputter pressure Co and Cu: $7 \cdot 10^{-3}$ Torr, T=RT sputter pressure 500NiO : $1 \cdot 10^{-3}$ Torr, T=200°C sputter deposition rate (Å/s) : Cu=2, NiO=0.5, Co=2	
sample number	composition
941280	500NiO+5Co+30Cu
941281	500NiO+10Co+30Cu
941282	500NiO+15Co+30Cu
941283	500NiO+20Co+30Cu
941284	500NiO+40Co+30Cu
941285	500NiO+80Co+30Cu

substrate : glass, grown in field base pressure : $4 \cdot 10^{-7}$ Torr, sputter pressure Co and Cu: $7 \cdot 10^{-3}$ Torr, T=RT sputter pressure NiO : $1 \cdot 10^{-3}$ Torr, T=200°C sputter deposition rate (Å/s) : Cu=2, NiO=0.5, Co=2	
sample number	composition
941286	50NiO+30Co+30Cu
941287	100NiO+30Co+30Cu
941288	200NiO+30Co+30Cu
941289	500NiO+30Co+30Cu
941290	1000NiO+30Co+30Cu
941291	2000NiO+30Co+30Cu

substrate : glass, grown in field base pressure : $4 \cdot 10^{-7}$ Torr, sputter pressure Co and Cu: $7 \cdot 10^{-3}$ Torr, T=RT sputter pressure NiO : $1 \cdot 10^{-3}$ Torr, T=RT sputter deposition rate (Å/s) : Cu=2, NiO=0.5, Co=2	
sample number	composition
941292	30Co+50NiO
941293	30Co+100NiO
941294	30Co+200NiO
941295	30Co+500NiO
941296	30Co+1000NiO
941297	30Co+2000NiO

substrate : glass, grown in field base pressure : $4 \cdot 10^{-7}$ Torr, sputter pressure $Ni_{80}Fe_{20}$ and Cu: $7 \cdot 10^{-3}$ Torr, T=RT sputter pressure 500NiO : $1 \cdot 10^{-3}$ Torr, T=200°C sputter pressure 100NiO : $1 \cdot 10^{-3}$ Torr, T=RT sputter deposition rate (Å/s) : $Ni_{80}Fe_{20}$=2, NiO=0.5, Co=2	
sample number	composition
950152	500NiO+30$Ni_{80}Fe_{20}$+20Cu+30$Ni_{80}Fe_{20}$+12Cu+100NiO
950153	500NiO+25$Ni_{80}Fe_{20}$+20Cu+25$Ni_{80}Fe_{20}$+12Cu+100NiO
950154	500NiO+20$Ni_{80}Fe_{20}$+20Cu+20$Ni_{80}Fe_{20}$+12Cu+100NiO
950155	500NiO+15$Ni_{80}Fe_{20}$+20Cu+15$Ni_{80}Fe_{20}$+12Cu+100NiO
950156	500NiO+10$Ni_{80}Fe_{20}$+20Cu+10$Ni_{80}Fe_{20}$+12Cu+100NiO
950157	500NiO+5$Ni_{80}Fe_{20}$+20Cu+5$Ni_{80}Fe_{20}$+12Cu+100NiO

substrate : glass base pressure : $4 \cdot 10^{-7}$ Torr, sputter pressure Fe and Cr: $7 \cdot 10^{-3}$ Torr, T=RT sputter pressure 500NiO : $1 \cdot 10^{-3}$ Torr, T=200°C sputter pressure 100NiO : $1 \cdot 10^{-3}$ Torr, T=RT sputter deposition rate (Å/s) : Fe=2, NiO=0.5, Cr=2	
sample number	composition
950162	200NiO+30Fe+9Cr+30Fe+50NiO
950163	200NiO+25Fe+9Cr+25Fe+50NiO
950164	200NiO+20Fe+9Cr+20Fe+50NiO
950165	200NiO+15Fe+9Cr+15Fe+50NiO
950166	200NiO+10Fe+9Cr+10Fe+50NiO
950167	200NiO+5Fe+9Cr+5Fe+50NiO

substrate : SiO_2, baselayer : 200Ru, toplayer : 30Ru base pressure : $5 \cdot 10^{-7}$ Torr, sputter pressure : $7 \cdot 10^{-3}$ Torr sputter deposition rate (Å/s) : Ru=1, Cu=2, Co=2	
sample number	composition
950184	75Co+6Ru+25Co+30Cu+2Ru+250Co
950185	75Co+6Ru+25Co+30Cu+5Co+2Ru+245Co
950186	75Co+6Ru+25Co+30Cu+10Co+2Ru+240Co
950187	75Co+6Ru+25Co+30Cu+20Co+2Ru+230Co
950188	75Co+6Ru+25Co+30Cu+40Co+2Ru+210Co
950189	75Co+6Ru+25Co+30Cu+80Co+2Ru+170Co
950190	75Co+6Ru+25Co+30Cu+120Co+2Ru+130Co
950191	75Co+6Ru+25Co+30Cu+160Co+2Ru+90Co
950192	75Co+6Ru+25Co+30Cu+200Co+2Ru+50Co
950193	75Co+6Ru+25Co+30Cu+250Co+2Ru

substrate : SiO_2, baselayer : 200Ru, toplayer : 30Ru base pressure : $4 \cdot 10^{-7}$ Torr, sputter pressure : $7 \cdot 10^{-3}$ Torr sputter deposition rate (Å/s) : Ru=1, Cu=2, Co=2	
sample number	composition
950194	75Co+6Ru+25Co+30Cu+25Co+5Ru+300Cu
950195	75Co+6Ru+25Co+30Cu+25Co+10Cu+5Ru+290Cu
950196	75Co+6Ru+25Co+30Cu+25Co+20Cu+5Ru+280Cu
950197	75Co+6Ru+25Co+30Cu+25Co+40Cu+5Ru+260Cu
950198	75Co+6Ru+25Co+30Cu+25Co+80Cu+5Ru+220Cu
950199	75Co+6Ru+25Co+30Cu+25Co+120Cu+5Ru+180Cu
9501100	75Co+6Ru+25Co+30Cu+25Co+160Cu+5Ru+140Cu
9501101	75Co+6Ru+25Co+30Cu+25Co+200Cu+5Ru+100Cu
9501102	75Co+6Ru+25Co+30Cu+25Co+250Cu+5Ru+50Cu
9501103	75Co+6Ru+25Co+30Cu+25Co+300Cu+5Ru

substrate : glass sputter pressure Co and Cu: $7 \cdot 10^{-3}$ Torr, T=RT sputter pressure 500NiO : $1 \cdot 10^{-3}$ Torr, T=200-220°C sputter pressure 100NiO : $1 \cdot 10^{-3}$ Torr, T=RT sputter deposition rate (Å/s) : Cu=2, NiO=0.5, Co=2	
sample number	composition
950274	500NiO+20Co+20Cu+20Co+12Cu+100NiO
950275	500NiO+30Co+20Cu+30Co+12Cu+100NiO
950276	500NiO+40Co+20Cu+40Co+12Cu+100NiO
950277	500NiO+60Co+20Cu+60Co+12Cu+100NiO
950278	500NiO+80Co+20Cu+80Co+12Cu+100NiO
950279	500NiO+100Co+20Cu+100Co+12Cu+100NiO

substrate : glass
base pressure : $3 \cdot 10^{-7}$ Torr, sputter pressure Co and Cu: $7 \cdot 10^{-3}$ Torr, T=RT
sputter pressure 500NiO : $1 \cdot 10^{-3}$ Torr, T=200-220°C

sample number	composition
950280	500NiO+20Co+20Cu+20Co+12Cu
950281	500NiO+30Co+20Cu+30Co+12Cu
950282	500NiO+40Co+20Cu+40Co+12Cu
950283	500NiO+60Co+20Cu+60Co+12Cu
950284	500NiO+80Co+20Cu+80Co+12Cu
950285	500NiO+100Co+20Cu+100Co+12Cu

substrate : glass, grown in field
base pressure: $3 \cdot 10^{-7}$ Torr, sputter pressure Co and Cu: $7 \cdot 10^{-3}$ Torr, T=RT
sputter pressure 500NiO : $1 \cdot 10^{-3}$ Torr, T=200-220°C
sputter pressure 100NiO : $1 \cdot 10^{-3}$ Torr, T=RT
sputter deposition rate (Å/s) : Cu=2, NiO=0.5, Co=2

sample number	composition
950286	500NiO+20Co+20Cu+15Co+12Cu+100NiO
950287	500NiO+20Co+20Cu+20Co+12Cu+100NiO
950288	500NiO+20Co+20Cu+25Co+12Cu+100NiO
950289	500NiO+20Co+20Cu+30Co+12Cu+100NiO
950290	500NiO+20Co+20Cu+40Co+12Cu+100NiO
950291	500NiO+20Co+20Cu+50Co+12Cu+100NiO

substrate : glass, grown in field
base pressure: $5 \cdot 10^{-7}$ Torr, sputter pressure Co and Cu: $7 \cdot 10^{-3}$ Torr, T=RT
sputter pressure 500NiO : $1 \cdot 10^{-3}$ Torr, T=200-220°C
sputter pressure 100NiO : $1 \cdot 10^{-3}$ Torr, T=RT
sputter deposition rate (Å/s) : Cu=2, NiO=0.5, Co=2

sample number	composition
950295	500NiO+20Co+20Cu+70Co+12Cu+100NiO
950296	500NiO+20Co+20Cu+90Co+12Cu+100NiO
950297	500NiO+20Co+20Cu+120Co+12Cu+100NiO
950298	500NiO+20Co+20Cu+150Co+12Cu+100NiO
950299	500NiO+20Co+20Cu+200Co+12Cu+100NiO
9502100	500NiO+20Co+20Cu+300Co+12Cu+100NiO

substrate : SiO_2, baselayer : 30Cr, toplayer : 30Cr
base pressure : $2 \cdot 10^{-7}$ Torr, sputter pressure : $7 \cdot 10^{-3}$ Torr
sputter deposition rate (Å/s) : Cr=2, Cu=2, Co=2

sample number	composition
9502106	75Co+7Cr+25Co+30Cu+100Co
9502107	75Co+7Cr+25Co+1Cr+30Cu+1Cr+100Co
9502108	75Co+7Cr+25Co+2Cr+30Cu+2Cr+100Co
9502109	75Co+7Cr+25Co+3Cr+30Cu+3Cr+100Co
9502110	75Co+7Cr+25Co+4Cr+30Cu+4Cr+100Co
9502111	75Co+7Cr+25Co+6Cr+30Cu+6Cr+100Co
9502112	75Co+7Cr+25Co+15Cu+2Cr+15Cu+100Co
9502113	75Co+7Cr+25Co+15Cu+4Cr+15Cu+100Co
9502114	75Co+7Cr+25Co+15Cu+6Cr+15Cu+100Co
9502115	75Co+7Cr+25Co+15Cu+12Cr+15Cu+100Co

substrate : glass, grown in field base pressure: $2 \cdot 10^{-7}$ Torr, sputter pressure $Ni_{80}Fe_{20}$ and Cu: $7 \cdot 10^{-3}$ Torr, T=RT sputter pressure 500NiO : $1 \cdot 10^{-3}$ Torr, T=200°C sputter pressure 100NiO : $1 \cdot 10^{-3}$ Torr, T=RT	
sample number	composition
9502171	$500NiO+20Ni_{80}Fe_{20}+20Cu+15Ni_{80}Fe_{20}+12Cu+100NiO$
9502172	$500NiO+20Ni_{80}Fe_{20}+20Cu+20Ni_{80}Fe_{20}+12Cu+100NiO$
9502173	$500NiO+20Ni_{80}Fe_{20}+20Cu+25Ni_{80}Fe_{20}+12Cu+100NiO$
9502174	$500NiO+20Ni_{80}Fe_{20}+20Cu+30Ni_{80}Fe_{20}+12Cu+100NiO$
9502175	$500NiO+20Ni_{80}Fe_{20}+20Cu+40Ni_{80}Fe_{20}+12Cu+100NiO$
9502176	$500NiO+20Ni_{80}Fe_{20}+20Cu+50Ni_{80}Fe_{20}+12Cu+100NiO$

substrate : glass, grown in field base pressure: $2 \cdot 10^{-7}$ Torr, sputter pressure $Ni_{80}Fe_{20}$ and Cu: $7 \cdot 10^{-3}$ Torr, T=RT sputter pressure 500NiO : $1 \cdot 10^{-3}$ Torr, T=200-220°C sputter pressure 100NiO : $1 \cdot 10^{-3}$ Torr, T=RT sputter deposition rate (Å/s) : Cu=2, NiO=0.5, $Ni_{80}Fe_{20}$=2	
sample number	composition
9502177	$500NiO+20Ni_{80}Fe_{20}+20Cu+70Ni_{80}Fe_{20}+12Cu+100NiO$
9502178	$500NiO+20Ni_{80}Fe_{20}+20Cu+90Ni_{80}Fe_{20}+12Cu+100NiO$
9502179	$500NiO+20Ni_{80}Fe_{20}+20Cu+120Ni_{80}Fe_{20}+12Cu+100NiO$
9502180	$500NiO+20Ni_{80}Fe_{20}+20Cu+150Ni_{80}Fe_{20}+12Cu+100NiO$
9502181	$500NiO+20Ni_{80}Fe_{20}+20Cu+200Ni_{80}Fe_{20}+12Cu+100NiO$
9502182	$500NiO+20Ni_{80}Fe_{20}+20Cu+300Ni_{80}Fe_{20}+12Cu+100NiO$

substrate : glass base pressure: $3 \cdot 10^{-7}$ Torr, sputter pressure Co and Cu: $7 \cdot 10^{-3}$ Torr, T=RT sputter pressure NiO : $1 \cdot 10^{-3}$ Torr sputter deposition rate (Å/s) : Cu=2, NiO=0.5, Co=2	
sample number	composition
	(500NiO at 200°C, 100NiO at RT)
950301	500NiO+20Co+20Cu+20Co+12Cu+100NiO
950302	500NiO+20Co+20Cu+40Co+12Cu+100NiO
950303	500NiO+20Co+20Cu+60Co+12Cu+100NiO
	(500NiO and 100NiO at RT)
950304	500NiO+20Co+20Cu+20Co+12Cu+100NiO
950305	500NiO+20Co+20Cu+40Co+12Cu+100NiO
950306	500NiO+20Co+20Cu+60Co+12Cu+100NiO

substrate : SiO_2 base pressure : $2{\cdot}10^{-7}$ Torr, sputter pressure : $7{\cdot}10^{-3}$ Torr sputter deposition rate (Å/s) : Ru=1, Cu=2, Co=2	
sample number	composition
9503122	200Ru+100Co+30Ru
9503123	200Ru+250Co+30Ru
9503124	200Ru+500Co+30Ru
9503125	200Ru+1000Co+30Ru
9503126	200Ru+2000Co+30Ru
9503127	200Ru+100Cu+30Ru
9503128	200Ru+200Cu+30Ru
9503129	200Ru+500Cu+30Ru
9503130	200Ru+1000Cu+30Ru
9503131	200Ru+2000Cu+30Ru

substrate : glass, grown in field base pressure: $3{\cdot}10^{-7}$ Torr, sputter pressure Co and Cu: $7{\cdot}10^{-3}$ Torr, T=RT sputter pressure 500NiO : $1{\cdot}10^{-3}$ Torr, T=200°C sputter pressure 100NiO : $1{\cdot}10^{-3}$ Torr, T=RT sputter deposition rate (Å/s) : Cu=2, NiO=0.5, Co=2	
sample number	composition
9503212	500NiO+20Co+20Cu+20Co+12Cu+100NiO
9503213	500NiO+20Co+20Cu+30Co+12Cu+100NiO (500NiO at higher T)
9503214	500NiO+20Co+20Cu+50Co+12Cu+100NiO
9503215	500NiO+20Co+20Cu+70Co+12Cu+100NiO
9503216	500NiO+20Co+20Cu+90Co+12Cu+100NiO

substrate : glass, grown in field base pressure: $3{\cdot}10^{-7}$ Torr, sputter pressure Co and Cu: $7{\cdot}10^{-3}$ Torr, T=RT sputter pressure 500NiO : $1{\cdot}10^{-3}$ Torr, T=200°C sputter pressure 100NiO : $1{\cdot}10^{-3}$ Torr, T=RT sputter deposition rate (Å/s) : Cu=2, NiO=0.5, Co=2	
sample number	composition
9503217	500NiO+20Co+20Cu+30Co+12Cu+100NiO
9503218	500NiO+20Co+20Cu+60Co+12Cu+100NiO
9503219	500NiO+20Co+20Cu+100Co+12Cu+100NiO
9503220	500NiO+20Co+20Cu+130Co+12Cu+100NiO
9503221	500NiO+20Co+20Cu+180Co+12Cu+100NiO
9503222	500NiO+20Co+20Cu+280Co+12Cu+100NiO

substrate : SiO_2 base pressure : $2 \cdot 10^{-7}$ Torr, sputter pressure : $7 \cdot 10^{-3}$ Torr sputter deposition rate (Å/s) : Ru=1, Cu=2	
sample number	composition
950403	250Ru
950404	500Ru
950405	1000Ru
950406	1500Ru
950407	2000Ru
950408	200Ru+1000Cu+30Ru
950409	200Ru+2000Cu+30Ru
950410	200Ru+4000Cu+30Ru
950411	200Ru+7000Cu+30Ru
950412	200Ru+10000Cu+30Ru

Bibliography

[Alph95] E.A.M. van Alphen, and W.J.M. de Jonge, Phys. Rev. B. **51**, 8182 (1995).

[Bai88] M.N. Baibich, J.M. Boto, A. Fert, F. Nguyen Van Dau, F. Petroff, P. Etienne, G. Cruezet, A. Friedrich, and J. Chazelas, Phys. Rev. Lett. **61**, 2472 (1988)

[Baum91] Peter Baumgart, Bruce A. Gurney, Dennis R. Wilhoit, Thao Nguyen, Bernard Dieny, and Virgil S. Speriosu, J. Appl. Phys. **69**, 4792 (1991).

[Bel94] P. Belien, R. Schad, C.D. Potter, G. Verbanck, V.V. Moshchalikov, Y. Bruynseraede, Phys. Rev. B. **50**, 9957 (1994).

[Bloem] P.J.H. Bloemen, *Metallic Multilayers*, PhD thesis, Eindhoven University of Technology, 1993.

[Bong95] R. Bongers, Master's thesis, Eindhoven University of Technology, Department of Physics, 5600 MB Eindhoven, The Netherlands, june 1995.

[Cam89] R.E. Camley, and J. Barnas, Phys. Rev. Lett. **63**, 664 (1989).

[Dien92] B. Dieny, P. Humbert, V.S. Speriosu, S. Metin, B.A. Gurney, P. Baumgart, and H. Lefakis, Phys. Rev. B **45**, 806 (1992).

[Dien93] B. Dieny, V.S. Speriosu, J.P. Nozières, B.A. Gurney, A. Vedyayev, and N. Ryzhanova, Magnetism and Structure in Systems of Reduced Dimension, Ed. R.F.C Farrow et al., Plenum Press, New York, 279 (1993).

[Fal92] Randolph Q. Hood and L.M. Falicov, Phys. Rev. B. **46**, 8287 (1992).

[Fert82] I.A. Campbell, and A. Fert, in *Ferromagnetic Materials*, Vol. 3, Ch. 9, pp. 747, edited by E.P. Wohlfarth, North-Holland Company, 1982.

[Frei93] P.P. Freitas, I.G. Trindade, L.V. Melo, N. Barradas, and J.C., Magnetism and Structure in Systems of Reduced Dimension, Ed. R.F.C. Farrow et al., Plenum Press, New York, 343 (1993).

[Full92] Eric E. Fullerton, David M. Kelly, J. Guimpel, Ivan K. Schuller, and Y. Bruynsereade, Phys. Rev. Lett. **68**, 859 (1992).

[Gurn93] B.A. Gurney, V.S. Speriosu, J-P. Nozieres, H. Lefakis, D.R. Wilhoit, and O.U. Need, Phys. Rev. Lett **71**, 4023 (1993).

[Grün86] P. Grünberg, R. Schreiber, Y. Pang, M.B. Brodsky, and H. Sowers, Phys. Rev. Lett. **57**, 2442 (1986).

[Haar94] F.L. Haarman, *Design and Realization of an automated Magneto-Optical Kerr Effect (MOKE) magnetometer*, ontwerpersopleiding fysische instrumentatie, Eindhoven, 1994.

[Hall92] M.J. Hall, B.J. Hickey, M.A. Howson, C. Hammond, M.J. Walker, D.G. Wright, D. Greig and N. Wiser, J. Phys. Condens. Matter **4**, L495 (1992).

[Hall93] M.J. Hall, B.J. Hickey, M.A. Howson, D. Greig, and N. Wiser, J. Magn. Magn. Mater. **121**, 421 (1993).

[Heuvel] J. van den Heuvel, *Theorie van de CIP magnetoweerstand in magnetische multilagen*, internal report, Eindhoven university of Technology, 1994.

[Hon94] Shigeo Honda, and Masahiko Nawate, Proceedings of the 3rd international symposium on magnetic materials, processes and devices, Volume **94** (6), 189 (1994).

[Huai93] Y. Huai, R.W. Cochrane, and M. Sutton, J. Appl. Phys. **73**, 5530 (1993).

[Huang93] T.C. Huang, J.P. Nozieres, V.S. Speriosu, B.A. Gurney, and H. Lefakis, Appl. Phys. Lett. **62**, 1478 (1993).

[John91] Johnson, and Camley, Phys. Rev. B. **44**, 9997 (1991).

[Jung94] R. Jungblut, R. Coehoorn, M.T. Johnson, J. aan de Stegge, and A. Reinders, J. Appl. Phys. **75**, 6659 (1994).

[Kit86] C. Kittel, *Introduction to solid state physics.*, New York, Wiley, 1986.

[Land95] S. Landheer, Master's thesis, Eindhoven University of Technology, Department of Physics, 5600 MB Eindhoven, The Netherlands, 1995.

[Lub61] Fred E. Luborsky, J. Appl. Phys. **32**, 171S (1961).

[Melo93] L.V. Melo, P. Monteiro, and P.P. Freitas, J. Magn. Magn. Mater. **121**, 390 (1993).

[Mott64] N. Mott, Adv. Phys. **13**, 325 (1964).

[Obi92] Y. Obi, K. Takanashi, Y. Mitani, N. Tsuda, and H. Fujimori, J. Magn. Magn. Mater. **104-107**, 1747 (1992).

[Oguri92] Akira Oguri, Yasuhiro Asano and Sadamichi Maekawa, J. Phys. Soc. Jpn. **61**, 2652 (1992).

[Pap86] D. Papaconstantopoulos, *Handbook of the Band Structures of Elemental Solids*, Plenum, New York, 1986.

[Par90] S.S.P. Parkin, N. More, and K.P. Roche, Phys. Rev. Lett. **64**, 2304 (1990).

[Par93] S.S.P. Parkin, Phys. Rev. Lett. **71** (1993) 1641.

[Par94] S.S.P. Parkin, 14th Int. Coll. on Magnetic Films and Surfaces & E-MRS Symp. on magnetic Ultrathin Films, Multilayers, and Surfaces, Düsseldorf, August 29 - September 2, 1994.

[Petr93] E. Petroff, A. Barthelemy, A. Hamzic, A. Fert, P. Etienne, S. Lequien, and G. Creuzet, J. Magn. Magn. Mater. **93**, 95 (1991).

[Qian] S. Qian, *The sheet resistance measurement of thin films*, internal report, Eindhoven University of Technology, 1994.

[Roer94] R.A. van de Roer, Master's thesis, Eindhoven University of Technology, Department of Physics, 5600 MB Eindhoven, The Netherlands, august 1994.

[Roth58] W.L. Roth, Phys. Rev. **110**, 1333 (1958).

[Sour94] R.L.H. Sour, Master's thesis, Eindhoven University of Technology, Department of Physics, 5600 MB Eindhoven, The Netherlands, december 1994.

[Soe93] S. Soeya, S. Tadokoro, T. Imagawa, and M. Fuyama, J. Appl. Phys. **74**, 6297 (1993).

[Speriosu93] V.S. Speriosu, J.P. Nozieres, B.A. Gurney, B. Dieny, T.C. Huang and H. Lefakis, Phys. Rev. B. **47**, 11579 (1993).

[Schad] R. Schad, C.D. Potter, G. Verbanck, V.V. Moshchalkov, Y. Bruynseraede, J. Dekoster, and G. Langouche, *The effect of step like interface roughness on the Giant Magnetoresistance in epitaxial(100) Fe/Cr superlattices*, to be published.

[Suzuki93] Motofumi Suzuki and Yasunori Taga, J. Appl. Phys. **74**, 4660 (1993).

[Tos93] G. Tosin, L.F. Schelp, M. Carara, J.E. Schmidt, A.A. Gomes, and M.N. Baibich, J. Magn. Magn. Mater **121**, 399 (1993).

[Viret] M. Viret, I. Auneau, and J.M.D. Coey, *Anisotropic magnetotransport properties of cobalt thin films*, Physics Department, Trinity College, Dublin 2, Ireland, to be published.

[Wied79] H.H. Wieder, *Laboratory notes on electrical and galvanomagnetic measurements*, Materials science monographs 2, Elsevier, Amsterdam, 1979.

[Will95] M.M.H. Willekens, Th.G.S.M. Rijks, H.J.M. Swagten and W.J.M. de Jonge,*Effects of interface intermixing on the magnetoresistance of spin-valves with uncoupled Co-layers*, to be published in J. Appl. Phys.

[Yam93] Haruki Yamane, Yoshinori Maeno, and Masanobu Kobayashi, J. Magn. Magn. Mater. **126**, 320 (1993).

Acknowledgements

Afstuderen doe je niet alleen en kan nooit tot een goed einde komen zonder de hulp van anderen. Daarom wil ik iedereen bedanken die bij mijn afstuderen betrokken waren, met name

Erwin van Alphen
Gerrie Baselmans
Pascal Bloemen
Rini Bongers
Hans Dalderop
Paul van der Heijden
Rob van Kempen
Siebe Landheer
Henk Munsters
Jef Noijen
Marc van Opstal
Marc Ponjée
Shengwei Qian
Theo Rijks
Wijnand Versteeg

en in het bijzonder *Henk Swagten* en *Marc Willekens* voor de goede en intensieve begeleiding en *prof. W. de Jonge* voor het mogelijk maken van mijn afstuderen.